Low-frequency dynamics in various disordered materials examined via fluorescence spectroscopy of incorporated chromophores

Yoshiro Ichino

Dissertation in Physics
Graduate School of Science
Osaka University
1997

Abstract

We have developed a site-selective fluorescence-excitation spectroscopy to measure hole-burning-free fluorescence-line-narrowing spectra including zero-phonon fluorescence lines for a wide variety of disordered materials incorporated with chromophores.

We have obtained the density of states of low-frequency host vibrational modes weighted by the coupling strength between the electronic state of the chromophore and the host vibrations (WDOS) for doped polymers, sol-gel-derived inorganic gels and molecular glass by analyzing the site-selective excitation spectrum at low temperatures. A universal feature has been found in WDOS spectra not only for polymeric systems but also for a number of molecular glasses when they are rescaled with respect to the peak energies. Several theoretical models proposed previously are reviewed and it is verified if they are appropriate for interpreting the universal behavior of WDOS spectra.

Site-selective fluorescence spectra have been obtained at various temperatures below the glass transition temperatures for several molecular glasses and compared with those calculated on the basis of the WDOS and the linear Frank-Condon interaction. In most cases, the calculated site-selective fluorescence spectra have reproduced the measured ones fairly well up to the glass transition temperatures, which indicates that the host vibrations are regarded as harmonic modes at whole temperatures below the glass transition temperature. In the case of chlorophyll b-doped 1-propanol glass, however, the calculated spectra have deviated from the measured

spectra even far below the glass transition temperature.

Nanosecond time-resolved site-selective fluorescence spectroscopy has been performed for chlorophyll b-doped 1-propanol glass at 60K. Temporal broadening of the fluorescence spectrum has been observed in the nanosecond scale which strongly indicates the relaxational behavior occurs even below the glass transition temperature. From these results, we set forth a hypothesis that the solvent-shell which has the different structure from the bulk glass is formed in the vicinity of a chromophore and the melting of this shell is observed even at a glassy state temperature.

Our results of WDOS are compared with Raman and inelastic neutron scattering data obtained by Sokolov's research group and the frequency dependence of the coupling coefficient in WDOS is discussed.

A new experimental technique to obtain the single-site absorption and fluorescence spectra independently has been developed, where hole-burning, site-selective fluorescence and fluorescence-excitation spectroscopies are combined. The difference spectrum of the site-selective excitation spectra before and after the hole-burning corresponds to the single-site absorption spectrum, while the similar difference spectrum of site-selective fluorescence spectrum corresponds to the single-site fluorescence spectrum. This technique has been applied to a chlorin-doped polystyrene film and it has been revealed that the mirror-symmetry relationship between single site absorption and fluorescence spectra roughly holds in this case. This result indicates that the optical spectra of this system can be roughly interpreted in terms of the linear Frank-Condon-type electron-phonon interaction which has been assumed in the analytical procedure of the determination of WDOS.

Contents

List of Figures

List of Tables

Chapter 1

Introduction

Numerous attempts have been made on the low-frequency vibrational modes in disordered materials in recent years [1-36]. The vibrational density of states (DOS) of these modes in a perfect crystal can be approximately described by the Debye continuum model and is well known to be proportional to the square of vibrational frequency. In the case of disordered systems, however, the DOS in the low-frequency region does not follow this power law of the vibrational frequency at all, which is supposed to be caused by the nonuniformity in these materials.

A number of experimental studies using low-frequency Raman scattering and inelastic neutron scattering have revealed so far that the anomalous excess modes compared to the Debye phonon modes surely exist in the low-frequency region, which has been called the Boson peak. This unique shape of the DOS has been found not only for inorganic oxide glasses [10,11,13-18,23-28] and organic polymers [1,2,7-10,12] but also for amorphous semiconductors [19-22] and molecular glasses [3-6,7,8]. The Boson peak is usually observed at sufficiently low temperatures while the relaxational contribution is not negligible and overcomes Boson peak at higher temperatures [3,4,9].

Malinovsky and his coworkers found the universal function for the densities of states of the low-frequency vibrational modes in polymers by means

of inelastic neutron scattering [12] and Raman scattering [13].

In addition, direct comparison between Raman and neutron scattering spectra for polymeric systems has been made by Sokolov and coworkers [7,8,10] and has clarified the vibrational frequency dependence of the light-to-vibration coupling coefficient in the low-frequency Raman scattering spectra. It is surprising that thus obtained frequency dependence of coupling coefficient is also universal among several polymeric systems they examined. This result shed a new light on the study of low-frequency dynamics in disordered systems because it has a possibility to verify existing theoretical models.

Various theoretical models, on the other hand, have been proposed so far to interpret the anomaly of DOS in disordered systems [12, 14, 15, 19, 23, 26, 34, 35, 36]. For example, a fractal model is one of the most widely accepted models to explain the anomaly in disordered materials such as silica aerogels [14-18,36] and amorphous semiconductors [19,20]. This model assumes the fractal network geometry and the superlocalized vibrational excitations in these disordered matrices. Malinovsky has proposed a cluster model for the interpretation of his result about the universality of DOS [11,13]. He concluded that the universal function he found could be derived from the size distribution of clusters in disordered materials. Although, as apparently shown in these examples, theoretical models proposed so far have succeeded in explaining the low-frequency dynamics for their particular cases of disordered materials, most of them remain insufficient for interpreting the universal behavior appeared in a fairly wide variety of materials. For example, monomeric disordered materials have never been concerned in the cluster model, where such a broad distribution of the cluster size which is assumed in polymeric disordered systems can hardly be considered. In the case of fractal models, it is still doubtful if all of disordered materials including molecular glasses and polymers have fractal

geometry.

One of motivations of our study in this thesis lies in the point, Why is such an anomalous shape of DOS found in a wide variety of disordered materials? We approach this theme from another point of view. Namely, we intend to investigate the low-frequency dynamics probed by the fluorescence spectra of incorporated chromophore molecules at low temperatures.

Site-selection spectroscopies including the hole-burning and the site-selective fluorescence, have been widely employed for various dye-doped disordered materials [37-40,50,52-66,71,74,75]. Transition energies from the electronic ground state to the excited state of a chromophore molecule in a disordered matrix are usually inhomogeneously distributed, which is caused by the inhomogeneity of the local configuration of the host matrix in the vicinity of the chromophore. Absorption and conventional fluorescence spectra for dye-doped disordered systems are broad and structureless because of this inhomogeneous broadening of the site-energy. Site-selection techniques could be powerful tools to extract the homogeneous spectrum from such an inhomogeneous broadening.

Ahn and coworkers succeeded for the first time in measuring the exact intensities of both zero-phonon line and the phonon-sideband of the site-selective fluorescence spectrum for organic polymers doped with porphyrin-like dye molecules at low temperatures [61-65]. This result has been obtained by utilizing the time-resolved technique together with the conventional site-selection spectroscopy. Namely, they employed a synchronously pumped cw mode-locked dye laser system as an excitation source and a time-correlated single-phonon counting method for detection [67,68]. This made it possible to determine the densities of states of low-frequency vibrational modes weighted by the electron-vibration coupling strength (WDOS) via the quantitative analysis. Although it had been widely known

before this work that the phonon-sideband component of the hole spectrum or the site-selective fluorescence spectrum contains information of the low-frequency vibrational modes in host matrices, quantitative analysis had not been performed because of the lack of the exact intensities of the zero-phonon component.

It is no doubt that this development enables us to look more carefully into the low-frequency dynamics on the local structure of the host matrices in the vicinity of the dye molecule. This work has revealed that thus obtained WDOS spectra only depend on the host matrices and are almost identical between various polymers on a normalized scale with respect to the peak frequencies of each WDOS spectra.

It is fairly important to examine whether the universal shape of the WDOS spectra exists even for other disordered materials such as inorganic gels and molecular glasses. However, site-selective fluorescence spectroscopy has only limited applications due to the hole-burning effects. Photoexcitation of probe molecules often causes conformational change of the surrounding host molecules in the disordered systems because of localized degrees of freedom which is called *two-level systems*. In this case, long-time irradiation of laser light for the measurement of fluorescence results in persistent spectral hole burning and prevents quantitative analysis of the site-selective fluorescence spectrum. This effect is particularly serious for ionic dye-doped systems or dye-doped molecular glasses.

We have developed a hole-burning-free site-selective fluorescence spectroscopy, namely, the time-resolved site-selective fluorescence-excitation spectroscopy [59,60]. This can be performed by using the continuous scan of the wavelength of the tunable dye laser together with the time-correlated single-photon counting method. This enables us to investigate the low-frequency dynamics of a much wider variety of disordered materials. In our investigation, we employed organic polymers, inorganic gels prepared

via the sol-gel method and alcoholic/non-alcoholic molecular glasses as disordered materials.

In this thesis, we will present our experimental results for recent three years concerning the low-frequency dynamics investigated via the site-selective fluorescence and excitation spectra of incorporated dye molecules.

Theoretical backgrounds required for the interpretation of the site-selective excitation spectrum, single-site absorption spectrum and WDOS will be described in Chapter 2.

In Chapter 3, we will firstly show the experimental setup for the site-selective excitation spectroscopy, then will present the chemical aspects of our research: the way we chose both host materials and guest molecules and the way we prepared the samples such as sol-gel glasses.

The main part of this thesis is Chapter 4 in which various experimental results will be shown. In Section 1, we will present the results on the conventional spectroscopy, i.e., absorption and conventional fluorescence spectra for dye-doped molecular glasses. In Section 2 we will describe the results of the site-selective excitation spectra together with the analytical procedure to extract single-site spectrum. WDOSs for various dye-doped disordered systems will be shown and compared with one another in Section 3. The universality of WDOSs not only for polymeric matrices but also for the monomeric molecular glasses will be presented in this section. Previously obtained WDOSs for dye-doped organic polymers will be compared to Raman or neutron scattering spectra in Section 4. Various theoretical models which were proposed so far will be reviewed with respect to the interpretation of the universal profile of WDOS in Section 5. In the latter part of this section we will present our standpoint that the superlocalized vibration in the strongly disordered systems is most likely the origin of the low-frequency modes which appeared in WDOS.

In Section 6, the temperature dependence of the site-selective fluorescence spectra will be shown together with that of the spectra calculated on the basis of obtained WDOS. The local melting postulate derived from these results will be presented in this section. We will describe the analytical and experimental procedures of double-selection technique to determine the single-site absorption and fluorescence spectra independently and then will verify the validity of mirror-symmetry relation in these spectra in the last section, Section 7.

Finally we will conclude this study in the end of this thesis, in Chapter 5.

Chapter 2

Theoretical Background

2.1 Spectral shape function

In this section, we will obtain the general formulation of a single-site absorption spectrum of an impurity center in a solid on the basis of a dynamical theory.

The shape function of the absorption spectrum which corresponds to the transition from the electronic ground state $|g\rangle$ to the excited state $|e\rangle$ can be written as

$$a_T(\omega_1;\omega_0) \propto \sum_n P_{gn} \sum_m \left|\langle em|\hat{V}|gn\rangle\right|^2 \delta(\omega-\omega_1) \tag{2.1}$$

$$W_{em} - W_{gn} = \hbar\omega, \qquad W_{e0} - W_{g0} = \hbar\omega_0 \tag{2.2}$$

where ω_1, T, $\hat{V}$ and n,m indicate the operator of light-electron interaction, lattice vibrational levels at $|g\rangle$ and $|e\rangle$ respectively, and P_{gn} shows the thermal distribution of the lattice vibration at $|g\rangle$

$$\begin{aligned} P_{gn} &= \frac{e^{-\beta W_{gn}}}{\sum_n e^{-\beta W_{gn}}} \\ \beta &= \frac{1}{k_B T}. \end{aligned} \tag{2.3}$$

When the electric dipole approximation is employed for the light-localized electron interaction, $\hat{V}$ can be written as

$$\hat{V} = \sum_l i\sqrt{\frac{\hbar\omega_l}{2\varepsilon_0 V}}(\hat{\mu}_l \hat{a}_l{}^+ - \hat{\mu}_l{}^+ \hat{a}_l). \tag{2.4}$$

where $\hat{a}_l{}^+$, $\hat{a}_l$ are the photon creation and annihilation operators respectively and $\hat{\mu}_l{}^+$, $\hat{\mu}_l$ indicate the electric dipole-moment operators corresponding to the transitions $|g\rangle \rightarrow |e\rangle$ and $|e\rangle \rightarrow |g\rangle$, respectively. Further, V, ε_0 and ω_l are the volume of the space which provides the boundary condition of the electromagnetic wave, the dielectric constant in the vacuum and the angular frequency of the light with the mode number l.

Then Eq.(2.1) can be rewritten by using Eq.(2.4) as

$$\begin{aligned} a_T(\omega_1;\omega_0) &= \sum_n P_{gn} \sum_m \left|\langle em|\hat{\mu}^+|gn\rangle\right|^2 \delta(\omega-\omega_1) \\ &= \frac{1}{2\pi}\int_{-\infty}^{\infty} dt \sum_n \sum_m P_{gn}\langle gn|\hat{\mu}|em\rangle\langle em|\hat{\mu}^+|gn\rangle e^{i(\omega_1-\omega)t}. \end{aligned} \tag{2.5}$$

Eq.(2.5) can be described using the density matrix $\hat{\rho}_j(\beta) \equiv e^{-\beta\hat{H}_j}$ as

$$\begin{aligned} a_T(\omega_1;\omega_0) &= \frac{1}{2\pi}\int_{-\infty}^{\infty} dt e^{i\omega_1 t} \frac{\mathrm{Tr}\left[\hat{\rho}_g(\beta-\frac{it}{\hbar})\mu_{ge}\hat{\rho}_e(\frac{it}{\hbar})\mu_{eg}\right]}{\mathrm{Tr}\left[\hat{\rho}_g(\beta)\right]} \\ \sum_n e^{-\beta W_{gn}} &= \sum_n \langle gn|e^{-\beta\hat{H}_g}|gn\rangle. \end{aligned} \tag{2.6}$$

Under these approximations, the shape function of the absorption spectrum is described as follows

$$a_T(\omega_1;\omega_0) = \frac{|\mu_{eg}|^2}{2\pi}\int_{-\infty}^{\infty} dt e^{i\omega_1 t} f^*(t), \tag{2.7}$$

where

$$f^*(t) = \frac{\mathrm{Tr}\left[\hat{\rho}_g(\beta-\frac{it}{\hbar})\hat{\rho}_e(\frac{it}{\hbar})\right]}{\mathrm{Tr}\left[\hat{\rho}_g(\beta)\right]}. \tag{2.8}$$

Here we assume that only Frank-Condon linear term contributes to the electron-phonon interaction. Namely, the curvatures of adiabatic potentials at $|g\rangle$ and $|e\rangle$ are identical with each other and the displacement between each of the potential minima is given as Δ. Then the following equation holds:

$$|em(q)\rangle = |gn(q-\Delta)\rangle\,. \tag{2.9}$$

When we use q-expression

$$\mathrm{Tr}[\hat{\rho}_j] = \int dq\langle q|\hat{\rho}_j|q\rangle \qquad (j=g,e) \tag{2.10}$$

in Eq.(2.8), it can be rewritten as

$$f^*(t) = \frac{\iint\langle q|\hat{\rho}(\beta-\frac{it}{\hbar})|\bar{q}\rangle\langle\bar{q}-\Delta|\hat{\rho}(\frac{it}{\hbar})|q-\Delta\rangle dqd\bar{q}}{\int\langle q|\hat{\rho}(\beta)|q\rangle dq}. \tag{2.11}$$

When the wave function $|q\rangle$ is assumed as the harmonic oscillator, the following equation can be obtained as

$$|q\rangle = \sqrt{\frac{\alpha}{\sqrt{\pi}2^n n!}}e^{-\frac{\alpha^2q^2}{2}}H_n(\alpha q), \tag{2.12}$$

where

$$H_n(x) = e^{x^2}\frac{(-2i)^n}{\sqrt{\pi}}\int_{-\infty}^{\infty}u^n e^{-u^2+2iux}du. \tag{2.13}$$

Substituting Eq.(2.12) and Eq.(2.13) into Eq.(2.11), we obtain the following equation:

$$\begin{aligned} f^*(t) = \exp[-i\omega_0 t - (\omega\Delta^2/2\hbar)\{&(2n_T(\omega)+1) - n_T(\omega)e^{i\omega t} \\ &-(n_T(\omega)+1)e^{-i\omega t}\}], \end{aligned} \tag{2.14}$$

where $n_T(\omega)$ is a Bose factor.

Because the lattice vibration actually contains a number of harmonic modes, Eq.(2.14) should be rewritten as

$$\begin{aligned} f^*(t) &= \exp[-i\omega_0 t - \sum_\lambda \frac{\omega_\lambda\Delta^2}{2\hbar}\{(2n_T(\omega_\lambda)+1) - n_T(\omega_\lambda)e^{i\omega_\lambda t} \\ &\qquad -(n_T(\omega_\lambda)+1)e^{-i\omega_\lambda t}\}] \\ &= \exp\{-i\omega_0 t + S_T(t) - S_T(0)\} \end{aligned} \tag{2.15}$$

where

$$S_T(t) = \int_0^\infty d\omega s(\omega) \left\{ (n_T(\omega) + 1) e^{-i\omega t} + n_T(\omega) e^{i\omega t} \right\} \tag{2.16}$$

and

$$\begin{aligned} s(\omega) &= \sum_\lambda \frac{\omega_\lambda {\Delta_\lambda}^2}{2\hbar} \delta(\omega - \omega_\lambda) \\ &= \sum_\lambda {\xi_\lambda}^2 \delta(\omega - \omega_\lambda). \end{aligned} \tag{2.17}$$

Here, $s(\omega)$ shows the density of phonon states weighted by the strength of electron-phonon coupling ξ_λ^2 (hereafter abbreviated as WDOS). When we substitute Eq.(2.15) into Eq.(2.7) and then normalize the total integral of $a_T(\omega_1;\omega_0)$ to unity, we finally obtain the shape function of single-site absorption spectrum as follows:

$$a_T(\omega_1;\omega_0) = \frac{1}{2\pi} \int_{-\infty}^{\infty} dt \exp\{i(\omega_1 - \omega_0)t + S_T(t) - S_T(0)\}. \tag{2.18}$$

The experimentally-measured absorption spectrum $A_{abs}(\omega)$ is proportional to $\omega a_T(\omega)$ instead of $a_T(\omega)$.

2.2 Weighted density of phonon states

When we assume that only the linear Frank-Condon-type interaction contributes to the electron-phonon coupling, a mirror-symmetry relation holds between the shape function of the single-site absorption and fluorescence spectra, because the phonon frequencies of the electronic ground state $|g\rangle$ and the excited state $|e\rangle$ are strictly identical under such an assumption.

Therefore, the shape function of the single-site fluorescence spectrum can be described as

$$f_T(\omega_p;\omega_0) = \frac{1}{2\pi}\int_{-\infty}^{\infty} dt \exp\{i(\omega_0-\omega_p)t + S_T(t) - S_T(0)\}, \tag{2.19}$$

where ω_p and ω_0 represent the angular frequency of light and that of the zero-phonon line, respectively. Replacing ω_0 with $\omega = \omega_0 - \omega_p$ in Eq.(2.19), we obtain the following equation:

$$f_T(\omega) = \frac{1}{2\pi}\int_{-\infty}^{\infty} dt e^{i\omega t} e^{S_T(t)} e^{-S_T(0)}. \tag{2.20}$$

$e^{S_T(t)}$ in Eq.(2.20) can be expanded by employing Taylor-expansion as

$$e^{S_T(t)} = \sum_{m=0}^{\infty} \frac{[S_T(t)]^{(m)}}{m!}. \tag{2.21}$$

Inverse Fourier transform of $S_T(t)$ in Eq.(2.16) is described as follows:

$$\begin{aligned} s_T(\omega) &= \frac{1}{2\pi}\int_{-\infty}^{\infty} dt S_T(t) e^{i\omega t} \\ &= s(\omega)\{n_T(\omega)+1\} + s(-\omega)n_T(-\omega), \end{aligned} \tag{2.22}$$

where $s_T(\omega)$ is called the *phonon function*. Eq.(2.22) indicates that the phonon function at finite temperature T can be obtained by using the phonon function at 0K $s(\omega)$ (WDOS) and Bose factor $n_T(\omega)$.

The first and the second terms of the right side of Eq.(2.22) correspond to the Stokes component caused by creation of phonons and the anti-Stokes component due to annihilation of phonons, respectively.

When we substitute Eq.(2.21) into Eq.(2.19) and replace $e^{S_T(0)}$ as $\alpha_T^{'}$, the following relation can be derived:

$$f_T(\omega) = \alpha_T^{'}\delta(\omega) + \Phi_T(\omega), \tag{2.23}$$

where

$$\begin{aligned}\Phi_T(\omega) &= \sum_{m=1}^{\infty} \Phi_T^{(m)}(\omega) \\ &= \sum_{m=1}^{\infty} \frac{\alpha_T^{'}}{m!} \cdot \frac{1}{2\pi} \int_{-\infty}^{\infty} dt e^{i\omega t} [S_T(t)]^m. \end{aligned} \tag{2.24}$$

In Eqs.(2.23) and (2.24), $\delta(\omega)$, $\Phi_T(\omega)$ and $\alpha_T^{'}$ represent the zero-phonon fluorescence line, the phonon-sideband and Debye-Waller factor, respectively.

$\Phi_T^{(m)}$ in Eq.(2.24), which means the m-phonon contribution in the phonon-sideband $\Phi_T(\omega)$, can be expressed using $s_T(\omega)$ as

$$\begin{aligned}\Phi_T^{(m)}(\omega) = \frac{\alpha_T^{'}}{m!} \int_{-\infty}^{\infty} d\omega_1 \int_{-\infty}^{\infty} d\omega_2 \cdots \int_{-\infty}^{\infty} d\omega_m s_T(\omega_1) s_T(\omega_2) \\ \times \cdots s_T(\omega_m) \delta(\omega - \omega_1 - \omega_2 \cdots - \omega_m). \end{aligned} \tag{2.25}$$

When we multiply both sides of Eq.(2.24) by $e^{-i\omega t^{'}}$, perform an integration over ω and substitute Eq.(2.19), then we obtain the following equation:

$$\int_{-\infty}^{\infty} d\omega \Phi_T(\omega) e^{-i\omega t^{'}} = \alpha_T^{'} \left[e^{S_T(t^{'})} - 1 \right]. \tag{2.26}$$

When we differentiate Eq.(2.26) by $t^{'}$ and perform reverse Fourier transform, the following integral equation is derived:

$$\omega \Phi_T(\omega) = \alpha_T^{'} \omega s_T(\omega) + \int_{-\infty}^{\infty} d\omega^{'} \Phi_T(\omega - \omega^{'}) \omega^{'} s_T(\omega^{'}). \tag{2.27}$$

At T=0, Eq.(2.27) can be expressed as

$$\omega \Phi_0(\omega) = \alpha_0^{'} \omega s_0(\omega) + \int_0^{\omega} d\omega^{'} \Phi_0(\omega - \omega^{'}) \omega^{'} s_0(\omega^{'}). \tag{2.28}$$

In this integral equation, $\Phi_0(\omega)$ corresponds approximately to the phonon-sideband of the single-site fluorescence spectrum obtained from the site-selective fluorescence spectrum at liquid helium temperature. The Debye-Waller factor $\alpha_0'(\omega)$, which corresponds to the ration of the integral intensity of the zero-phonon line to that of the total fluorescence spectrum, is also determined experimentally from the site-selective fluorescence spectrum.

In conclusion, WDOS $s_0(\omega) \equiv s(\omega)$ can be determined by solving Eq.(2.28) numerically.

2.3 Site-selective fluorescence and excitation spectra

We illustrate in this section that the single-site spectrum can be obtained from the site-selective fluorescence or fluorescence-excitation spectrum.

Actual single-site absorption and fluorescence spectra $a_T^{'}(\omega)$, $f_T^{'}(\omega)$ are expressed by using the shape functions $a_T(\omega)$, $f_T(\omega)$ discussed in the preceding sections as

$$\begin{aligned} a_T^{'}(\omega) &\propto \omega a_T(\omega), \\ f_T^{'}(\omega) &\propto \omega^3 f_T(\omega). \end{aligned} \tag{2.29}$$

When we use relations in Eq.(2.29) and furthermore assume that the single-site spectrum is site-energy-independent, which seems to be adequate for the host-guest systems we investigate, site-selective fluorescence (SSF) and fluorescence-excitation (SSE) spectra can be described exactly in the same form as

$$F(\omega;\omega_L) \propto \int G(\omega')\omega_L a_T(\omega_L-\omega')\omega^3 f_T(\omega-\omega')d\omega', \tag{2.30}$$

where ω and ω_L represent the angular frequency of the detected fluorescence and that of the exciting tunable laser, respectively. $G(\omega^{'})$ shows the site-energy distribution function. The difference between SSF and SSE only lies in the scanning parameters, ω for SSF and ω_L for SSE, respectively.

When we divide the shape functions of single-site absorption/fluorescence spectra into two components, zero-phonon lines and phonon-sidebands, as

$$\begin{aligned} a_T(\omega_L-\omega') &= a_{zpl}(\omega_L-\omega') + a_{psb}(\omega_L-\omega') \\ &= \delta(\omega_L-\omega') + a_{psb}(\omega_L-\omega') \end{aligned} \tag{2.31}$$

$$\begin{aligned} f_T(\omega-\omega') &= f_{zpl}(\omega-\omega') + f_{psb}(\omega-\omega') \\ &= \delta(\omega-\omega') + f_{psb}(\omega-\omega'), \end{aligned} \tag{2.32}$$

then Eq.(2.30) can be rewritten as the sum of four components as follows:

$$\begin{aligned} F(\omega;\omega_L) \;\propto\; & {\omega_L}^4 G(\omega_L) \\ & + \omega_L \omega^3 G(\omega_L) f_{psb}(\omega - \omega_L) \\ & + \omega_L \omega^3 G(\omega) a_{psb}(\omega_L - \omega) \\ & + \omega_L \omega^3 \int G(\omega') a_{psb}(\omega_L - \omega') f_{psb}(\omega - \omega') d\omega'. \end{aligned} \tag{2.33}$$

The first and the second components correspond to the zero-phonon and the phonon-sideband fluorescence caused by the resonant zero-phonon absorption, respectively. The third and the last components, on the other hand, correspond to the zero-phonon and the phonon-sideband fluorescence due to the phonon-sideband absorption, respectively. The site-energy distribution function $G(\omega')$ can be obtained from the first component, which can be experimentally determined by plotting the fluorescence intensity of the zero-phonon line with a fixed power of the excitation laser.

It can be found that, as seen in Eq.(2.30), the shape functions of single-site absorption $a_T(\omega_L - \omega')$ and the single-site fluorescence $f_T(\omega - \omega')$ cannot be determined independently from the experimental results $F(\omega;\omega_L)$ and $G(\omega')$. Hence, in order to solve Eq.(2.30) numerically, we need an assumption that the mirror symmetry relation holds between the shape functions of single-site absorption and fluorescence as

$$f_T(\omega - \omega') = a_T(\omega' - \omega). \tag{2.34}$$

This relationship holds if we assume that only the linear Frank-Condon electron-phonon interaction contributes to the optical spectrum at low temperatures. This assumption seems to be valid in the cases of our samples with a fairly weak electron-phonon coupling, which will be discussed more carefully in the later section. Employing this mirror symmetry relation in Eq.(2.30), we finally obtain the following equation:

$$F(\omega;\omega_L) \propto \int G(\omega') \omega_L a_T(\omega_L - \omega') \omega^3 a_T(\omega' - \omega) d\omega'. \tag{2.35}$$

It is obvious that the shape function of the single-site spectrum $a_T(\omega_L - \omega')$ can be obtained from experimentally determined site-selective fluorescence/excitation spectrum $F(\omega; \omega_L)$ and the site-energy distribution function $G(\omega')$.

Chapter 3

Experiment

3.1 Experimental setup

In this section, we will describe the experimental setup for the site-selective fluorescence/fluorescence-excitation spectroscopy in detail. It is particularly noteworthy that we employed the time-correlated single-photon counting method combined with the site-selective fluorescence measurement, which enabled us to measure the zero-phonon fluorescence intensity quantitatively for dye-doped disordered systems without suffering from the scattering of excitation laser light. It should also be noted that we have succeeded in obtaining the *hole-burning-free* site-selective excitation spectrum including zero-phonon fluorescence line for the first time.

This technique makes it possible to determine the weighted density of states of low-frequency vibrational modes for a number of dye-doped disordered materials with high hole-burning efficiencies such as organic molecular glasses and sol-gel-derived inorganic gels.

3.1.1 Laser system

Our experimental setup employed for the excitation laser system is shown in Fig.1.

We employed a cw mode-locked dye lasers system (Spectra Physics model 376B) synchronously pumped by a cw mode-locked Ar^+ ion laser (Spectra

Physics model 2020) as an excitation source. A DCM dye laser was used for the tunable light source of site-selective fluorescence spectroscopy in most cases, while R6G dye laser was used for the excitation source only when we measured the selective fluorescence spectra at the higher energy side of the site-energy distribution in oxazine 4-doped SiO_2 gel. Both dyes DCM and R6G were purchased from Exciton Inc. The frequency of the AO modulation in the mode-locker driver was set to about 41MHz, which produced the cw mode-locked pulses with their intervals of 12.2ns. This DCM-tunable dye laser system provided light pulses in the spectral range of 630-690nm with a pulse duration of less than 10 ps and an average power of 50mW.

The lasing wavelength could be selected by adjusting the angle of an intracavity-placed birefringent filter which was rotated by the stepping motor. This motor was controlled by the pulse motor controller(Ampére PPMD805), which was in turn controlled by the personal computer(PC).

The output power of the dye laser was reduced to about 25mW by a neutral density filter and then was stabilized by an external laser power controller(Thorlabs CR200A). We confirmed that it could stabilize the output power of the dye laser during the wavelength scan with a relatively high scanning speed.

The stabilized laser light went through the first wedged substrate(WS1) dividing the incident beam into two reflected beams and one transmitted one. One of the reflected beams was led to the photodetector(PD1) for monitoring the stability of the laser power. The other reflected part first passed through the solid-gap etalon(CVI, FSR$\sim$4.9cm^{-1}) and then the transmitted interference signal was detected by another photodetector(PD2). Both signals detected by PD1 and PD2 were converted to digital signals by a 2ch-A/D converter(Union Data UAD98WA) and then stored in the computer PC.

The transmitted beam at WS1 was again split to three parts by another wedge-shaped substrate(WS2). One of the reflected beams was focused onto a fast *pin*-type photodiode, whose output signal was used as a stop pulse of a time-to-amplitude converter in the time-correlated single photon counting system. Another part of the reflected beams was used to measure roughly the wavelength of the dye laser by a 0.25-m single-grating portable monochromator(Nikon G250). These two wedged substrates are much more useful in minimizing the fluctuation of the output light due to the interference effect than the standard glass plates.

The power of the transmitted laser beam was again reduced to μW order by using an absorption-type neutral density filter (also chosen to minimized interference). The laser beam was passed through a polarizer sheet (PL1) in order to select polarization perpendicular to the experimental bench, and was finally used as an excitation source.

The excitation power was finally reduced to $0.5\sim5\mu$W, which was determined for each experiment considering the hole-burning efficiency and the fluorescence quantum efficiency of each sample. The spot size at the surface of the sample was about ϕ1mm, which corresponds to the power density of about $0.1\sim1$mW/cm^2. Any focusing lenses were not used in front of the samples to minimize the excitation power density and hence to minimize the hole-burning effect.

The power instability of the excitation laser light while scanning the laser wavelength for any unexpected reasons, including the wavelength-dependence of the transmittance of the polarizer and the neutral density filter, was carefully checked by using a photodetector replaced with the cryostat before starting our measurement sequences.

3.1.2 Detection system

Fluorescence from the sample was analyzed by a single monochromator (Chromatix CT103, 1-m focal length, F=6.8) and detected by a cooled photomultiplier (Hamamatsu R928p). The cross-polarized analyzer sheet (PL2) in front of the entrance slit of the monochromator played an important role in minimizing the perpendicularly polarized scattered laser light which mainly originated from the surface of the sample or the inner part of the cryostat. In the case of polymers or inorganic gels with an excellent optical quality, most of the scattered light could be easily removed by using this polarizer-analyzer pair. In most cases of liquid-quenched molecular glasses, however, the frozen sample had a number of microcracks and local strains which caused randomly polarized scattering light. In this case, it is quite difficult to improve markedly the fluorescence-scattering ratio only by using the polarizer-analyzer pair and accordingly the rejection of the scattered light using the time-domain method plays an indispensable role, which will be discussed later.

The mount of the cryostat was specially designed to be movable mechanically in both horizontal and vertical directions, which greatly helps us to select a position of the sample with the best optical quality for laser excitation.

Absorption spectra were also measured by using a 50W tungsten lamp, which is focused on the sample with exactly the same size of the excitation light. The power of this light was reduced by using neutral density filters to the order of μW at the surface of the sample.

3.1.3 Cryogenic system

For organic polymers, a section of film of uniform color was cut from the dried film and was used as a sample. For inorganic gels, a fragment with

appropriate size (~5mm×5mm) was used. A special care was taken for liquid-quenched molecular glasses because almost all of the liquids chosen as samples have fairly low melting points and thereby should be prevented from vaporization during the loading process of samples. A previously prepared dye solution was poured quickly into a glass cell with the dimensions of $10\times10\times1mm^3$ stored in ice water. As soon as filled up, it was sealed up tightly at the top of the cell. Thus prepared samples were placed in a continuous-flow liquid-helium cryostat (Oxford CF1204). To obtain a liquid-quenched glass with a good optical quality, the cooling rate was set at the maximum value of our cryogenic system (~10K/min). The temperature of the sample was monitored by a thermocouple during the measurement and was controlled within ±0.5K.

3.1.4 Electronic devices

The time-correlated single-photon counting technique is frequently employed for the measurement of fluorescence lifetime with the order of nanoseconds and microseconds and was described elsewhere in detail [67, 68]. The positive pulse signal with a duration of ~1nsec was negatively amplified by a 300MHz preamplifier (Kuranishi WP11), discriminated (EG&G T105/NL), and was fed into a time-to-amplitude converter (TAC, Ortec 467) as a stop pulse of time-correlated single photon counting (TCSPC). The negative output pulse from the photomultiplier was also discriminated (Ortec Constant Fraction Discriminator 583), delayed (Ortec 425A) and was fed into TAC as a start pulse of TCSPC. Since TAC converts the time interval between the start and stop pulses into output pulse amplitude, the pulse-height distribution of the output of TAC gives the time profile of the photon-detection probability by the photomultiplier. The output pulse was analyzed by a multichannel analyzer (Canberra series 35-plus) and then transmitted to another personal computer. Out-

put pulses from the photomultiplier were also counted by a gated photon counter (Stanford Research SR400) and then were collected by the computer PC2. This *non-time-resolved* counts are also used as experimental data, which will be described in the later section.

3.2 Sample preparation

3.2.1 Chlorophyll b

We employed chlorophyll b as a dopant molecule for most of the molecular glasses we investigated because of its advantages compared with other dyes [52-56].

Chlorophyll b has a similar structure to other chlorins including chlorin-e_6 and bacteriochlorins. A chlorin ring which is commonly contained in these chlorin-type molecules is one of variations of a porphyrin ring, where one of tetrapyrroles of porphyrin ring which causes the large π-electronic system is oxidized. Chlorophyll b is characteristic in comparison with other chlorins with respect to a long hydrocarbon side group and a cyclopentanone ring which coexists with a chlorin ring as a part of the π-electronic system.

It should be noted that chlorophyll b has a solubility into alcoholic solvents, which cannot usually be seen in porphyrins without any hydrophilic side groups. It may be interpretable as the effect of hydrogen-bonds between the alcoholic molecules and the oxygen atom in a cyclopentanone ring of chlorophyll b. In addition, chlorophyll b is also soluble into benzene and alkylbenzenes such as toluene and isopropylbenzene, which can be roughly explained if we consider that the polarity of chlorophyll b is not so high compared with other chlorins due to the long hydrocarbon side-group. Chlorin ring itself has a centro-asymmetric structure as described above and hence is polar by nature, which enables us to explain the insolubility of chlorins to benzene and alkylbenzenes. In the case of chlorophyll b, however, its polarity might be canceled by the existence of the large nonpolar side-group. This may explain why chlorophyll b has a solubility to nonpolar solvents.

We conclude that chlorophyll b is especially suitable for our aim of re-

search to investigate the low-frequency dynamics of glass-forming liquids because of its solubility in a variety of organic solvents.

Chlorophyll b (CAS no.519-62-0, MW=907.51) was extracted from leaves of spinach. Detailed procedure of extraction of chlorophyll b is described elsewhere and hence is omitted in this article. Chlorophyll b was employed not only as solute of organic solvents but also as that of polystyrene matrix.

A great care should be taken to handle chlorophyll b molecule because of its extremely high light-sensitivity in the solution form. For example, hydroxylic solution of chlorophyll b can be completely bleached within several hours under the daylight. Chlorophyll b was dissolved into various solvents in the dark. The solution was bubbled with a nitrogen gas, tightly sealed, and stored in the dark.

3.2.2 Other dyes and polymer samples

Because chlorophyll b cannot be used as a dopant of sol-gel inorganic matrices due to the irresistibility to an acid condition and some of organic polymers due to insolubility to them, alternatives of chlorophyll b have to be chosen for these applications.

Zn-phthalocyanine (ZnPc) was particularly selected only for the dopant of poly(butyl acrylate) (PBA, Aldrich), because most of dyes, whose electronic states are known to be weakly coupled to the host vibrations, could not be dispersed successfully into PBA.

Oxazine 4 perchlorate was one of the best choices for the dopant of sol-gel-derived matrices because it has a fairly high heat- and acid-resistibility and a weak electron-phonon coupling strength. Although free base porphyrins might be also incorporated into sol-gel matrices, they are known to coexist as a dication form (H_4P^{+4}) and a neutral form (H_2P) in inorganic

gels, which are possibly caused by the residual silanol groups remaining unreacted in gels. In the case of metal-substituted porphyrins, on the other hand, they cannot be dispersed into gel matrices as their original forms because the metal atoms in them tend to be removed under the acid condition required for gelation process. Oxazine 4 was also used as a dopant of poly(vinyl butyral) (PVB, purchased from Nakarai Tesque). ZnPc and oxazine 4 were purchased from Aldrich and Eastman Kodak, respectively. Mg-octaethylporphyrin (MgOEP) was employed as an alternative dopant of chlorophyll b into nonpolar molecular glasses. MgOEP (CAS no.20190-35-4, MW=557.09) was prepared by a variant of the method by Fuhrhop and Mauzerall.

Molecular structures of all of the dye molecules we employed are shown in Fig.3.

Dye-doped polymer samples were prepared by mixing dye solutions with polymer solutions, casting them onto glass plates and drying them in the dark for several days. Colored transparent films were finally obtained with an optical density of $\sim$1.0 at the absorption maximum.

In the case of poly(butyl acrylate) (PBA), however, its glass transition temperature is lower than the room temperature and hence it exhibits a highly viscous liquid. Therefore, dye-doped PBA was put directly onto the slide glass and used as a sample.

Chemical structures of organic polymers we used as samples are shown in Fig.4.

3.2.3 Sol-gel method

Chromophore-doped inorganic gels were prepared by a so-called *sol-gel* technique. This novel technique enables one to make an inorganic glass at room temperature from the alkoxide solution via hydrolysis and polycon-

densation processes. Incorporation of organic dye molecules into inorganic host matrices has not been achieved due to heat-irresistibility of organic dyes until the sol-gel method was developed. Much attention has been paid on both the basic property and possibility for applications of sol-gel derived inorganic and organic-inorganic hybrid glasses in the last decade.

The procedure of sample preparation by the sol-gel method is as follows. To begin with, the initial solution containing tetraethoxysilane (TEOS), tetraisopropoxytitanate (TPOT) (only used for SiO_2–TiO_2 bicomponent gel), ethanol and oxazine 4 perchlorate were mixed and stirred by a magnetic stirrer for an hour. This mixed solution was kept at about 75°C, near the boiling temperature of ethanol, under reflux. Alkoxides TEOS and TPOT were purchased from Nakarai Tesque. Next, the mixed solution was still continuously stirred while pouring 0.1N hydrochloric acid quite slowly as an acid catalyst for hydrolysis reaction. The solution was stirred one more hour after finishing adding the acid and then poured into a polystyrene container. After heating it up to 70°C to evaporate ethanol and water for 20 days, finally we obtained a dried transparent gel whose optical density is about 1.0 at the absorption maximum in the visible region.

The molar ratio of materials for preparing our samples is listed in Table.1.

^{1}H-NMR spectroscopy has revealed that, in acid-catalyzed sol-gel reaction, linearly linked siloxane (≡Si–O–Si≡) chain grows in the mixed solution, which seems to be considerably different from the case of fused silica with a dense, three-dimensional linkage [80].

3.2.4 Molecular glasses

Glass-forming solvents we investigated can be divided into three groups, alcohols, alkylbenzenes and alkanes.

Alcohols

Rigid structure due to hydrogen bonds between hydroxyl groups of individual molecules is possibly expected in alcoholic glasses. It can also be considered that the structures of alcohol glasses with two or three hydroxyl groups are more rigid and network-like compared with that of monohydroxyl alcohols. This structural difference may be also reflected on the difference of the glass transition temperature (T_g) and the accessibility to a glassy state. Alcohols with m-hydroxyl groups (m=2,3) and the number of carbons $n(C)$=3 are highly viscous even at room temperature and have relatively high T_gs (160$\leq T_g \leq$180). Glassy states of these alcohols can be quite easily obtained even under moderate cooling rate [3,4].

In contrast, monohydroxylic alcohols with $n(C)$=3 or 4 have lower viscosity at room temperature and lower T_g (100$\leq T_g \leq$140 in most cases) than those for multi-hydroxylic alcohols [5, 29]. To our knowledge, the glassy states for monohydroxylic alcohols can be obtained under the quick quenching in the case of 3$\leq n(C) \leq$6. On the contrary, it is much difficult to obtain a uniform glassy state for alcohols with $n(C) \leq$2 or $n(C) \geq$7 where polycrystallization occurs even under quick quenching and snow-like solids are obtained.

Alcoholic solvents, 1-propanol, 2-propanol, 1-butanol, 2-butanol, propylene glycol, trimethylene glycol and glycerol are all purchased from Nakarai Tesque and used as solvents of our samples without further purification and dehydration treatment. These alcohols are selected with respect to its small $n(C)$(=3 or 4), low glass-transition temperature (100K$\leq T_g \leq$160K

in most cases) and variation of the number of hydroxyl group m contained in a single molecule (m=1 for propanols and butanols, m=2 for two glycols and m=3 for glycerol).

A small content (less than 1%) of residual water might be involved in these alcoholic solvents without any dehydration treatment. Renge suggested that water molecules have higher ligation efficiency to the magnesium atom centered in a chlorophyll molecule than that of alcoholic molecules [69]. A doubt may arise if the WDOS profiles of chlorophyll b-doped alcoholic solvents are not determined by the alcoholic solvent molecules themselves, but merely by the small amount of water molecules which are effectively ligated to the chlorophyll molecule.

Such a problem, however, is not supposed to be so serious in the case of our aim of research, because the low-frequency vibrations we are looking into are caused not by the motion of a single solvent molecule but by that of the structure containing a number of solvent molecules located around the dye molecule [72]. The variety of the peak frequency of WDOS for frozen alcohol solutions, described in the later sections, clearly shows the validity of the above discussion.

Alkylbenzenes and alkanes

In contrast with the rigid structure in alcoholic glasses, a more fragile structure caused by the weak Van der Waals intermolecular forces may be formed in alkylbenzenes and alkanes.

Benzene itself is never vitrified even under the fastest quenching, while benzene derivatives with side groups of hydrocarbons, which are called alkylbenzenes, are vitrifiable under a certain cooling condition [5].

Alkanes are also known to be polycrystalized with some exceptions under the normal cooling conditions. n-alkanes with $n(C) \geq 6$ form semi-crystalline phases by fast cooling, which are called *Spol'skii* matrix [52,

53]. Some of alkanes with side branches, on the other hand, can be vitrified with fast quenching, which may be caused by the steric hindrance effect of these branched molecules.

Benzene, toluene, isopropylbenzene and 3-methypentane were used as solvents in this work which are all purchased from Nakarai Tesque.

The molecular structures of organic solvents we employed are listed in Fig.5. Parameters such as molecular weights and glass transition temperatures for these solvents are also listed in Table.2 [4, 5, 29, 31].

Chapter 4

Results and discussion

4.1 Conventional spectroscopy in dye-doped molecular glasses

In this section, we show results of the stationary absorption and off-resonantly excited fluorescence spectra for dye-doped molecular glasses. Absorption spectra for these systems are more complicated than that for doped polymers, which is supposed to be caused by the variety of local configuration around each dye molecule in the glassy state. These systems are also useful in examining the spectral change accompanied by the glass transition because the glass transition temperatures of them are far below the ambient temperatures and therefore the spectroscopic research can be easily performed for both fluid state and glassy state.

4.1.1 Chlorophyll b-doped alcoholic solutions

Fig.6 shows the absorption spectrum of chlorophyll b-doped 1-butanol, 2-butanol and 1-propanol solutions at 300K and 4K. All these solvents are in fluid states at 300K and in glassy states at 4K. Absorption spectra for these solutions at room temperature are almost identical with one another, which have Gaussian-like Q_y-bands with peak wavelengths of about 6480Å and Soret bands (B bands) with those of 4670Å[69]. At 4K, however, the shape of Q_y-band in each frozen solution varies with one another and is not

Gaussian-like. Two Gaussian components with peak wavelengths of 6580Å and 6620Å whose intensity ratio varies with each alcoholic solvent, may contribute to the unusual shapes of Q-bands at 4K. This shape function is supposed to appear by the splitting of the energy level in the lowest excited state due to the different configuration of the surrounding frozen solvent molecules, which is caused during the process of vitrification.

We should mention the possibility that chlorophyll *dimers* in frozen solvents might cause the additional band in the Q_y band region. The dimer band was found also in the lower energy side of monomer band in chlorophyll *a*-doped polystyrene film [74] and n-hexane solution with a high dopant concentration more than 10^{-3}M [81]. In our case of frozen alcoholic solution, however, the dopant concentration is sufficiently low. And more, such an additional band does not appear at room temperature in our case. Therefore, it is quite hard to consider the possibility of the existence of chlorophyll dimers. In conclusion, we may be able to say that the origin of the lower band in our case is not the chlorophyll dimers but the splitting of energy levels due to the difference in local configuration of solvent molecules.

Temperature dependence of Q-band absorption

It is also remarkable in Fig.6 that the peak energies of both Q_y and Soret absorption bands shift to the lower energies with decreasing temperature. This temperature-dependence in the absorption band could only be seen in the fluid state. In contrast, absorption spectra obtained at various temperatures below T_g were fairly identical for all of the alcoholic glasses doped with chlorophyll b we investigated. This can be well interpreted by considering the temperature dependence of the site-energy distribution function. The site-energy of each dye molecule is different from one another due to the difference of local configuration of solvent molecules. Each

configuration is supposed to be completely *frozen* at glassy state below T_g, which may cause the site-energy distribution.

Temperature dependence of the absorption maximum energy at fluid state is then roughly estimated by the polarity of both solvent and solute molecules and by the temperature-dependence of the refractive index of host matrices. As a matter of fact, the peak shift to lower energy with decreasing temperature was also found in the case of toluene-benzene-mixture doped with chlorophyll-b and also in 3-methylpentane doped with octaethylchlorin (OEC), while the reverse temperature-dependence, namely, the peak shift to higher energy with decreasing temperature, was found in 3-methypentane doped with Mg-octaethylporphyrin.

When we calculate the resonance fluorescence spectra at temperatures higher than 4K by employing WDOS spectrum obtained at 4K, the determination of site-energy distribution function is always required at every temperature. The site-energy distribution function obtained at 4K was, however, also applied for calculation at temperatures higher than 4K in accordance with the discussion shown above.

Fluorescence spectra and site-energy distributions

Absorption and ordinary fluorescence spectra at 4K for chlorophyll b-doped alcoholic glasses are superimposed in Fig.7. In contrast with the case of absorption spectra shown above, fluorescence spectra obtained for the doped glasses resemble with one another with a peak wavelength of $\sim$6710Å .

Although it remains unclear why such a similarity appears only in the fluorescence spectra, it might possibly be explained by assuming the low quantum yield of the higher energy part of the Q_y absorption band.

Ordinary fluorescence spectra were obtained using 5145Å line of an Ar^+-ion laser as the excitation light. These fluorescence spectra have been

corrected for the reabsorption effect as follows:

$$F_T(\omega, \omega_L) = \frac{A_T(\omega_L) + A_T(\omega)}{1 - 10^{-[A_T(\omega_L)+A_T(\omega)]}} F'_T(\omega, \omega_L), \tag{4.1}$$

where $F'_T(\omega, \omega_L)$ and $F_T(\omega, \omega_L)$ represent the fluorescence spectra before and after the correction respectively, and $A_T(\omega)$ is the optical density at ω.

When we employ 5145Å line as the excitation light of chlorophyll-doped glasses, it can be considered that all of the chromophore molecules are off-resonantly excited and therefore all sites in the site-energy distribution uniformly contribute to the ordinary fluorescence spectrum as follows:

$$F_{ord}(\omega) \propto \int G(\omega')\omega^3 f_T(\omega - \omega')d\omega'. \tag{4.2}$$

Accordingly, the shape of the higher energy side of $F_{ord}(\omega)$ can be regarded as the shape of the higher energy side of the site-energy distribution if the electron-phonon coupling is sufficiently weak and the contribution of the phonon sideband in $f_T(\omega - \omega')$ is small.

On the other hand, since the absorption spectrum of chromophores incorporated in the solid-state materials is described as

$$A(\omega) \propto \int G(\omega')\omega a_T(\omega - \omega')d\omega', \tag{4.3}$$

the shape of the lower-energy side of the absorption spectrum $A(\omega)$ corresponds to the lower-energy side of the site-energy distribution in the case of systems with weak electron-phonon coupling.

In conclusion, the site-energy distribution function $G(\omega')$ can be estimated as the shape of the overlapped area between the absorption and off-resonance fluorescence spectra.

In Fig.7, Gaussian functions fitted both for the higher energy side of $f_T(\omega)$ and for the lower energy side of $a_T(\omega)$ are shown together with absorption and fluorescence spectra. Although being a rough estimation,

this can reproduce fairly well the experimentally obtained site-energy distribution in most cases. Examples will be shown in a later section.

Furthermore, thus obtained Gaussian functions for these samples resemble quite well with one another with respect to both the bandwidth and the peak energy, which reveals that the distribution of site-energy at frozen state does not apparently depend on the species of solvent molecules themselves.

4.1.2 MgOEP-doped non-alcoholic glasses

Fig.8 shows the absorption spectra of MgOEP-doped isopropylbenzene and 3-methypentane obtained at 300K and 4K.

The absorption spectra at room temperature resemble with each other and also are quite similar with those obtained for MgOEP-doped polymers [61]. They have two bands in the visible region with their peak wavelengths at 5800Å and 5430Å , which correspond to the lower $Q(0,0)$ band and the higher $Q(1,0)$ vibronic band, respectively.

The absorption spectra at 4K, however, have more complicated profiles than those obtained at room temperature. It is particularly noteworthy that the lowest $Q(0,0)$ band splits into two bands for MgOEP-doped 3-methylpentane glass at 4K.

Fluorescence spectra of these samples at 4K are shown together with absorption spectra in Fig.9. The additional fluorescence band, which appears as a shoulder at the lower energy side of the original fluorescence band in the case of isopropylbenzene, can be seen more clearly in 3-methylpentane doped with MgOEP, whose intensity is almost the same as the main band.

To clarify the origin of the additional fluorescence band, we measured the site-selective fluorescence spectra at various site-energies, which are shown in Fig.10. When we excited mainly the higher part of the split lowest energy band (site(a) in Fig.10), the fluorescence spectrum has only a

phonon-sideband, which means that the site-selectivity at this site-energy was fairly good. In contrast, the site-selective fluorescence spectra with the excitation energies (b) and (c) contain additional bands, which appeared at around 5880Å for both cases. Such a non-site-selectivity of these fluorescence bands means that their origin is the fluorescence from the off-resonantly excited molecules. More careful observation of Fig.10(c), however, reveals that the resonantly (site-selectively) excited component remains to a certain content in the fluorescence spectrum obtained by lower-energy band excitation, which means that the site-selectivity exists in the lower-energy band. This result is also confirmed by the measurement of the distribution of the zero-phonon intensity shown in Fig.11, which clearly indicates that the site-energy distribution has two peaks. The origin of such a splitting of the site-energy distribution is unknown at this stage.

4.2 Site-selective excitation spectrum

Site-selective fluorescence spectrum can be obtained as simply as the conventional off-resonant fluorescence spectrum by scanning the wavelength of the monochromator under the irradiation of laser light with a fixed wavelength. This technique, however, can be applied only to the limited cases of host-guest systems which have an extremely low hole-burning efficiency. Most of dye-doped disordered systems we employed as samples in this work, however, have a relatively high non-photochemical hole-burning efficiency due to the local rearrangement of the host matrices even at low temperatures. Consequently, we employed the site-selective *excitation* spectroscopy to determine WDOS for our samples instead of the site-selective fluorescence spectroscopy. This novel technique can be performed by scanning the wavelength of the tunable laser for excitation and detecting fluorescence at a fixed wavelength.

As a preliminary experiment, we employed a polychromatic measurement for site-selective *fluorescence* spectroscopy by employing a liquid N_2-cooled-CCD detector and a triple-grating monochromator. This multichannel measurement has a great advantage that the exposure time can be established to be much shorter than that in the case of a monochromatic measurement. Because the fluorescence spectrum detected via the CCD-multichannel measurement is not time-resolved, it has no means to remove the scattering of the excitation laser light, which makes it much difficult to evaluate the zero-phonon fluorescence intensity required in the analytical procedure to determine WDOS. In the case of polymer samples with excellent optical quality without any strains and cracks, almost all of the scattered laser light might be rejected by using a pair of a polarizer and a cross-polarized analyzer as described previously. In most cases including sol-gel derived inorganic gels and liquid-quenched molecular glasses,

however, a large quantity of randomly polarized scattering light may pass through the polarizer-analyzer pair and may saturate the CCD detector.

Accordingly, we judged that a CCD-multichannel measurement must be inappropriate for our quantitative research.

Fig.12 shows the site-selective excitation spectrum for chlorophyll b-doped propylene glycol glass obtained at 4K. Figs.12(a) and (b) show the time-resolved spectra obtained via the time-to-amplitude converter (TAC) and the non-time-resolved ones via the gated photon counter (GPC), respectively. Both spectra have been corrected for the reabsorption effect using Eq.(4.1). The resonance fluorescence line has a width of about 3cm^{-1}, which is determined by the system resolution and is considered to be much broader than the homogeneous linewidth determined by the dephasing process. As shown in Fig.12(c), the shapes of the phonon-sideband components in these spectra coincide with each other, which indicates that these two spectra are equivalent to be employed for the numerical analysis. In contrast, the relative intensity of the resonance line ($\omega_L = \omega$) obtained via GPC is much larger than that obtained via TAC, which clearly indicates that the scattered laser light contained to a great content in the spectrum obtained via GPC is highly suppressed in the spectrum via the time-correlated single-photon counting method. This can be also recognized in Fig.13, which shows the time profiles of the excitation laser pulses and the zero-phonon fluorescence. As shown in Fig.13, fluorescence lifetime of a dye molecule in a glassy matrix is of the order of nsec which is comparable with the pulse interval. We can see here that only the photons which come after the end of the excitation laser pulses are selectively counted via the time-correlated single-photon counting. It goes without saying that the non-time-resolved fluorescence-excitation spectrum has a great advantage with respect to the signal-to-noise ratio which

is required for obtaining WDOS spectrum with an excellent quality, while the time-resolved measurement is needed to determine the intensity of the zero-phonon fluorescence line.

Therefore, we have decided to use time-resolved spectrum for the zero-phonon resonance line and non-time-resolved spectrum for the phonon-sideband.

The phonon-sideband part of the site-selective excitation spectrum shown in Fig.12 contains not only the resonantly excited component but also the off-resonantly excited one because of the large inhomogeneous broadening of the transition energy of the doped chromophores.

The shape of the site-selective excitation spectrum can be described as Eq.(2.29) and thereby the site-energy distribution function has to be determined to obtain the single-site spectrum and WDOS. This could be obtained by measuring the zero-phonon fluorescence at various laser wavelengths with fixed power. The laser power used for this measurement is almost the same as that in measuring the full shape of the spectrum as shown above. In most cases including MgOEP and chlorophyll b-doped disordered systems, decrease of zero-phonon fluorescence intensity caused by a hole-burning effect in a short time required only for the measurement of the zero-phonon line is negligible. In the case of oxazine 4-doped disordered systems, however, the non-photochemical hole-burning efficiency is much higher than that of other dyes and the hole-burning effect while measuring the zero-phonon fluorescence intensities is not negligible. Hence in these cases we measured zero-phonon intensities with the laser wavelength scanning just in the vicinity of each detection wavelength, which is considered to be one of variations of the site-selective excitation spectroscopy.

The site-energy distribution of chlorophyll b-doped propylene glycol obtained for the above-mentioned method is shown in Fig.14 together with

the absorption spectrum both obtained at 4K. The data points were corrected for the reabsorption effect and the instrumental response in the whole detection system. The correction for reabsorption was performed by following the relation

$$G(\omega_L) = \frac{2A_T(\omega_L)}{1 - 10^{-2A_T(\omega_L)}} G'(\omega_L), \tag{4.4}$$

which can be easily derived from Eq.(4.1) by replacing ω with ω_L.

The site-energy distribution $G(\omega')$ should be a smoothly continuous curve in Eq.(2.35) in order to calculate the single-site spectrum $a_T(\omega_L - \omega)$ numerically. In Fig.14 we fit the site-energy distribution with the Gaussian function:

$$G(\omega_L) = \frac{1}{\sqrt{2\pi\sigma}} \exp\left[-\frac{(\omega_L - \omega_c)^2}{2\sigma^2}\right]. \tag{4.5}$$

We can also successfully fit the site-energy distribution with a single Gaussian function in the cases of other molecular glasses doped with chlorophyll b, while the summation of two or three Gaussian functions must be employed for oxazine-4 doped inorganic gels and a *skewed* Gaussian function is required for MgOEP doped disordered system. The unique shape of site-energy distribution in oxazine 4-doped gels is supposed to arise from the variety of coupling between dyes and host matrices. On the other hand, the skewed shape of site-energy distribution function in MgOEP-doped disordered systems may be caused by the degenerate energy levels of MgOEP.

4.3 Determination of WDOS

4.3.1 Analytical procedure

In this section, we describe the analytical procedure to determine WDOS spectrum numerically from experimentally obtained site-selective fluorescence or fluorescence-excitation spectrum.
When we transform the variables ω_L and ω' in Eq.(2.35) into Ω and Ω' as

$$\omega_L - \omega = \Omega$$

$$\omega' - \omega = \Omega',$$

then we obtain the following equation:

$$F(\omega;\omega+\Omega) \propto (\omega+\Omega)\int G(\omega+\Omega')a_T(\Omega-\Omega')a_T(\Omega')d\Omega'. \tag{4.6}$$

The anti-Stokes component of phonon-sideband in the site-selective fluorescence or excitation spectrum is extremely small due to the small occupation number of phonons at liquid helium temperature and hence is negligible.

When we regard ω as the origin of the shift-energy axis and replace $F(\omega;\omega+\Omega)$ and $G(\omega+\Omega')$ with $\tilde{F}(\Omega)$ and $\tilde{G}(\Omega')$ respectively, Eq.(4.6) is then rewritten as

$$\tilde{F}'(\Omega) = (\omega+\Omega)\int_0^{\Omega} \tilde{G}(\Omega')a_T(\Omega-\Omega')a_T(\Omega')d\Omega'. \tag{4.7}$$

Dividing the area of integration into groups of the small area ϵ as $\Omega = n\epsilon$ and $\Omega' = j\epsilon$ (n, j=1,2,...) and replacing $\tilde{F}'(\Omega)$, $\tilde{G}(\Omega)$ and $a_T(\Omega)$ with $\tilde{F}'_n$, $\tilde{G}_j$ and a_j respectively, then we can derive the summation form of Eq.(4.7) as

$$\tilde{F}'_n = (\omega+n\epsilon)\sum_{j=0}^{n} \epsilon\, \tilde{G}_j a_j a_{n-j}. \tag{4.8}$$

In the case of n=0, Eq.(4.8) can be described as

$$\tilde{F}_0' = \epsilon\omega G_0 a_0 a_0 \tag{4.9}$$

As $\tilde{F}_0'$ and $\tilde{G}_0$ have been obtained experimentally, a_0 can be determined by Eq.(4.9). It should be mentioned that we regard the integral intensity of zero-phonon fluorescence line as $\tilde{F}_0'$, which has a finite bandwidth ($\sim$3cm^{-1} in FWHM) determined by the resolution of the monochromator.

Next in the case of $n = 1$, Eq.(4.8) leads to

$$\tilde{F}_1' = \epsilon(\omega + \epsilon)(\tilde{G}_0 a_0 a_1 + \tilde{G}_1 a_1 a_0). \tag{4.10}$$

Here $\tilde{F}_1'$, $\tilde{G}_0$, $\tilde{G}_1$ are given and a_0 has been already determined in Eq.(4.9), and therefore we obtain a_1 numerically.

$\tilde{F}_2'$ can be determined in a similar way as the case of n=1,2 as follows:

$$\tilde{F}_2' = \epsilon(\omega + 2\epsilon)(\tilde{G}_0 a_0 a_2 + \tilde{G}_1 a_1 a_1 + \tilde{G}_2 a_2 a_0). \tag{4.11}$$

We can finally obtain the single-site spectrum $a_T(\omega')$ as a series of a_j by repeating this procedure shown above.

Fig.15 shows the single-site spectrum of chlorophyll b-doped 1-propanol glass determined via the analytical procedure shown above using the experimentally obtained site-selective excitation spectrum (also shown in Fig.15 as a reference) and the site-energy distribution function described in the preceding section. The Debye-Waller factor, which is the proportion of the intensity of the zero-phonon line to the total fluorescence intensity, can also be determined to be about 0.6.

As shown in Eq.(2.24), the single-site spectrum contains not only 1-phonon contribution but also m(=2,3,...)-phonon contributions. Accordingly, the phonon-sideband spectrum in the single-site spectrum does not directly correspond to WDOS. As seen in Eq.(2.28), the 1-phonon function at 0K $s_0(\Omega)$ can be obtained from the phonon-sideband of the single-site spectrum at 0K Φ_0.

To solve this integral equation numerically, firstly we define new variables as

$$x = \frac{\Omega}{\Omega_0}$$

$$y = \frac{\Omega'}{\Omega_0}$$

$$\tilde{s}(x) = x s_0(x\Omega_0) = x s_0(\Omega)$$

$$\phi(x) = \Phi_0(x\Omega_0) = \Phi_0(\Omega),$$

where Ω_0 is an arbitrary value. Phonon-sideband spectrum $\Phi_0(\Omega)$ should be normalized to the total integral intensity of $1 - \alpha_0'$ before performing the analytical procedure shown below.

We can derive the following equation from the integral equation Eq.(2.28) using these new expression as

$$\tilde{s}(x) = \frac{1}{\alpha_0'}[x\phi(x) - \int_0^x \phi(x-y)\tilde{s}(y)dy]. \tag{4.12}$$

Here we set a boundary condition as $\tilde{s}(0) = 0$ and divide the area of integration into a group of a small area ϵ like $x = n\epsilon$ and $y = m\epsilon$ (n, m=1,2,...). Then we can derive the following relation:

$$\tilde{s}_n = \frac{1}{\alpha_0'}\Big[n\epsilon\phi_n - \sum_{m=1}^{n-1} \epsilon\phi_{n-m}\tilde{s}_m\Big]. \tag{4.13}$$

$\tilde{s}_1$ is determined from Eq.(4.13) in the case of $n = 1$,

$$\tilde{s}_1 = \frac{\epsilon}{\alpha_0'}\phi_1, \tag{4.14}$$

where Debye-Waller factor α_0' has been already determined from the single-site spectrum described above.

In the case of $n = 2$, Eq.(4.13) can be expressed as

$$\tilde{s}_2 = \frac{\epsilon}{\alpha_0'}(2\phi_2 - \phi_1\tilde{s}_1), \tag{4.15}$$

where $\tilde{s}_2$ can be determined from experimentally given ϕ_1 and ϕ_2, and $\tilde{s}_1$ given in Eq.(4.14).

As a consequence, we obtain WDOS $s(\Omega)$ numerically as a series of $\tilde{s}_n$ by repeating the above-mentioned procedure.

In Fig.16 we show the WDOS spectrum together with the single-site spectrum for chlorophyll b-doped 1-propanol glass determined via this analytical procedure using the single-site spectrum.

4.3.2 WDOSs for various systems

Following the analytical procedure described above, we obtained WDOSs for various disordered systems doped with chromophores.

WDOS for dye-doped polymeric systems

WDOS spectra for dye-doped polymeric systems including organic polymers and inorganic gels are shown in Fig.17, where the intensities are normalized with respect to the peak intensities. We found that these WDOS profiles resemble well with one another in spite of a wide variety of host-guest systems we examined, while their peak frequencies are slightly different with one another.

In Table.3 we list the peak frequencies of WDOSs for these samples. The peak frequencies were determined from smooth curves obtained by averaging values of the several adjacent data for each data points of raw WDOS spectra. It is not surprising that the peak frequencies of WDOSs for inorganic gels are comparable to those of organic polymers if we consider that the linearly linked siloxane chains like Si–O–Si or Si–O–Ti–O–Si play an important role in the formation of glass structures as mentioned previously. This structure in gels is supposed to be formed during the gelation process including hydrolysis and polycondensation reaction with

the acid catalysis. This structure seems to be considerably different from that of the fused silica glass with a dense, three-dimensional network of SiO_4, and is rather similar to that in some types of organic polymers where covalently bonded hydrocarbon chains are responsible for these structures.

Peak frequencies of WDOSs for various organic polymers which were determined in the previous work are also listed in Table 3 as references. It can be found that the peak frequency of WDOS for poly(vinyl butyral) is fairly higher compared with other polymers. This might indicate the rigid network in PVB caused by the interchain coupling via the hydrogen bonds between residual hydroxyl groups contained in the PVB chains.

Noticing the similarity in the shapes of WDOS spectra, we superimpose them in Fig.18 where each frequency is rescaled by dividing frequencies by each peak frequency listed in Table.3. Surprisingly, these coincide with one another within the experimental or analytical errors, which indicates that the WDOS profiles for dye-doped polymeric disordered systems we investigated can be commonly described as a *universal* function curve.

Fig.19 shows the similar plot for WDOS spectra of MgOEP-doped polymers obtained previously [63]. We found here that all of the rescaled WDOS spectra for doped polymers also coincide with one another and furthermore, trace the universal curve which has been obtained in this work.

We may conclude from these results that the universal curve actually exists in WDOS profiles of a wide variety of polymeric disordered systems doped with chromophores.

WDOS for dye-doped monomeric systems

Figs.20 and 21 show the WDOS spectra for dye-doped alcoholic glasses and non-alcoholic glasses, respectively. Almost all of WDOS spectra shown in two figures are fairly similar with one another and also similar with those

obtained for doped polymeric systems shown above. WDOS obtained for 3-methylpentane doped with MgOEP, however, might be one of the exceptions, which has a broad hump in the region from $50cm^{-1}$ to $100cm^{-1}$.

In addition, two distinct peaks can be seen at around $170cm^{-1}$ and $270cm^{-1}$ in Fig.21 for isopropylbenzene and 3-methylpentane both doped with MgOEP, which are possibly assigned to the *intramolecular* vibrations of MgOEP because the shift frequencies of these peaks are fairly identical with each other in spite of the difference of host molecular glasses.

Peak frequencies of WDOSs for dye-doped molecular glasses are listed in Table 4.

We notice in this table that WDOS for various doped molecular glasses employed in this work can be classified into two groups: one group with a higher peak frequency at around $25cm^{-1}$ and the other with a lower peak frequency at around $18cm^{-1}$.

Among others, peak frequencies of WDOSs for dye-doped glycerol and 3-methylpentane are particularly higher compared with those for other molecular glasses. Glycerol has three hydroxyl groups and hence may form a network structure or large clusters via the hydrogen bonds between hydroxyl groups of adjacent molecules, which is supposed to be one of the reasons of high peak frequency. Relatively high peak frequencies of WDOSs for alcohols with two hydroxyl groups, propylene glycol and trimethylene glycol ($25cm^{-1}$ for both) may be interpreted by the similar concept as shown above.

On the contrary, the high peak frequency cannot be explained simply by the same concept in the case of dye-doped 3-methylpentane because it has neither hydroxyl groups nor other functional side groups, and hence only the weak Van der Waals intermolecular forces between each molecules may play a role in forming the glassy structure in this case.

With respect to monohydroxylic alcohols, two *n*-alcohols, 1-propanol

and 1-butanol, are involved in the group with higher peak frequencies while the other two *iso*-alcohlos are involved in the group with lower peak frequencies. We assume that such a difference in the peak frequency of WDOS is caused by the presence or absence of the steric effect of alcoholic molecules, which is discussed later again.

Two alkylbenzenes, toluene-benzene-mixture and isopropylbenzene are involved in the group with lower peak frequencies, which might be interpreted in terms of randomly oriented benzene rings roughly determine the structure of the glassy state while the side groups, methyl group for toluene and isopropyl group for isopropylbenzene, do not play an important role in glass formation. It also means that the steric effect in isopropyl side-group is not responsible for determining the local structure of the glass.

The similar plots as shown in Fig.18 for polymeric systems are also performed for dye-doped alcoholic and non-alcoholic molecular glasses in Figs.22(a) and (b) respectively. Almost all the rescaled WDOSs for alcoholic glasses coincide with one another as clearly seen in Fig.22(a), while 1-propanol and 2-propanol are exceptions. With respect to the non-alcoholic glasses in Fig.22(b), the difference of shapes of rescaled WDOSs between 3-methypentane and two alkylbenzenes is apparently observed.

It is quite surprising that all profiles for molecular glasses we investigated except for propanols and 3-methypentane trace the universal curve obtained for polymeric disordered systems, which indicates clearly that the universal curve holds not only for polymeric systems but also for monomeric ones.

It remains unsolved at this stage, however, why the exceptional profiles of WDOSs are observed for two propanols and 3-methypentane as shown above.

Solvent shell of alcoholic glasses

Let us look more closely at WDOS obtained for alcoholic glasses doped with chlorophyll b molecules.

Considering that our results on WDOSs for alcoholic glasses are inconsistent with those obtained from the Raman scattering spectroscopy as mentioned above, it might be considered that what our site-selective fluorescence-excitation spectroscopy observes is not equivalent with the low-frequency dynamics of *bulk* matrix observed by Raman scattering spectroscopy. The electronic state of doped chromophore can *feel* dynamics on the local structure of solvent molecules which are located in the vicinity of the chromophore. If the glassy structure around the chromophore is determined by the particular coupling between the solvent molecules and the chromophore, the solvent *shell* which has a different structure from the bulk glass might be formed.

Pack and co-workers [73] proposed a *solvation shell* model to explain the anomalous behavior of spectral diffusion in resorufin-doped ethanol glass probed by the photon echo experiments. According to their concept, a *shell* structure of solvent molecules might be formed in the vicinity of the chromophore, which has a higher degree of order than that of the outer part of the solvent shell. Such a highly ordered structure may be induced by the electronic structure of the dye molecule itself.

Although the origin of the formation of the solvent shell remains unclear, the particular ligation form of solvent molecules to the chlorophyll, as proposed by Renge [69], may be one of the possible reason, which will be discussed in the following section.

4.3.3 Universality of WDOS

We have found the universal profile of *weighted* vibrational densities of states (WDOS) $s(\omega)$ which can be applied not only to polymeric disordered materials but also to monomeric molecular glasses. It should be mentioned here that thus obtained WDOS s(ω) contains two contributions; the actual density of vibrational states $g(\omega)$ and the vibrational frequency dependence of the coupling coefficient with the electronic states of doped chromophores $\xi(\omega)$, as shown in Eq.(4.16):

$$\begin{aligned} s(\omega) &= \sum_{\lambda} {\xi_\lambda}^2 \delta(\omega - \omega_\lambda) \\ &= \xi(\omega) g(\omega). \end{aligned} \tag{4.16}$$

We have shown in the preceding subsection that the universal profile is found for a considerably wide variety of dye-doped disordered systems. It apparently suggests that we should examine the possibility of the universality for both $g(\omega)$ and $\xi(\omega)$.

Let us review again the wide variety of host-guest systems we employed.

Firstly we consider the variety in disordered host materials. Organic polymer including PBA, PVB and those investigated previously [63] have a rigid medium-range structure due to covalently bonded hydrocarbon chains. Inorganic gels obtained via the sol-gel method are characterized by the linearly-linked siloxane chain and the interchain coupling, which seems to be somewhat similar to those of organic polymers. In contrast with these polymeric systems, molecular glasses are considered to have more fragile structures which are mainly based on clusters containing several molecules. Alcoholic glasses are relatively rigid compared with other molecular glasses which have hydrogen bond-based clusters or network structures. Non-alcoholic molecular glasses without any hydroxyl groups including alkylbenzenes and alkanes are supposed to be vitrified only due to the weak Van der Waals intermolecular forces and hence are expected

to be more *fragile* than alcoholic glasses.

As seen above, we have examined both *polymeric* materials (polymer and inorganic gels) and *monomeric* ones (alcoholic/nonalcoholic molecular glasses). Nevertheless, the shape of the obtained WDOS for these host materials hardly depend on the polymericity of them. It may suggest the universality of $g(\omega)$ for various types of disordered materials.

Secondly, we should mention the variety of incorporated chromophores. Oxazine 4 incorporated in sol-gel matrices and in PVB is a cationic dye. Namely, it is polar and hence has a permanent dipole moment in the electronic ground state. Porphyrin-type macromolecules, chlorophyll b, MgOEP and Zn-phthalocyanine are much less polar than oxazine 4 due to its centrosymmetric or quasi-centrosymmetric molecular structures, which means that they have no permanent dipoles but may have induced dipoles. Accordingly, the variety lying in the polarity of doped dye molecules leads to the variety of the type of electron-vibration interaction such as dipole-dipole, dipole-induced dipole interactions.

We may conclude from the above discussion concerning the variety of host materials and polarity of chromophores that the universal function of WODS is possibly composed of the universal function of vibrational density of states $C(\omega)$ and that of the coupling coefficient $\xi(\omega)$.

The universality of coupling coefficient $\xi(\omega)$ is expected to be derived from the theoretical models of electron-phonon interaction. Several theoretical models have been proposed so far [42-51], which enable us to interpret the temperature dependence of the homogeneous linewidth. Unfortunately, however, there is no theoretical work concerning the frequency dependence of coupling coefficient $\xi(\omega)$. To our knowledge, the electron-vibration coupling coefficient has been assumed to be frequency-independent even in latest theories.

The universal profile of density of vibrational states $g(\omega)$, on the other

hand, has been frequently discussed so far with respect to the geometrical characteristics of disordered materials [11,13] and superlocalized vibrations on the strongly disordered network [82, 85]. Some of these theoretical models will be reviewed more carefully in Section 5.

Finally, we should mention the WDOS spectrum obtained for a chromoprotein.

In Fig.23, the WDOS spectrum of Zn-protoporphyrin-substituted myoglobin (Zn-Mb) rescaled using the peak frequency (25cm^{-1} in this case) is shown together with those for three glassy systems [87]. It indicates that the WDOS spectrum for Zn-Mb deviates from those for other systems just above the peak frequency, while an pronounced peak at $E/E_{max} = 5$ can be assigned to the intramolecular vibration of Zn-protoporphyrin IX. This deviation may arise from the difference of the structure between proteins and amorphous systems.

A protein can be regarded as a kind of disordered material in a sense because it contains polypeptide chains. However, in contrast with the case of usual disordered systems involving inorganic glasses, organic polymers and liquid-quenched glasses whose structures cannot be determined uniquely, one can obtain information on structures of proteins by X-ray diffraction measurements. This advantage makes it possible to perform computational experiments on the density of states of the low-frequency vibrational modes for real proteins such as a normal-mode analysis and a molecular dynamics simulation. These works have revealed so far that the possible origin of the low-frequency vibrational modes in proteins is the collective motion extending to almost of all containing atoms such as the so-called *accordion* motion of an α-helix.

We believe that comparisons between DOSs of low-frequency vibrations in proteins obtained from the spectroscopic technique such as inelastic

neutron scattering and that from the computational approach will shed new light on the concept of the low-frequency dynamics in various kinds of disordered materials [?].

4.4 Comparison of WDOS, Raman and neutron scattering spectra

4.4.1 Raman scattering and inelastic neutron scattering

Low-frequency dynamics in disordered materials has been examined by employing the inelastic neutron scattering and Raman scattering spectroscopy.

Inelastic neutron scattering spectroscopy is superior to Raman scattering spectroscopy in several points to investigate the low-frequency dynamics in disordered materials. One of these advantages is that the *real* density of states of vibrational modes can be obtained by means of this experimental technique if all of the scattering events are assumed to be completely incoherent with one another. In addition, this technique does not require an optical transparency at all and thereby powder or flake materials can be included in objects of study. Furthermore, information on both q- and ω-space can be obtained in this spectroscopy, because a neutron scattering occurs while preserving the total energy and the total momentum. It has an disadvantage, however, that it is quite difficult to obtain data with good signal to noise ratio even for an extremely long accumulation time.

The low-frequency Raman scattering, on the other hand, is superior to the neutron scattering spectroscopy with respect to the excellent data quality. It is also advantageous to investigate vibrational behavior in the extremely low-frequency regime below 10cm^{-1} by employing a double- or triple-grating monochromator.

The absence of translational symmetry or long-range order in disordered materials relaxes the selection rule in light scattering so that all of the low-frequency vibrational modes in the Brillouin zone participate in the first-order Raman scattering [32]. Shuker and Gammon suggested that Raman scattering intensity at low-frequency region could be described as

$$I_{RS}(\omega) \propto C(\omega)g(\omega)(1+n(\omega))/\omega, \tag{4.17}$$

where $C(\omega)$, $g(\omega)$ and $n(\omega)$ represent the light-to-vibration coupling coefficient, vibrational density of states and the Bose-Einstein occupation number, respectively. *Reduced* Raman scattering spectrum is frequently used from Eq.(4.17) as

$$\begin{aligned} I_{red}(\omega) &\propto I_{RS}(\omega)/(1+n(\omega)) \\ &\propto C(\omega)g(\omega)/\omega. \end{aligned} \tag{4.18}$$

In most cases of disordered materials, reduced Raman spectra obtained at various temperatures below the glass transition temperature are nearly identical with one another in the low-frequency region, which clearly indicates that the low-frequency vibrational excitation modes can be regarded as the *Boson* excitation. This is why the characteristic peak commonly appeared in the low-frequency region of Raman spectra is usually called a *Boson peak.*

As shown in Eq.(4.18), even the *reduced* Raman scattering spectrum does not directly reveal the *real* DOS $g(\omega)$ but contains the coupling coefficient $C(\omega)$. We conclude that DOS $g(\omega)$ can never be obtained from Raman scattering spectroscopy by itself.

Recently, Sokolov and coworkers compared the inelastic neutron scattering spectra $I_{INS}(\omega)$ and the Raman scattering spectra $I_{RS}(\omega)$ for a-SiO_2, poly(styrene)(PS) and poly(butadiene)(PB) in the low-frequency region [8, 7]. They found from this comparison that these two spectra were connected with each other by the following relation:

$$\frac{I_{INS}(\omega)}{\omega^2} \propto \frac{I_{red}(\omega)}{\omega^2} \qquad \text{at} \qquad \omega > \omega_{max}, \tag{4.19}$$

where ω_{max} is a boson peak frequency.

From Eqs.(4.18) and (4.19), $C(\omega)$ can be determined as

$$C(\omega) \sim \omega \qquad \text{at} \qquad \omega > \omega_{max}. \tag{4.20}$$

Eq.(4.20) holds in all of the investigated disordered systems, and accordingly we conclude that thus obtained $C(\omega)$ is universal for all of disordered materials. It should be noted that this $C(\omega)$ was determined experimentally without any theoretical assumptions. Sokolov also arrived at the same conclusion from the comparison of Raman scattering spectra and data from the heat capacity measurement [10].

This $C(\omega)$ behavior cannot be explained by the theoretical models previously proposed for the low-frequency dynamics in disordered materials. For example, frequency-dependence of light-vibration coupling coefficient is not considered at all in soft-potential model [23-27] or dipole-induced-dipole scattering model where the second order Raman scattering is assumed, and $C(\omega) \propto \omega^2$ for damped acoustic plane-wave model [8, 10]. Fracton model proposed by Alexander [34-36] suggests

$$C(\omega) \propto \omega^{\frac{2\tilde{d}}{D}}, \tag{4.21}$$

where $C(\omega) \propto \omega$ holds only under the assumption of the ideal linearly-linked polymer ($D = 2$ and $\tilde{d} = 1$ following his description).

4.4.2 Comparison of WDOS with Raman/neutron data for polymers

As described above, WDOS means the vibrational density of states *weighted* by the electron-vibration coupling strength; i.e.,

$$s(\omega) \propto \xi(\omega) g(\omega). \tag{4.22}$$

Because the vibrational density of states $g(\omega)$ can be obtained directly from the inelastic neutron scattering measurement, $\xi(\omega)$ might be determined from the comparison between WDOS and the neutron scattering spectrum. Moreover, if we assume the relation Eq.(4.20) for Raman spectroscopy, $\xi(\omega)$ can also be determined from the comparison between WDOS and Raman spectrum.

In the present subsection we compare WDOS spectra obtained in our previous work [61-65] with Sokolov's experimental results of inelastic neutron scattering and Raman scattering for organic polymers [8] and Kanaya's results of neutron scattering only for PMMA [1]. This comparison was made for three organic polymers, poly(styrene)(PS), poly(methyl methacrylate)(PMMA) and poly(butadiene)(PB).

In Figs.24, we plot WDOS spectra together with $g(\omega)/\omega^2$ obtained by neutron scattering and $I(\omega)/\omega(n(\omega)+1)$ and $I(\omega)/\omega^2(n(\omega)+1)$ by Raman scattering in both-logarithmic scale. All of these WDOSs were obtained by employing Mg-octaethylporphyrin as a dopant. First of all, we can see in these figures that $I(\omega)/\omega^2(n(\omega)+1)$ coincides with $g(\omega)/\omega^2$ fairly well in the frequency region $\omega > \omega_{max}$ in PB, and the rough agreement between these spectra can be also found in PS. In both cases of PB and PMMA, the shapes of $I(\omega)/\omega(n(\omega)+1)$ are far apart from those of $g(\omega)/\omega^2$ in the region $\omega > \omega_{max}$. This result clearly indicates that the relation $C(\omega) \sim \omega$ actually holds for $\omega > \omega_{max}$.

Next let us look into the correlation between WDOS and Raman or neutron data. WDOS spectrum and $I(\omega)/\omega^2(n(\omega)+1)$ are surprisingly identical with each other in PMMA and the fairly good agreement can also be seen in PS and PB. We can conclude from this comparison that

$$\xi(\omega) \propto \frac{1}{\omega^2}. \tag{4.23}$$

For the lower frequency region $\omega < \omega_{max}$, the relation between WDOS and Raman or neutron scattering spectrum seems to be more complicated compared to the higher frequency region $\omega > \omega_{max}$. To begin with, let us verify the light-vibration coupling $C(\omega)$ in this frequency region. Fig.24(a) reveals that $g(\omega)/\omega^2$ is in fairly good agreement with $I(\omega)/\omega^2(n(\omega)+1)$ in PS. On the contrary, the agreement between these two spectra cannot be obtained in the case of PB as shown in Fig.24(c). Quasielastic scat-

tering caused by the relaxational motion may contribute to the Raman and neutron scattering spectra to some content even at low temperatures in the lower frequency region $\omega < \omega_{max}$. Contribution from the relaxational motion is supposed to depend on the fragility (proposed by Angell [31]), which makes it difficult to find out the behavior of $C(\omega)$ precisely at $\omega < \omega_{max}$. Sokolov concluded from the comparison for more materials in addition to three samples shown here that the frequency dependence of light-vibration coupling in the region $\omega < \omega_{max}$ is much weaker than that in the region $\omega > \omega_{max}$ or nearly constant. This is, however, merely a rough estimation and should be more complicated in actual. For example, Raman spectrum in the extremely low frequency region in disordered systems is supposed to be determined by the acoustic phonons as in the crystals and thus $C(\omega) \propto \omega^2$ [33].

Next we examine the electron-vibration coupling $\xi(\omega)$ in the lower frequency region $\omega < \omega_{max}$. The agreement between WDOS and $I(\omega)/\omega(n(\omega)+1)$ is fairly better than that between WDOS and $I(\omega)/\omega^2(n(\omega)+1)$ in this region for PS and PMMA, while $I(\omega)/\omega^2(n(\omega)+1)$ rather than $I(\omega)/\omega(n(\omega)+1)$ roughly coincides with WDOS. Although we should not say too much from such a small amount of experimental results, we might say that there lies a possibility that the behavior of $\xi(\omega)$ changes in the vicinity of the Boson peak ω_{max}; i.e.,

$$\xi(\omega) \sim \omega^{-\nu} \qquad (\nu < 2). \tag{4.24}$$

Anyway, much more efforts on such comparison is strongly needed at this stage.

4.5 Theoretical models of low-frequency dynamics

Latest Raman and neutron scattering experiments have revealed that the Boson peak can be observed for a wide variety of disordered materials including inorganic glasses [19-28], polymers [1,2,7,8,12] and molecular glasses [3-6].

In the present section, we introduce several models proposed so far for the qualitative interpretation of the Boson peak in disordered materials and examine them in connection with our results of WDOSs.

4.5.1 Various models of Boson peak

Cluster model

Several research groups have claimed that the shape of the Boson peak can be explained by the size distribution of clusters in disordered materials [11,13,21,22].

It is assumed in this model that the low-frequency modes arise from the cluster with a correlation length of an order of 10Å . The frequency of the vibration excited in the cluster with its size r is given by

$$\omega \approx \frac{v}{r}, \tag{4.25}$$

where v is the sound velocity in the medium. Eq.(4.25) shows that the excited vibration in the cluster follows the Debye-type dispersion.

In this model, the distribution of the cluster size is assumed to be expressed as

$$N(r) \approx \frac{N_0}{\sqrt{2\pi\sigma^2}} \exp\left(-\frac{[\ln(r/r_0)]^2}{2\sigma^2}\right). \tag{4.26}$$

It is obvious from the inverse proportional relation between ω and r in Eq.(4.25) that the vibrational density of states $g(\omega)$ is also given by the same function as Eq.(4.26); i.e.,

$$g(\omega) \approx \exp\left(-\frac{[\ln(\omega/\omega_0)]^2}{2\sigma^2}\right). \tag{4.27}$$

This empirical function is called *lognormal* function, which is often used to describe the final size distribution of the mechanically milled particles.

This model function can fit very well the universal profile of DOS of low-frequency vibrations obtained for polymers and inorganic amorphous materials by means of inelastic neutron scattering [11] as well as Raman scattering spectroscopy [13,21,22]. It is concluded in this model that the universal curve found in the low-frequency Raman or neutron spectrum is caused by the universality lying in the size distribution of clusters in disordered materials.

Although this model function has succeeded in explaining the universal profile of $g(\omega)$ qualitatively and hence has been widely accepted, it remains doubtful if it is acceptable for a variety of disordered materials including liquid-quenched molecular glasses. Linear dispersion relation of vibrational excitations in clusters means that the spherical modes or the surface modes should be assumed for these vibrations excited in spherical clusters. Such isotropic shapes of clusters could be considered in particular cases such as inorganic oxide glasses and amorphous semiconductors, while it could be hardly considered for linearly-linked organic polymers and sol-gel derived inorganic gels.

We conclude that this model is invalid as a model to explain the universal Boson peak profile.

Soft librational modes of glass-forming liquids

Yamamuro and coworkers measured the inelastic neutron scattering for molecular glasses without any particular intermolecular interaction except for the Van der Waals forces and found that the vibrational densities of states in these materials have Boson peaks which are quite similar to other

polymeric disordered materials [6]. They also found the relation between the peak frequency of the Boson peak ω_{max} and the molecular weight M as

$$\omega_{max} \sim \frac{1}{\sqrt{M}}. \tag{4.28}$$

He concluded from this result that the boson peak in these simple molecular glasses may arise from the softening of the librational modes of *individual* molecules. This conclusion, which indicates that the profile of DOS $g(\omega)$ in monomeric glasses is not determined by their macroscopic structure but by the single molecules themselves, can be accepted quite naturally. However, it is still open to question if such a librational motion in a single molecule contributes to the profile of WDOS in our case. As seen in the preceding section, the peak frequencies of WDOS for 3-methylpentane and toluene glasses are 27cm^{-1} and 18cm^{-1} respectively, while the molecular weights of these glasses are almost the same (MW=86.2 for 3MP and MW=92.1 for toluene). Our results clearly indicate that the peak frequencies of WDOSs do not follow the relation Eq.(4.28).

Only few attempts have so far been made for the study on the low-frequency dynamics in such simple molecular glasses due to the difficulty of obtaining glassy states with a good quality. Such a difficulty is caused by their low glass-transition temperatures ($T_g \leq$100K in most cases). Further investigation should be required in this field.

Fractons in the fractal network

Courtens, Tsujimi and their coworkers measured the depolarized Raman scattering, inelastic neutron scattering and Brillouin scattering spectra for base-catalyzed silica aerogels and analyzed their experimental data on the basis of the concept of the superlocalized vibrations on the fractal network, which are called *fractons*. They confirmed the unique structure with the

self-similarity in aerogels by means of the scanning electron microscopy (SEM). They suggested that the fractons could be seen when the characteristic scale of the fractal structure and the wavelength of the vibrational excitation are comparable; i.e.,

$$a < \lambda < \xi_{ac},$$

where a is the mean size of silica particles and ξ_{ac} is the acoustical correlation length, which is supposed to represent the mean size of SiO_2 *clusters* in silica aerogels. In the fracton regime, the vibrational density of states $g(\omega)$ and light-vibration coupling coefficient $C(\omega)$ can be written as

$$\begin{aligned} g(\omega) &\sim \omega^{\tilde{d}-1} \\ C(\omega) &\sim \omega^{\frac{2\tilde{d}}{D}}, \end{aligned} \tag{4.29}$$

where $\tilde{d}$ and D are the fracton and the fractal dimensions, respectively. When substituting Eq.(4.29) into Eq.(4.18), we obtain the reduced Raman intensity as

$$I_R(\omega) \sim \omega^{\nu}, \tag{4.30}$$

where

$$\nu = \tilde{d}(1 + \frac{2}{D}) - 1. \tag{4.31}$$

The power law of ω in Eq.(4.30) can be easily verified if a linear line appears in log-log plot of reduced Raman spectra.

The fractal model has been also employed for amorphous semiconductors by Ivanda and coworkers [19], and its possibility has also been examined by another group [20].

Ivanda claimed that the frequency-independence of the depolarization ratio in a wide frequency range (from the very low-frequency up to more than $1000cm^{-1}$) of Raman scattering spectra could be explained only by

the fractal-fracton model [19]. He also pointed out, in addition, that the anomalously long lifetime of low-frequency vibrations in amorphous semiconductors clearly indicates that these vibrations are superlocalized on the fractal network.

He represented the shape function of reduced Raman scattering spectrum in amorphous semiconductors as

$$I^R(\omega) \propto \omega^3(\omega^2 + \omega_{col}^2)^{\{\tilde{d}/D(\sigma+d-D)-\frac{5}{2}\}} \tag{4.32}$$

where ω_{col}, $\tilde{d}$ and D represent the phonon-fracton crossover frequency, spectral dimension and fractal dimension, respectively (σ is a correction factor). Although his expression of $I_R(\omega)$ does not follow a power-law of ω as shown in Eq.(4.30), this function can roughly reproduce the whole shape of Boson peak as shown in Fig.25.

Malinovsky and coworkers have pointed out [12] that the fracton regime could also be found in organic polymers as the unique ω^ν-relation in reduced Raman spectra as described above, which was also confirmed by Saikan and coworkers. These results suggests that the fractal regime exists in the scale of about 50Å, which has not been observed yet by the direct measurement of the microstructure by means of SEM or related spectroscopy. We think it is still doubtful if the fractal geometry actually exists in organic polymers. One of the reasons is that the fracton regime represented by the power-law of ω is too limited to regard this structure as a fractal.

We prepared SiO_2 and SiO_2-TiO_2 inorganic gels via the sol-gel method similar to the case of silica aerogels described above. We used the *acid* catalyst for hydrolysis and polycondensation reaction in our case in stead of the *base* catalyst in silica aerogels [78]. Silica or silica-titania gel under the acid condition has a structure characterized by the linearly-linked chain

bridged by siloxane bond as described previously, which is supposed to be far from the fractal structure [77, 80].

In addition, it can hardly be considered that the fractal structure exists in the monomeric molecular glasses such as alkane and alkylbenzene glasses, which are vitrified only due to the weak Van der Waals intermolecular forces.

We come to the conclusion that it might be impossible to explain the universality of the Boson peak profile for a variety of disordered materials only from the viewpoint of the geometrical *fractals*.

4.5.2 Concept of superlocalized vibrations

Recently, Foret and coworkers have performed both the small-angle inelastic neutron scattering and the inelastic X-ray scattering experiment for fused silica [85]. They argued that they found experimentally the direct evidence of the localized vibrations at the boson peak for the first time. When the q value of the dynamical structure factor $S(q,\omega)$ was sufficiently small, only the vibration with frequency ω, whose value could be derived from the normal dispersion relation, was detected. This shows that only the propagating acoustic phonons could be seen in the small q region. In contrast, when the q value increased, obtained scattering spectrum became broader and its peak frequency hardly depended on q.

Bermejo and coworkers performed the simulation of the low-frequency vibration on the basis of the molecular dynamics for several realistic glasses such as amorphous selenium and some molecular glasses and illustrated the localization of low-frequency vibrations by comparing the results obtained from the simulation of $S(q,\omega)$ for various q values [86]. They also found that the "hump" at the low-frequency arised not from the rotational motions but from the center-of-mass motions and concluded that the origin of the boson peak is not the intramolecular vibration but the collective

motion in a group of molecules.

Their results are fairly consistent with our recent findings on Raman scattering for molecular glasses. Distinct peaks whose frequencies are about two or three times larger than the frequency of the boson peak have been found for alkylbenzene glasses, while the corresponding peaks have never been seen in WDOS of dye-doped alkylbenzene glasses. In the case of Raman scattering, coupling of light with electric dipole contributes to the light scattering. Intramolecular vibrations including librations tend to induce electric dipoles and hence should be sensitive to the incident light. We suppose this is why these distinct peaks can be observed in Raman scattering of molecular glasses. In contrast, WDOS contains the coupling strength between the vibrations and the *electronic state* of the chromophore. Namely, the incident light couples to the electric dipole on the chromophore molecule, not to the dipole on the host molecule which arises the intramolecular vibrations. A fact that the intramolecular vibrations of the chromophore itself are always observed clearly in WDOS spectrum may support the above concept.

We support the fundamental idea that the origin of the boson peak is the localized vibrations arising from the collective motion of the group of molecules, and believe that this idea can also explain the origin of the characteristic shape of the WDOS spectrum.

However, the most important problem still remains unsolved: What is the origin of the universality we found in the shapes of WDOS spectra for a number of host-guest systems?

In the case of the weak scattering condition, a disordered system has three characteristic lengths, a wavelength, a scattering length and a localization length. When the vibrations are strongly localized, three scale parameters are virtually identical ("single-length scale postulate") and thereby only the wavelength can characterize the size of the system. Such

a strong scattering condition is often called *Ioffe-Regel* condition. Foret and coworkers [85] found that the Ioffe-Regel frequency ω_{IR}, which corresponds to the crossover frequency from the normal scattering condition to the Ioffe-Regel condition and can be roughly predicted from the result of the heat conductivity experiment, was remarkably close to the boson peak frequency ω_{bp} in the case of fused silica. If the relation

$$\omega_{IR} \sim \omega_{bp}$$

holds for various disordered systems, the universal shape of the density of states of low-frequency vibrational modes might be qualitatively interpreted in terms of the concept single-length scaling because only ω_{IR} is the parameter to determine the shape of the DOS spectrum in the low-frequency region. Although the universality of WDOS we have found seems to be more difficult to explain in comparison with the case of DOS because of the *coupling* part in WDOS, the above concept is the most likely interpretation for the present.

4.6 Temperature dependence in site-selective fluorescence spectra

In the present section, we discuss the temperature dependence of the site-selective fluorescence spectra for dye-doped molecular glasses. To begin with, let us describe the procedure of calculation to obtain the site-selective fluorescence spectrum $F_T(\omega_L, \omega)$ at a given temperature T.

4.6.1 Analytical procedure

As discussed in the previous section, 1-phonon function at a given temperature T is obtained by using WDOS which corresponds to the 1-phonon function at 0K as

$$\begin{aligned} s_T(\Omega) &= \frac{1}{2\pi}\int_{-\infty}^{\infty} dt S_T(t) e^{i\Omega t} \\ &= s(\Omega)\{n_T(\Omega)+1\} + s(-\Omega)n_T(-\Omega), \end{aligned} \tag{4.33}$$

where we assume that all of the vibrational modes contained in WDOS are regarded as harmonic modes at none-zero temperatures.

The m(=2,3,4,...)-phonon function at T is then obtained by

$$\begin{aligned} \Phi_T^{(m)}(\Omega) = \frac{\alpha_T'}{m!}\int_{-\infty}^{\infty} d\Omega_1 \int_{-\infty}^{\infty} d\Omega_2 \cdots \int_{-\infty}^{\infty} d\Omega_m s_T(\Omega_1) s_T(\Omega_2) \\ \times \cdots s_T(\Omega_m)\delta(\Omega - \Omega_1 - \Omega_2 \cdots - \Omega_m). \end{aligned} \tag{4.34}$$

The single-site fluorescence spectrum at temperature T can be described from Eq.(2.23) and Eq.(2.24) as

$$\begin{aligned} f_T(\Omega) &= \alpha_T'\delta(\Omega) + \Phi_T(\Omega) \\ &= \alpha_T'\delta(\Omega) + \sum_{m=1}^{\infty} \Phi_T^{(m)}(\Omega). \end{aligned} \tag{4.35}$$

The site-selective fluorescence spectrum at a given site-energy can be obtained using above-mentioned single-site spectrum $f_T(\Omega)$ and the site-energy distribution as

$$\tilde{F}'(\Omega) = (\omega + \Omega) \int_0^{\Omega} \tilde{G}(\Omega') f_T(\Omega - \Omega') f_T(\Omega') d\Omega'. \tag{4.36}$$

In conclusion, we can calculate the site-selective fluorescence spectrum $F_T(\omega_L, \omega)$ at a given ω_L and temperature T from WDOS spectrum $s(\omega)$ and the site-energy distribution function $G(\omega)$ under several theoretical assumptions; linear Frank-Condon electron-phonon interaction , the harmonicity of vibrational modes, temperature-independence of WDOS and the temperature-independence of $G(\omega)$.

These assumptions listed above are expected to hold true only in the *frozen* state below T_g while some of them may be violated in the fluid state. The site-energy distribution may be fixed at the frozen state, because the local configuration in the vicinity of the dye molecule is frozen and thereby only the local motions are permitted. This is also confirmed by the results shown previously that the peak energy and the bandwidth of the lowest optical absorption band are nearly constant at whole temperatures below T_g.

4.6.2 Results and discussion

Fig.26 shows the comparison between the measured site-selective fluorescence spectra and those calculated following the analytical procedure mentioned above in MgOEP-doped isopropylbenzene glass below $T_g(\sim 125\text{K})$. The calculated spectra are in fair agreement with the measured ones at all temperatures below T_g.

A similar comparison was performed in chlorophyll b-doped toluene-benzene-mixture and 1-butanol glasses, which are shown in Figs.27 and 28, respectively. The calculated spectra also reproduce well the measured ones at all temperatures below T_g ($\sim$120K for both glasses) in these samples.

The fairly good agreement in the comparison of measured and calculated site-selective spectra made for these systems tells us that the above

assumptions employed to calculate fluorescence spectra are valid in these cases.

Next, in Fig.29, we made comparisons between the measured spectra and the calculated ones for chlorophyll b-doped 1-propanol glass. Although they are in fair agreement with each other at 20K, the measured spectral widths are broader than those calculated at 40K and above. It should be noted that the poor agreement in these spectra is observed even far below the glass transition temperature T_g(~96K). Furthermore we should mention that the deviation between these spectra becomes larger with increasing temperature. To show this anomalous temperature dependence more clearly, we plot only the spectral bandwidth (FWHM) of both measured and calculated site-selective fluorescence spectra at various temperatures in Fig.30. The experimental value of the bandwidth of site-selective fluorescence spectrum at 120K is approximately three times larger than that expected from the analysis shown above.

This result suggests that one of these theoretical assumptions or more are broken down in the case of chlorophyll b-doped 1-propanol glasses. Such a temperature dependence could be also observed in 2-propanol doped with chlorophyll b where the deviation of measured spectrum from the calculated one is smaller than that in the case of 1-propanol glass. On the contrary, we could not find the apparent deviation for polyhydroxylic alcohols.

To figure out the origin of this anomalous behavior, we performed nanosecond time-resolved fluorescence spectroscopy at temperatures below T_g. Fortunately, this experimental technique does not require any further modification of the experimental setup for the site-selective fluorescence/excitation spectroscopy described in the previous section.

Fig.31 shows the time-resolved site-selective fluorescence spectra at 60K. Intensities of these spectra for various time-delay windows are normal-

ized so that they coincide with one another at both higher and lower energy edges (-200∼-100cm^{-1} and 200∼400m^{-1}, respectively) of these fluorescence spectra. The time-resolved fluorescence spectrum obtained for a delay time window of 0-1nsec corresponds to the fluorescence at the origin of the time delay for the time resolution of our system (up to 0.4nsec). We can find from this figure that the time-resolved fluorescence spectrum changes in a nanosecond time scale at 60K while such a behavior is not found below 40K.

This result clearly indicates that the energy relaxation which can be usually observed in the fluid state occurs even in the *frozen* state. Low-frequency vibrations at the bottom of the local potential minima in the potential with relatively small amplitude are regarded as harmonic modes. As the vibrational amplitude becomes larger, on the contrary, the low-frequency local vibrations are no longer in each local *pockets* and shift to the relaxational modes.

This concept of relaxational motion in the frozen state may be acceptable if we assume that the frozen structure of solvent molecules in the vicinity of the dye molecule begins to melt only in the limited area below the glass transition temperature of the *bulk* glass. We must consider that this local melting phenomenon is far from the so-called glass transition in bulk glasses, in which the cooperative motion extending to a macroscopic scale play an indispensable role.

The electronic state of the incorporated dye molecule as a localized center *feels* the vibrational or relaxational dynamics in the vicinity of the dye itself. Therefore, it is quite reasonable that the site-selective fluorescence spectrum reflects sensitively the host dynamics arising from the local structure. The local configuration of the solvent molecules in the vicinity of the dye molecule may be determined by the particular coupling to the certain part of the dye molecule via the dipolar interaction. This possi-

bly explains why the local melting occurs only in the chlorophyll b-doped 1-propanol system.

As discussed in the previous section, an alcoholic molecule tends to ligate to the oxygen atom in the cyclopentanone ring of chlorophyll b. This may be one of the origins to determine the local configuration in the vicinity of chlorophyll b, which is different from the bulk structure.

In contrast, alkylbenzenes (toluene and isopropylbenzene) have no particular coupling to the porphyrin-type molecules as MgOEP and chlorophyll b. Accordingly, the local configuration in the vicinity of the dye molecule in the case of dye-doped alkylbenzenes is the same as that of bulk matrix, which causes the coincidence between the measured and calculated site-selective fluorescence spectra up to the glass transition temperature as shown above.

It remains unsolved, however, why the local melting phenomenon is not found in chlorophyll b-doped 1-*butanol* glass.

4.7 Mirror-symmetry relation in single-site spectra

In the analytical procedure of the determination of WDOS, we assume that the mirror symmetry relationship holds between the shape functions of the single-site absorption $a_T(\omega_L - \omega')$ and fluorescence $f_T(\omega - \omega')$ as shown in Eq.(2.34). We propose in this section the novel technique to verify experimentally the validity of this assumption in dye-doped disordered systems.

Mirror symmetry relation about the zero-phonon line between the shape functions of absorption and fluorescence has been discussed theoretically in 1970's [42-45,46-49] and compared with experimental results of optical spectra of localized centers in crystals [43]. Small found the breakdown in the mirror symmetry relation in tetracene-doped p-terphenyl crystal at low temperatures and concluded that the breakdown was caused by the quadratic term of the electron-phonon coupling.

According to the theory concerning the linear and the quadratic terms in the Frank-Condon-type electron-phonon interaction, the degree of mirror asymmetry strongly depends on the strength of the quadratic term. Namely, the mirror symmetry relation exactly holds only under the linear Frank-Condon interaction. Quadratic term, on the other hand, causes the difference in the vibrational energy between the electronic states of localized center $|g\rangle$ and $|e\rangle$, which is considered to be the origin of the breakdown of the mirror symmetry relation between the shapes of phonon-sidebands in absorption and fluorescence spectra.

It should be noted that, considering the Herzberg-Teller(HT) mechanism where the q-dependence of the transition dipole moment is assumed in Eq.(2.10) for the electron-phonon interaction, even the linear term of HT interaction can violate the mirror symmetry relation.

In most cases of impurity centers in crystals, the inhomogeneous broad-

ening is smaller than homogeneous linewidth even at low temperatures, which enables us to measure the single-site absorption and fluorescence spectra by means of the conventional spectroscopy. To our knowledge, however, it has never been verified if the mirror symmetry holds in disordered materials doped with chromophores. One of the reasons may lie in the hole-burning effect in connection with using the laser light. Hole-burning effect inherently occurs in most disordered materials even at sufficiently low temperatures which is caused by the degrees of freedom in frozen local configurations, often called two-level systems(TLS). This effect makes it quite difficult to measure the site-selective fluorescence spectrum without any distortion because the fluorescence intensity decreases during the measurement by suffering from hole-burning.

4.7.1 Various experimental approaches

Since we have developed the novel site-selection spectroscopic technique called the site-selective fluorescence-*excitation* spectroscopy, several combinations of the variation of site-selection methods can be considered to verify the mirror symmetry relation.

Although we could successfully obtain site-selective *excitation* spectra including the zero-phonon lines for dye-doped disordered materials with high hole-burning efficiencies, it is very difficult to measure the site-selective *fluorescence* spectra accurately for these samples.

Several experimental techniques have been proposed so far for measuring the site-selective fluorescence spectrum without suffering from hole-burning.

Some of these employ another light together with the exicitation light to *restore* the burned hole. One of them has been proposed by Galaup [57], where he used the so-called *double-chopper double-excitation method.* When a photochemical reaction such as the tautomerization of protons

in porphyrin molecules occurs by laser irradiation at low temperatures, a photoproduct site may be generated, whose wavelength is apparently different from that of hole-burned site, within the broad absorption band. It depends on the type of photoreaction whether the transition energy of the photoproduct site ω_p is higher or lower than that of the educt (burned) site ω_b. Irradiation of ω_p light causes the backward-photoreaction and can put the generated photoproduct back to the original (educt) state. If one irradiates ω_p light together with ω_b light for fluorescence detection, the site-selective fluorescence spectrum can be measured without suffering from hole-burning. A double-chopper technique was utilized to cut off the back-reaction light ω_p during the measurement of site-selective fluorescence signal.

Although his technique may be applicable to a certain case, it has too many experimental limitations to be widely used.

Although a polychromatic measurement using a CCD detector may be another approach to the site-selective fluorescence spectrum as shown in the previous section, it is disadvantageous that the exact value of the zero-phonon fluorescence intensity cannot be measured in this method.

In the following subsections, we review some of experimental techniques which have a possibility to verify the validity of mirror symmetry relation.

Site-selective fluorescence/excitation spectrum and saturation effect

As shown previously, the shape functions of site-selective fluorescence (SSF) and excitation (SSE) spectra are commonly given as

$$F(\omega;\omega_L) \sim \int G(\omega')a_T(\omega_L-\omega')f_T(\omega-\omega')d\omega'. \tag{4.37}$$

Utilizing the saturation effect of absorption due to the bottleneck state T_1 in site-selective excitation measurement, we can obtain the single-site spectrum by the following procedure: When we compare the site-selective

excitation spectrum obtained under the weak irradiation power without any saturation and that obtained under the strong irradiation power where only the zero-phonon component of absorption may be saturated, the difference spectrum between these spectra corresponds to the single-site *fluorescence* spectrum. It can be understood if we see Eq.(2.33)

$$\begin{aligned} F(\omega;\omega_L) \propto\ & {\omega_L}^4 G(\omega_L) \\ & +\omega_L\omega^3 G(\omega_L) f_{psb}(\omega-\omega_L) \\ & +\omega_L\omega^3 G(\omega) a_{psb}(\omega_L-\omega) \\ & +\omega_L\omega^3 \int G(\omega') a_{psb}(\omega_L-\omega') f_{psb}(\omega-\omega') d\omega', \end{aligned} \tag{4.38}$$

where the first and the second terms correspond to the resonantly excited components whose intensities are affected by the zero-phonon hole at ω_L.

It should be noted that this technique itself has no possibility to determine the single-site *absorption* spectrum.

Fünfschilling and coworkers proposed a new method to determine the single-site absorption and fluorescence spectra from the site-selective fluorescence and excitation spectra [37]. We followed their algorithm in the analytical procedure and tried to determine the single-site spectrum by ourselves for chlorophyll-b doped polystyrene. However, the solution of each spectrum diverges and could not be successfully determined because this algorithm is extremely sensitive to a small noise in either site-selective spectrum.

Hole-burning spectroscopy

Absorption spectra before and after hole-burning are described commonly as

$$A(\omega,t) = \int G_0(\omega') e^{-\nu a(\omega_B-\omega')t} a(\omega-\omega') d\omega', \tag{4.39}$$

where $G_0(\omega)$, ν, t and ω_B represent the initial site-energy distribution, hole-burning efficiency, burning time and the wavelength of the laser,

respectively. Absorption spectrum before hole-burning corresponds to $A(\omega, 0)$. The hole spectrum can be derived from Eq.(4.39) as

$$\begin{aligned} H(\omega, t) &= A(\omega, 0) - A(\omega, t) \\ &= \int G_0(\omega')(1 - e^{-\nu a(\omega_L - \omega')t}) a(\omega - \omega') d\omega'. \end{aligned} \tag{4.40}$$

When the burning time t is sufficiently short, we can use the following relation:

$$e^{-\nu a(\omega_L - \omega')t} \approx 1 - \nu a(\omega_L - \omega')t. \tag{4.41}$$

Using Eq.(4.41), Eq.(4.40) can be rewritten as

$$H(\omega, t) \propto \int G_0(\omega') a(\omega_L - \omega') a(\omega - \omega') d\omega'. \tag{4.42}$$

Eq.(4.42) indicates that the single-site *absorption* spectrum can be determined *ideally* from the hole spectrum. However, it is in fact not easy to measure the hole spectrum precisely because of several restrictions.

In the actual measurement, the shape of the hole spectrum strongly depends on the total fluence (given as a product of burning time and power) of laser light used for hole-burning because of the difference lying in the condition of saturation between the zero-phonon line and the phonon sideband. It should be also noted that the change of the site-energy distribution $G(\omega)$ due to the photoproduct states induced by hole-burning is not considered in Eq.(4.42). In addition, spontaneous hole-filling effect may also distort the measured hole-spectrum.

In conclusion, hole-burning spectroscopy is insufficient for the determination of single-site absorption spectrum.

4.7.2 Double-selection spectroscopy

In this subsection we show that the single-site absorption and fluorescence spectra can be independently determined by employing hole-burning

spectroscopy as the site-selective *absorption* measurement together with the site-selective *fluorescence* spectroscopy. Since we use these two site-selection methods simultaneously, we call this novel technique a *double-selection spectroscopy.*

In this technique, we measure the difference spectra between before and after hole-burning for both site-selective fluorescence (SSF) spectrum and the site-selective excitation (SSE) spectrum.

In the case of the double-selection *fluorescence* spectrum, we first measure the SSF spectrum with the excitation laser ω_L. Then we burn a spectral hole with a burning light $\omega_B(=\omega_L)$ and again measure the SSF spectrum with the same excitation energy ω_L after hole-burning. Finally the difference spectrum between these spectra is obtained.

The measurement procedure of double-selection *excitation* spectrum is quite similar, while the energy of the fluorescence detection ω should be replaced with ω_L.

As shown in Eq.(4.39), site-distribution at ω' after hole-burning at ω_L for time t is given as

$$\begin{aligned} G(\omega', t) &= G_0(\omega') e^{-\eta a(\omega_L - \omega')t} \\ a(\omega_L - \omega') &= a_{zpl}(\omega_L - \omega') + a_{psb}(\omega_L - \omega'), \end{aligned} \tag{4.43}$$

where $a_{zpl}(\omega)$ and $a_{psb}(\omega)$ correspond to the zero-phonon and phonon-sideband components respectively.

The site-selective fluorescence spectrum at burning time t is

$$\begin{aligned} F(\omega, t) &\propto \int G(\omega', t) a(\omega_L - \omega') f(\omega - \omega') d\omega' \\ &= \int G_0(\omega') e^{-\eta a(\omega_L - \omega')} a(\omega_L - \omega') f(\omega - \omega') d\omega'. \end{aligned} \tag{4.44}$$

When t is sufficiently short, the difference spectrum between before and after hole-burning can be described using Eqs.(4.43) and (4.41) as

$$\Delta F(\omega, t) = F(\omega, 0) - F(\omega, t)$$

$$\propto \int G_0(\omega') \cdot \eta\{a_{zpl}(\omega_L - \omega') + a_{psb}(\omega_L - \omega')\}$$
$$\times a(\omega_L - \omega') f(\omega - \omega') d\omega'. \quad (4.45)$$

As seen in Eq.(4.45), the difference spectrum can be expressed as the convolution of the hole spectrum, single-site absorption spectrum and the single-site fluorescence spectrum.

Here we assume that the zero-phonon line in the single-site absorption spectrum $a_{zpl}(\omega_L - \omega')$ can be replaced with $\delta(\omega_L - \omega')$.

Let us consider firstly the case of double-detection SSE spectroscopy. Energy of the excitation laser light ω_L, which is a scanning parameter in this case, must be larger than that of the fluorescence detection ω because a molecule which absorbs $\omega_L (\leq \omega)$ can hardly emit fluorescence with the energy of ω at a very low temperature. It means that molecules with site-energy $\omega' \leq \omega_L$ do not contribute to the SSE spectrum. Because the change in the site-energy distribution $\Delta G(\omega)$ only lies in the energy $\omega' \leq \omega_B (= \omega_L)$, it can be concluded that only the zero-phonon hole can contribute to the difference spectrum in the case of SSE spectroscopy. The zero-phonon line of the difference spectrum corresponds to the zero-phonon fluorescence from the molecules which resonantly absorb the laser light $\omega_L = \omega$ through zero-phonon absorption. Namely,

$$\Delta F_{zpl}^{SSE}(\omega, \omega) \sim G_0(\omega) a_{zpl}(0) a_{zpl}(0) f(0). \quad (4.46)$$

The phonon-sideband part of the difference spectrum, on the other hand, corresponds to the zero-phonon fluorescence from the off-resonantly excited molecules whose transition energy ω' is larger than the detection energy ω through phonon-sideband absorption. Namely,

$$\Delta F_{psb}^{SSE}(\omega_L, \omega) \sim G_0(\omega) a_{zpl}(0) a_{psb}(\omega_L - \omega) f(0). \quad (4.47)$$

From Eqs.(4.46) and (4.47), we obtain the following relation:

$$\Delta F^{SSE}(\omega_L, \omega) \propto a(\omega_L - \omega), \quad (4.48)$$

which clearly indicates that the difference spectrum in double-detection SSE spectroscopy corresponds to the single-site absorption spectrum.

Next, we consider the double-detection SSF spectroscopy. In this case, it would be better to consider that the difference spectrum $\Delta F^{SSF}(\omega_L, \omega)$ has two components, fluorescence from the molecules which resonantly absorb the laser light ω_L through zero-phonon absorption line (ΔF_z^{SSF}) and that off-resonantly absorb ω_L through phonon-sideband absorption (ΔF_p^{SSF}).

The resonantly-excited component of the difference spectrum is caused by the zero-phonon hole at $\omega_B = \omega$ as

$$\begin{aligned} \Delta F_z^{SSF}(\omega_L, \omega) &\propto a_{zpl}(0) a_{zpl}(0) f(\omega_L - \omega) \\ &\propto f(\omega_L - \omega). \end{aligned} \tag{4.49}$$

On the other hand, off-resonantly excited component is express as

$$\Delta F_p^{SSF}(\omega_L, \omega) \propto \int a_{psb}(\omega_L - \omega') a_{psb}(\omega_L - \omega') f(\omega - \omega') d\omega'. \tag{4.50}$$

The ratio of phonon-sideband contribution ΔF_p^{SSF} to the total difference spectrum is determined by the relative intensity of phonon-sideband in single-site absorption spectrum and is roughly estimated by $(1 - \alpha_T')^2$ (α_T' is Debye-Waller factor) because ΔF_p^{SSF} requires at least twice of the phonon-sideband process. Consequently, off-resonantly excited component ΔF_p^{SSF} can be neglected if the electron-phonon coupling is sufficiently weak ($\alpha' \sim 1$).

In conclusion, the difference spectrum in double-detection SSF spectroscopy corresponds to the single-site *fluorescence* spectrum under the weak coupling approximation.

4.7.3 Sample preparation

As described above, a host-guest system with a relatively weak electron-phonon coupling strength must be selected as a sample for the double-selection spectroscopy. In addition, there are still many limitations for

selecting the appropriate samples. Properties of the host-guest system which are considered to be required for this method are listed below:

1. Burned spectral-hole should be thermally stable.
   (It should have an extremely low spontaneous hole-filling efficiency.)

2. Difference between the site energy of photoproduct state and that of the educt (burned) state should be large enough.
   (The change in the site-energy distribution should not influence the measurement of site-selective fluorescence/excitation spectra.)

3. Electron-vibration coupling should be fairly weak.
   (Debye-Waller factor should be large enough.)

4. Absorption band should be covered with the tuning curve of the tunable laser system.

The hole-burning mechanism required for the double-selection method is not the non-photochemical type but the photochemical one.

Change in the site-energy distribution induced by hole-burning lies not only in the zero-phonon hole and the pseudo-side-hole but also in the photoproduct state. In the nonphotochemical hole-burning mechanism, changes of the local configuration of the host material cause the change of the electronic transition energy of the guest molecule. Therefore, the change of the transition energy is fairly small, and moreover, the site-energy distribution of photoproduct states is much broader than the hole spectrum. It means that the site-distribution of the electronic transition energy in the region of interest for site-selective fluorescence/excitation spectra might be changed after hole-burning due to photoproduct states. These changes possibly distort the profile of measured site-selective fluorescence/excitation spectra. In addition, the photoproduct states of

non-photochemical hole-burning are thermally unstable in most cases and spontaneously come back easily to the original states.

In the photochemical hole-burning, on the other hand, the change in the chemical structure of the chromophore by irradiation of monochromatic light including tautomerization and photodissociation causes the photoproduct state. Therefore, it should be expected that the energy-distribution of the generated photoproduct states is much narrower than that in the case of nonphotochemical hole-burning and is far from the energy of the burned site. Moreover, the product states are in most cases stable and hardly come back without any irradiation.

In conclusion, the photochemical mechanism is much better than the non-photochemical one for double-selection technique.

The weakness of the electron-phonon coupling and the matching for our tunable laser system are also taken into consideration in addition to the burning mechanism discussed above, and finally we arrived at the conclusion that free-base chlorin is one of the best chromophores for the double-selection spectroscopy.

The steady form and the photoproduct form of free-base chlorin in n-hexane single crystals have the transition wavelength of 633.3nm and 574.2nm, respectively [52], which corresponds to the energy splitting of more than $1600cm^{-1}$. This splitting is much larger than that of a free-base porphyrin, ($\sim 100cm^{-1}$) in the same matrix. Since this splitting is not supposed to depend strongly on the host matrix, we can expect that change in site-energy distribution due to the photoproduct band does not affect the double-selection difference spectrum in chlorin-doped disordered materials.

We choose poly(styrene) as a host matrix, which is known to be chemically and thermally stable and to have an extremely low yield of spon-

taneous hole-filling. Chlorin e_6-doped poly(styrene) film was prepared as follows. First of all, both polystyrene and chlorin-e_6 (purchased from Porphyrin Products) were dissolved in a fresh chloroform in the dark. Then, these solutions were mixed together, casted onto glass plates and dried in the dark for a week. Moss-green-colored transparent film was finally obtained with the optical density of about 1.0 at the absorption maximum.

4.7.4 Results and discussion

Fig.32(a) shows the site-selective excitation spectra before and after hole-burning. Contribution from the scattered laser light has already been removed for both spectra. It can be found that both intensities of the zero-phonon fluorescence line and the particular part of the phonon-sideband with a small shift energy decrease after hole-burning, while the intensity of the phonon-sideband with the shift-energy higher than 300cm^{-1} remains unchanged.

Fig.32(b) clearly indicates that the shape of the phonon-sideband component in the site-selective excitation spectrum changes with the burning time.

The difference between the site-selective excitation spectra before and after hole-burning is shown in Fig.33(a). In Fig.33(b), the difference spectra at different stages of hole-burning are compared. It is obvious that the shape of the phonon-sideband of the difference spectrum in the case of deep spectral hole coincides with that in the case of shallow hole, which supports the idea shown above that the site-selective excitation spectrum is never affected by the pseudo-sidehole even in the case of deeply burned holes.

A preliminary measurement of the difference spectrum has been performed for oxazine 4 perchlorate-doped poly(vinyl butyral). Figs.34(a) and (b) show the site-selective excitation spectra before and after hole-

burning, and their difference spectrum, respectively. As shown clearly, the change in the phonon-sideband spectrum caused by hole-burning is not detectable at all in this case, while the distinct change in the zero-phonon line can be seen. One of the reasons why we could not detect the difference spectrum properly in this measurement may lie in the non-photochemical hole-burning mechanism in poly(vinyl butyral) doped with oxazine 4. Inhomogeneously-broadened photoproduct-site distribution caused by hole-burning possibly affects the phonon-sideband spectrum after hole-burning. Furthermore, the shape of the phonon-sideband spectrum after burning may be also affected by the laser-induced hole-filling effect.

Fig.35(a) shows the site-selective fluorescence spectra before and after hole-burning, where the scattering of excitation laser light has been removed. Change of fluorescence intensity can be also found both in zero-phonon line and in the phonon-sideband.

Fig.35(b) indicates the change in the phonon-sideband of the site-selective fluorescence spectrum during hole-burning process.

The difference between the site-selective fluorescence spectra before and after hole-burning is shown in Fig.36(a). The similar plot of Fig.33(b) is also drawn in Fig.36(b) in the case of the site-selective fluorescence spectrum, where both difference spectra correspond to those obtained for different stages of hole-burning process.

In contrast with the case of site-selective excitation spectra, however, we found that the shape of the phonon-sideband of the difference spectrum obviously depends on the burning time, corresponding to the hole depth. Even if the depth of the zero-phonon hole is saturated due to the long burning time, the depth of pseudo-sidehole remains growing larger proportional to the burning time. Accordingly, the long burning time may causes a large pseudo-sidehole compared to the zero-phonon hole. This

result confirms the concept shown above that the profile of the difference spectrum must be affected by the fluorescence from off-resonantly excited sites whose transition energies coincide with that of the pseudo-sidehole.

Finally we compare thus obtained difference spectra for both site-selective fluorescence and excitation spectroscopy, which correspond to the single-site fluorescence and absorption spectra respectively, in Fig.37. It can be found that the peak frequencies of phonon-sidebands for these difference spectra are identical with each other with its value of $\sim$15cm^{-1}. We also found that the whole shapes of the phonon-sideband part of these spectra are almost the same within the shift-energy of 150cm^{-1}. When we extend the region of interest to more than 400cm^{-1}, however, the violation of the mirror symmetry relation about the zero-phonon line can be seen as apparently shown in Fig.37(b). This might arise because the Debye-Waller factor in chlorin-doped poly(styrene) is much smaller than 1, which means that the electron-phonon coupling is not extremely weak and thereby the off-resonant component shown in Eq.(4.50) may play an important role in the difference spectrum.

In conclusion, we have succeeded in verifying that the mirror-symmetry relation in single-site absorption and fluorescence roughly holds in chlorin-doped poly(styrene) at low temperatures.

Chapter 5

Conclusion

In this work, we investigated the low-frequency dynamics for various disordered materials via the site-selective fluorescence or fluorescence-excitation spectrum of incorporated chromophores at low temperatures.

We developed a site-selective excitation spectroscopy where the continuous scan of the wavelength of the tunable dye laser was utilized together with the time-correlated single-photon method. This has a great advantage that the intensities of both the zero-phonon line and the phonon-sideband component are accurately determined even for dye-doped disordered materials with relatively high hole-burning efficiency. This technique enables us to examine the low-frequency dynamics in a wide variety of disordered materials including sol-gel derived inorganic gels and molecular glasses.

We obtained the densities of states of low-frequency vibrational modes weighted by the electron-vibration coupling strength (WDOS) for these dye-doped disordered materials following the analytical procedure on the basis of the linear Frank-Condon interaction from the site-selective excitation spectra. It was found that the shapes of thus determined WDOSs for a wide variety of disordered materials including polymeric materials and monomeric molecular glasses resemble fairly well with one another. Peak frequencies of WDOSs, however, reveal their own personalities for various disordered systems. It should be particularly mentioned that the

n-monohydroxylic alcohols doped with chlorophyll-b have relatively high peak frequencies of WDOSs compared to *iso*-monohydroxylic alcohols, which might be interpreted as due to the solvent-shell effect in the vicinity of chlorophyll b molecule.

We compared the WDOS spectra with other experimental data, Raman scattering and inelastic neutron scattering spectra in the low-frequency region for polymers. This comparison revealed that the electron-vibration coupling coefficient $\xi(\omega)$ in the frequency region higher than the peak frequency of WDOS ω_{max} is roughly proportional to $1/\omega^2$.

In order to determine the single-site absorption and fluorescence spectra independently in dye-doped disordered materials, we developed a novel site-selection spectroscopy called double-selection spectroscopy, where we employed the hole-burning spectroscopy together with both the site-selective fluorescence and excitation spectroscopy simultaneously. We came to the conclusion that chlorin-doped polystyrene is the most suitable host-guest system for our aim of research by taking various limitations for this method into consideration. Results from this approach clearly indicate that the mirror-symmetry relation holds roughly between single-site absorption and fluorescence spectra, which proves the validity of the linear FC interaction approximation employed in the analytical procedure of the determination of WDOS for the first time.

Acknowledgments

The author wishes to thank Professor Takashi Kushida for his guidance and valuable suggestions. He would like to express his thanks to Professor Shuichi Kinoshita for his enlightening comments. The author also wishes to thank Dr. Yasuo Kanematsu for his fruitful discussions and continuous co-operation throughout this research. He is indebted to Dr. Atusi Kurita for his valuable advice on the algorithm of the numerical calculation. He greatly thanks Mrs. Kuniko Hirata for sample preparation.

The author is grateful to Dr. Osamu Yamamuro in Department of Chemistry for many valuable suggestions from the chemical point of view. He is also indebted to Professor A.P.Sokolov in Max-Planck Institute for providing him experimental data on the Raman scattering.

Finally, the author thanks Mr. Naoki Hashimoto and all the members of Kushida & Kinoshita research group for their devoted assistance and stimulating discussions.

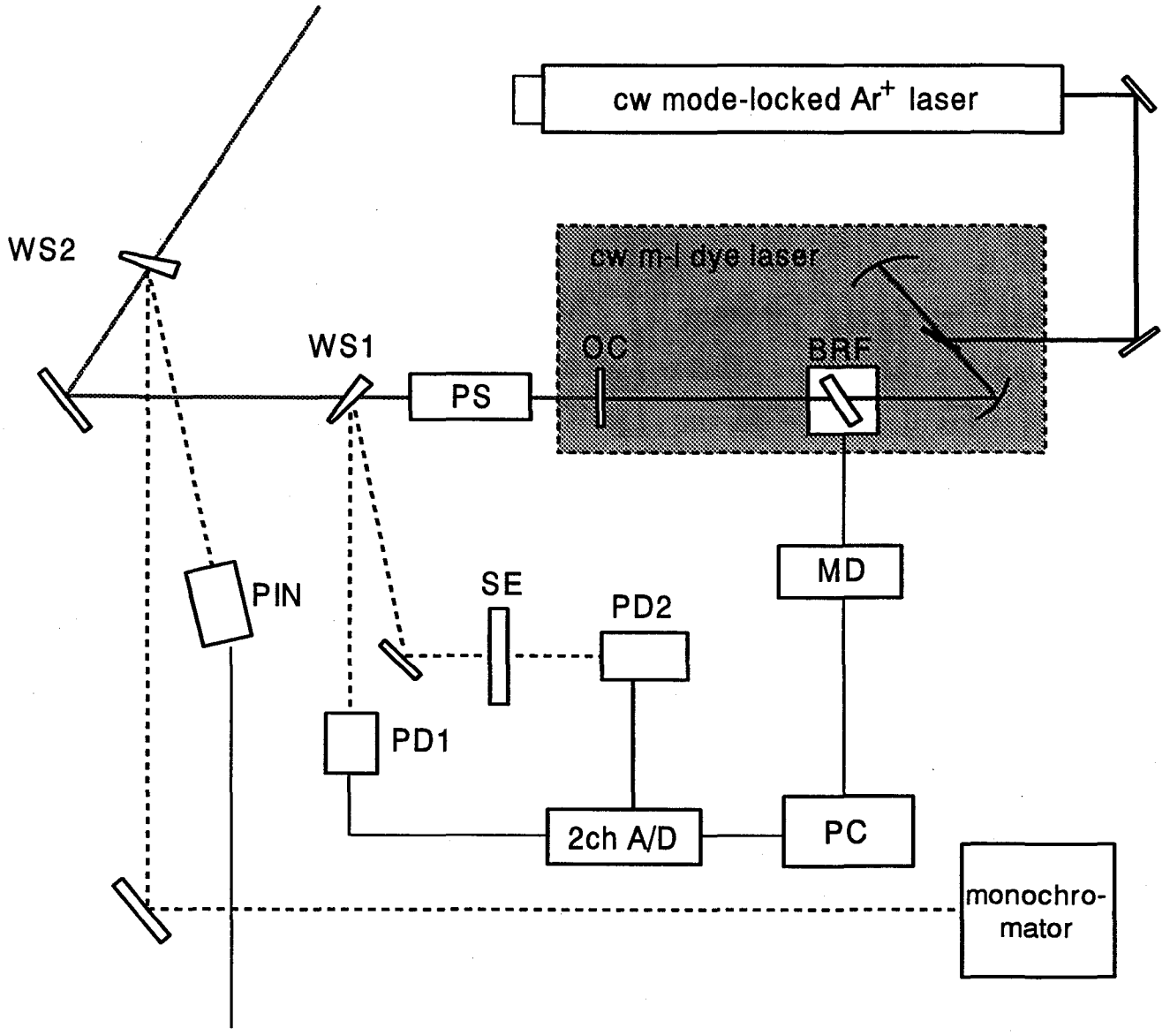

Figure 1: Experimental setup of excitation laser system for the site-selective fluorescence/excitation spectroscopy. WS1,WS2:wedged substrates, PS:laser power stabilizer, PD1,PD2:photodiodes, PIN:fast photodiode, SE:solid etalon, PC:personal computer, MD:stepping motor driver, OC:output coupler, BRF:birefringent filter.

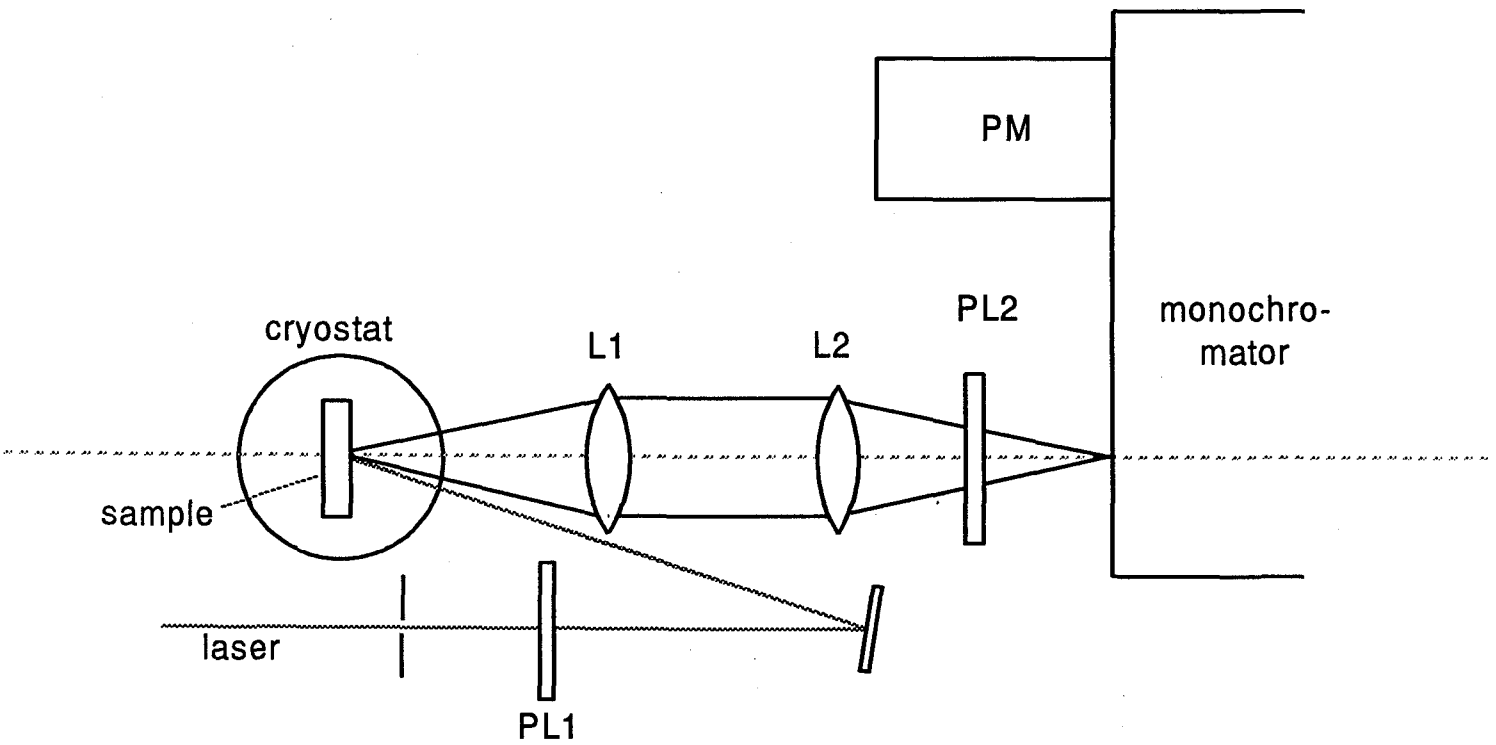

Figure 2: Experimental setup in front of the monochromator. PL1,PL2:polarizers, L1,L2:f=100mm lenses, PM:photomultiplier tube.)

Oxazine 4

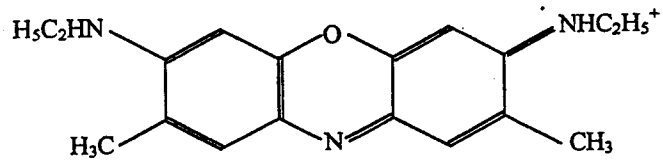

Mg-octaethylporphyrin (MgOEP)

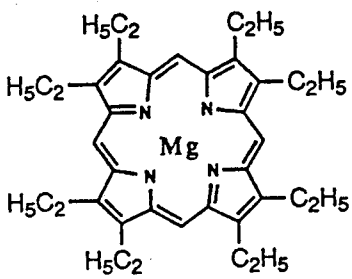

Chlorin e_6

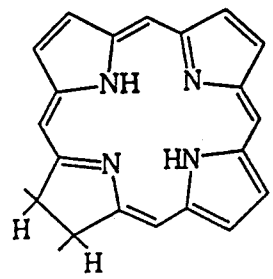

Zn-phthalocyanine

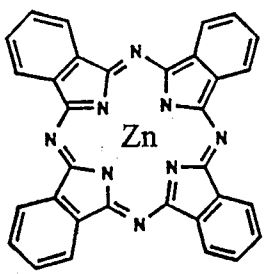

Chlorophyll-b

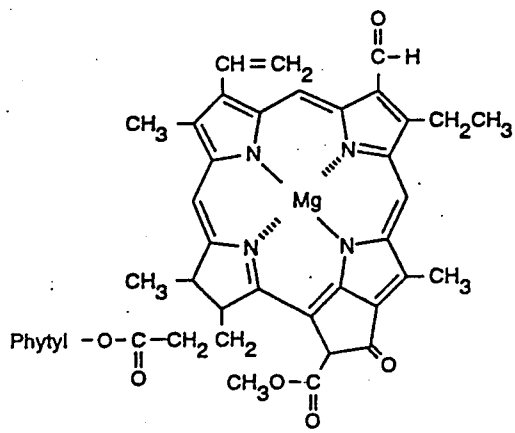

Figure 3: Chemical structures of dye molecules.

Polystyrene (PS)

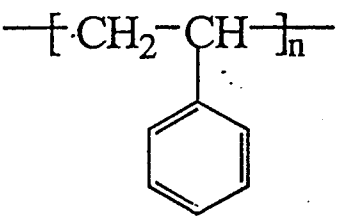

Polybutylacrylate (PBA)

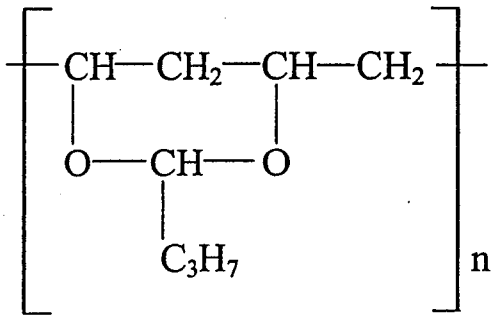

Polyvinylbutyral (PVB)

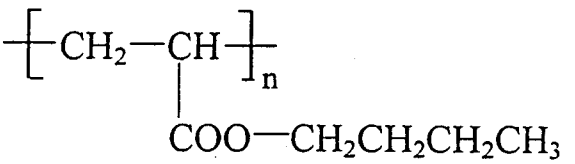

Figure 4: Chemical structures of organic polymers.

	TEOS	TPOT	ethanol	H_2O	HCl
SiO_2	1	—	4	4	0.01
SiO_2–TiO_2	0.95	0.05	8	4	0.01

Table 1: Molar ratio of materials for sol-gel synthesis of oxazine 4-doped SiO_2 and SiO_2-TiO_2.

1-propanol

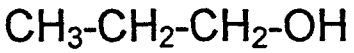

2-propanol

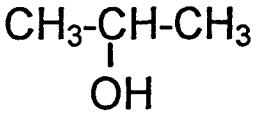

1-butanol

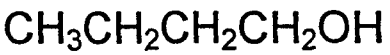

2-butanol

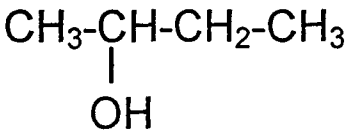

trimethylene glycol

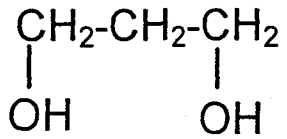

propylene glycol

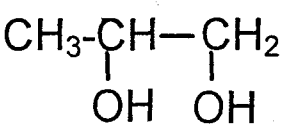

glycerol

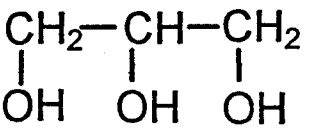

3-methylpentane

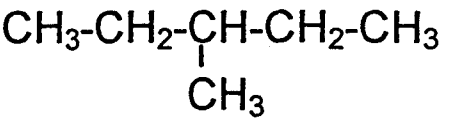

isopropylbenzene

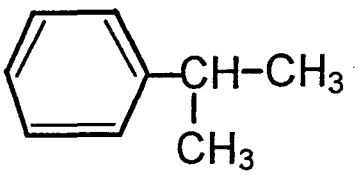

toluene

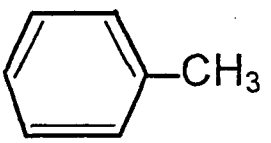

Figure 5: Chemical structures of organic solvents for molecular glasses.

Solvent	*M.W.*	*Tg* (K)
1-propanol	60.1	96[(d)]
2-propanol	60.1	121[(a)]
1-butanol	74.1	113[(a)]
2-butanol	74.1	120[(a)]
propylene glycol	76.1	172[(b)]
trimethylene glycol	76.1	152[(b)]
glycerol	92.1	194[(b)]
toluene-benzene	92.1	126[(c)]
isopropylbenzene	120.2	125[(d)]
3-methylpentane	86.2	77[(d)]

Table 2: Molecular weights(M.W.) and glass transition temperatures(T_g) for various organic solvents. See references (a)[29], (b)[84], (c)[31] and (d)[5].

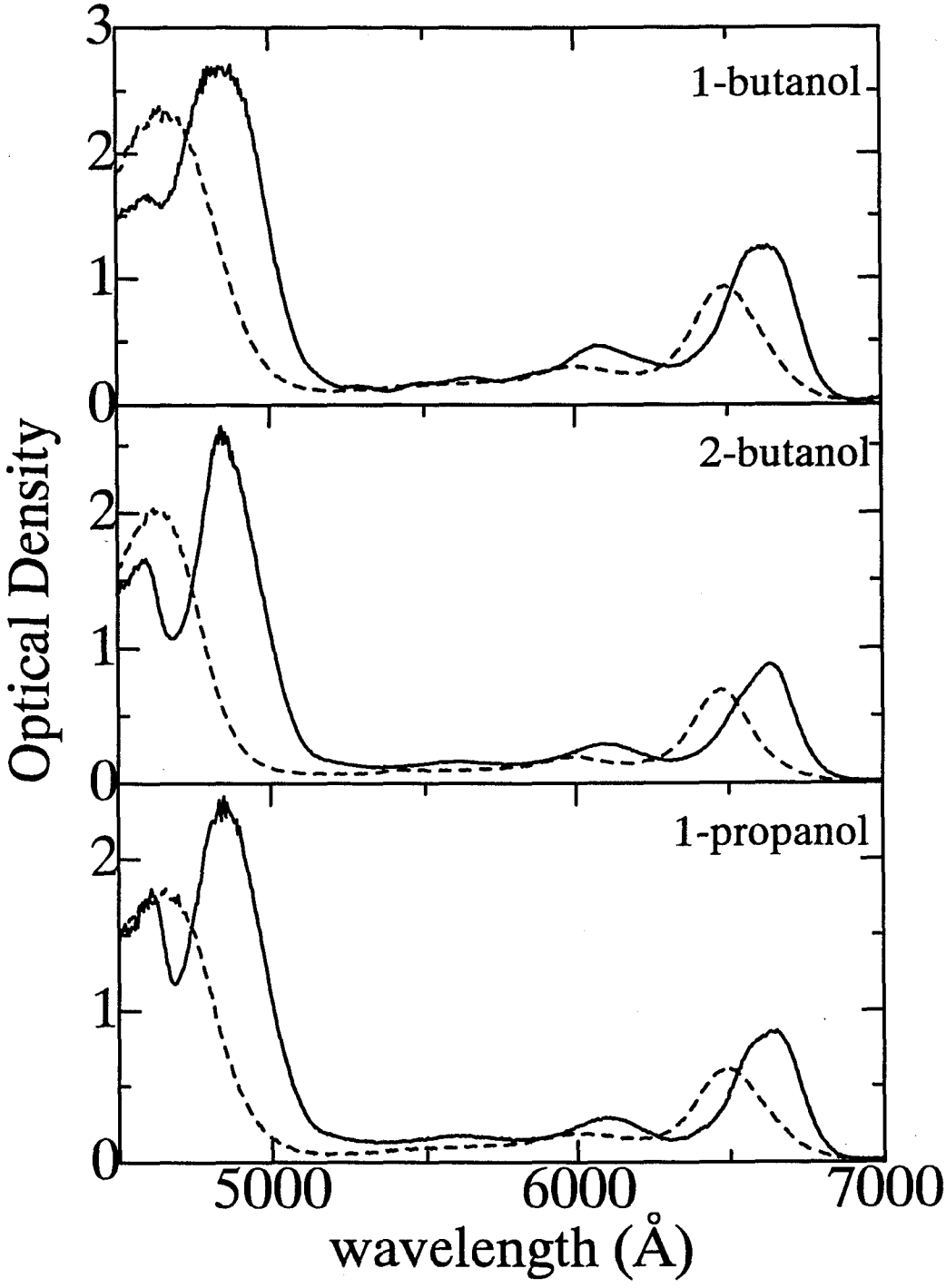

Figure 6: Absorption spectra of chlorophyll b-doped 1-butanol, 2-butanol and 1-propanol obtained at 4K(solid lines) and 300K(broken lines).

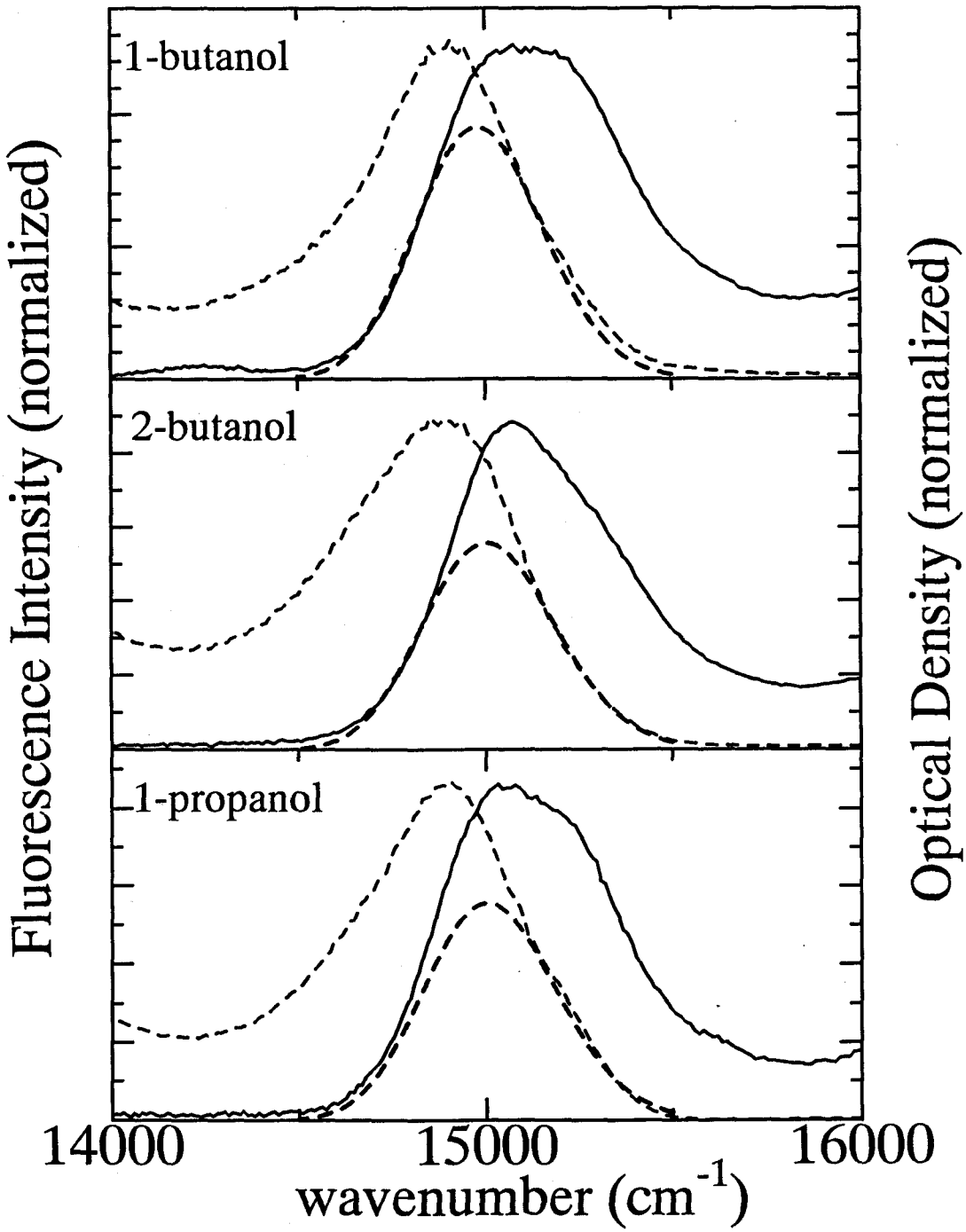

Figure 7: Absorption spectra(solid lines), off-resonance fluorescence spectra(thin broken lines) and the estimated site-energy distribution functions(thick broken lines) for the lowest excited-state of chlorophyll b-doped 1-butanol, 2-butanol and 1-propanol glasses at 4K. The wavelength of the excitation laser for the fluorescence spectra is 5145Å . Both intensities are normalized with their peak intensities.

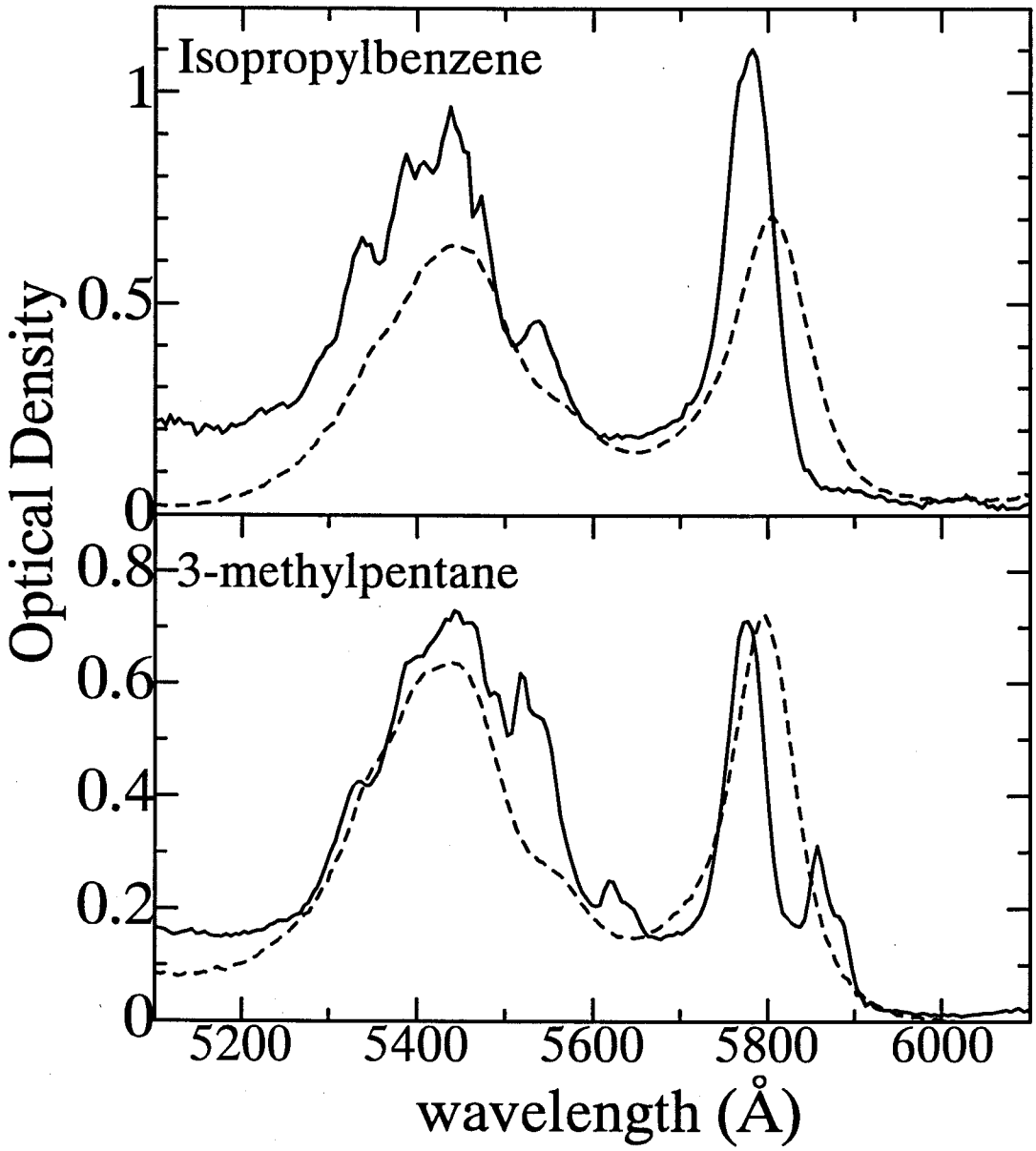

Figure 8: Absorption spectra for Mg-OEP-doped isopropylbenzene and 3-methylpentane at 4K(solid lines) and 300K(broken lines).

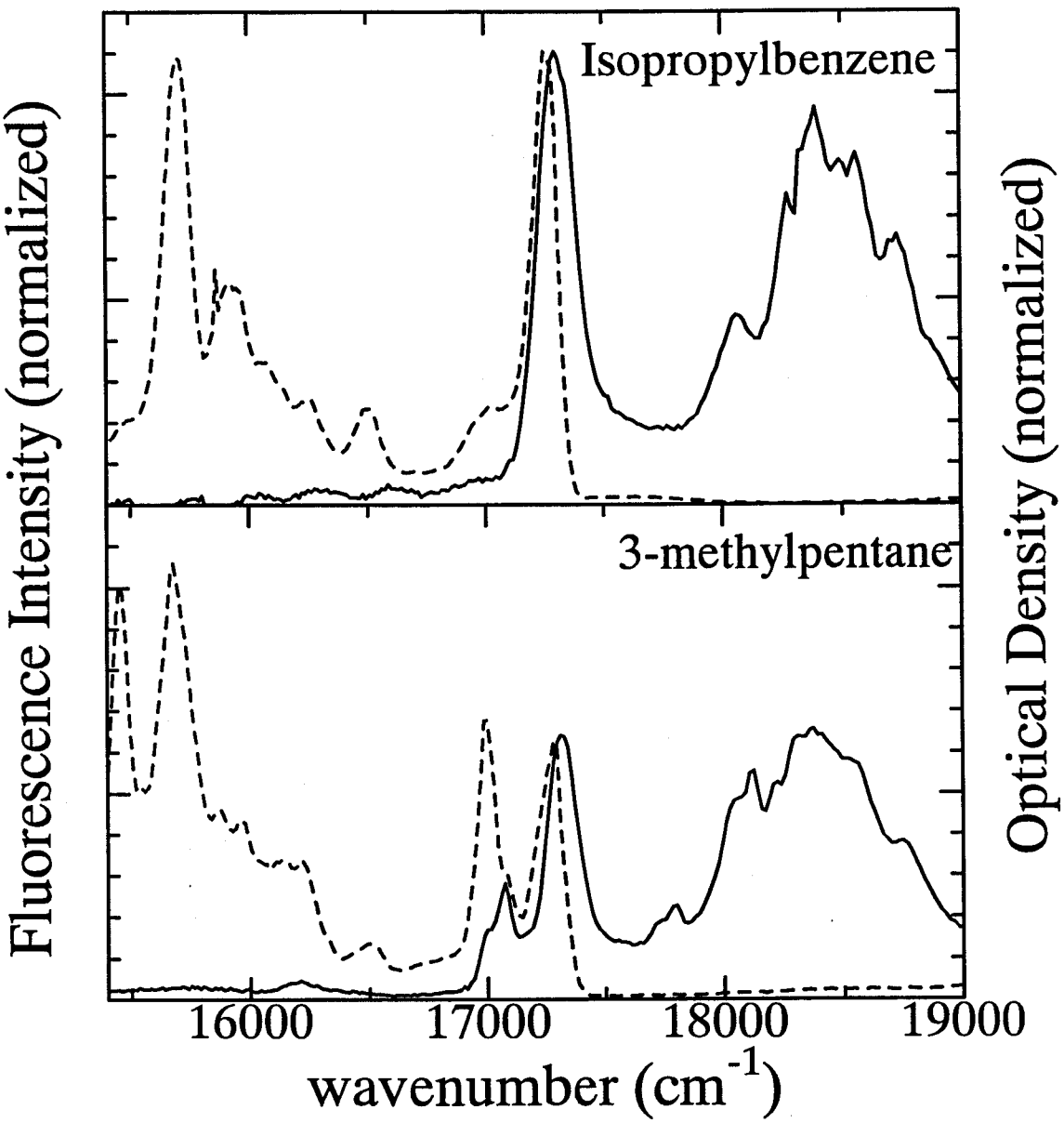

Figure 9: Absorption spectra(solid lines), off-resonance fluorescence spectra(broken lines) for Mg-OEP-doped isopropylbenzene and 3-methylpentane glasses at 4K. The wavelength of the excitation laser for these fluorescence spectra is 5145Å . Both intensities are normalized with their peak intensities.

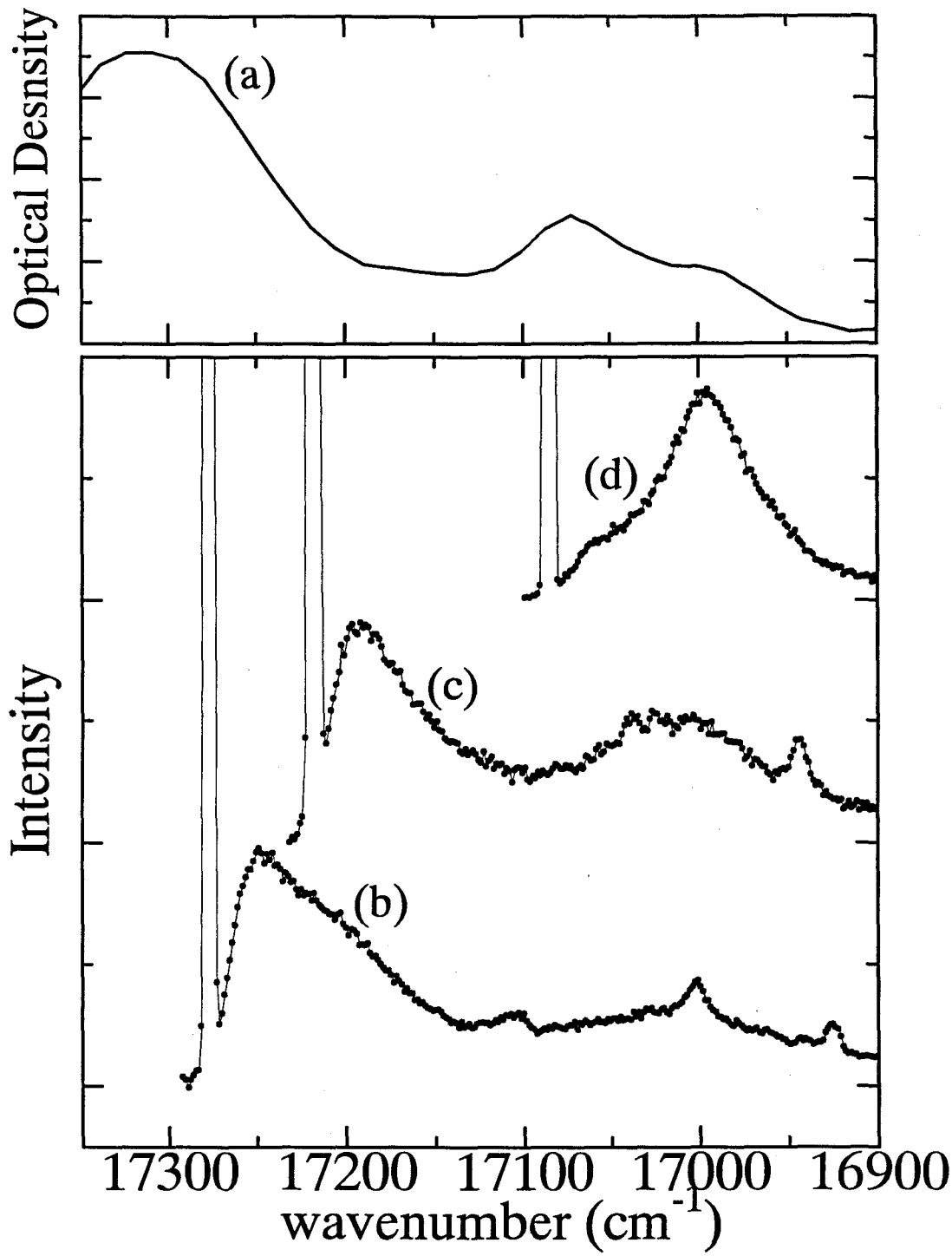

Figure 10: Site-selective fluorescence spectra for MgOEP-doped 3-methylpentane with excitation wavelengths of 5785Å($17286cm^{-1}$)(b), 5810Å($17218cm^{-1}$)(c) and 5855Å($17086cm^{-1}$)(d) together with the absorption spectrum (a).

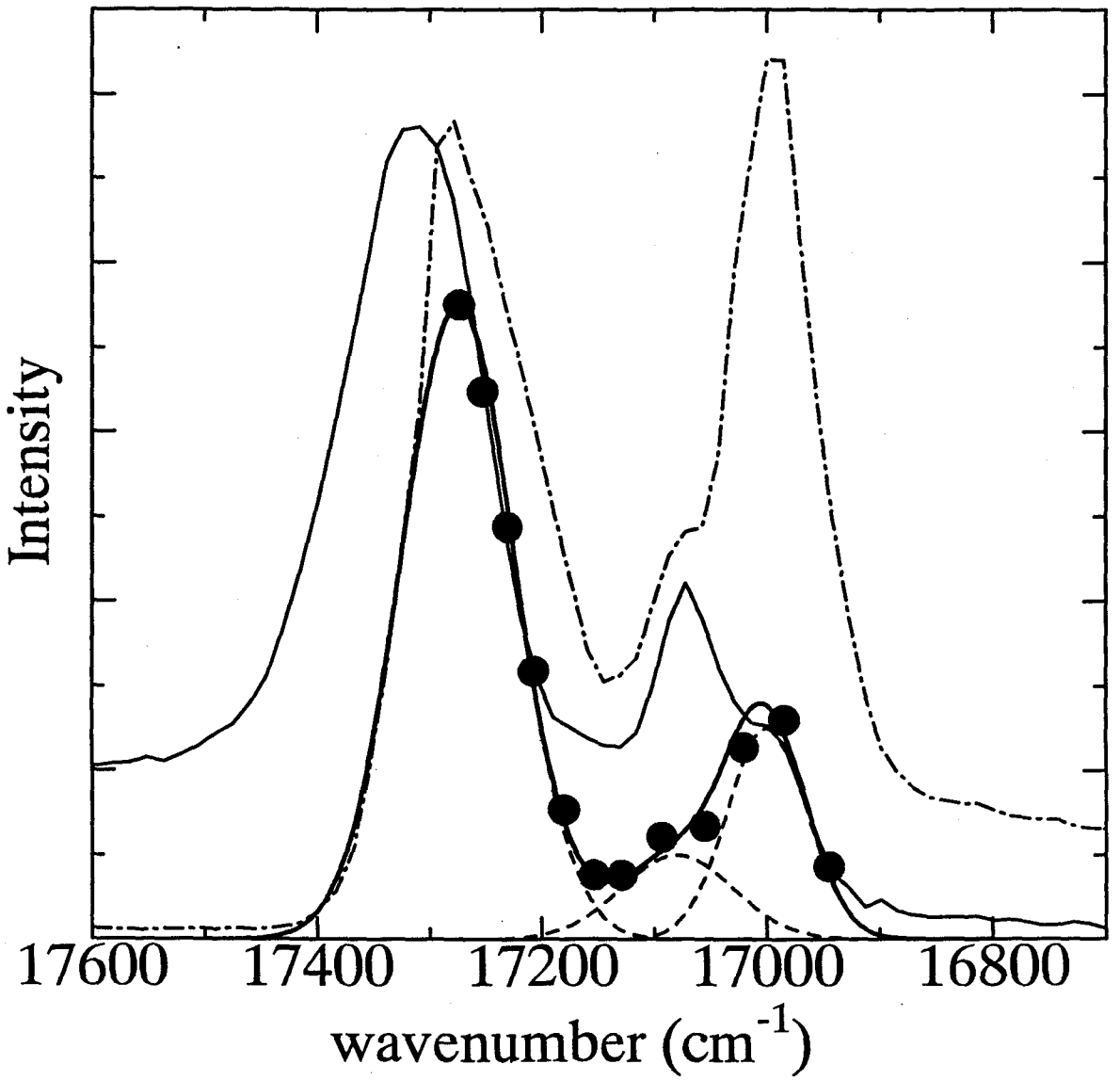

Figure 11: Distribution of the zero-phonon fluorescence intensity (circles) and fitted site-energy distribution function(thick solid line) for MgOEP-doped 3-methylpentane glass together with absorption (dotted broken line) and off-resonance fluorescence (solid line) spectra . This fitting function is the summation of three Gaussion functions (broken lines). Zero-phonon fluorescence intensities have been corrected for the reabsorption effect.

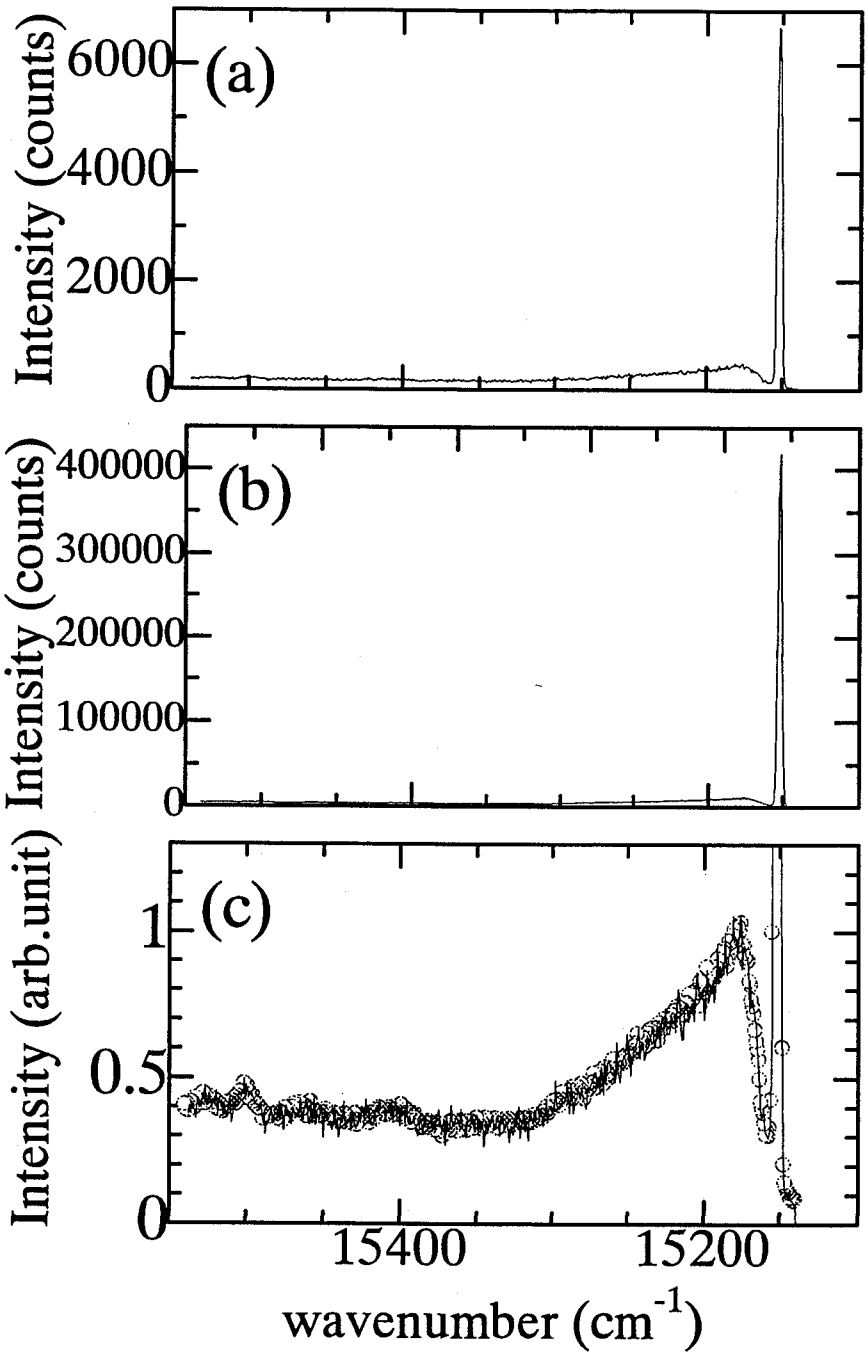

Figure 12: Time-resolved (a) and non-time-resolved (b) site-selective excitation spectrum for chlorophyll b-doped propylene glycol glass at 4K. The wavelength of the monochromator for detecting fluorescence was set to the lower energy side of the Q_y band, 6600ÅThe power of the excitation laser was 0.5mW/cm^2

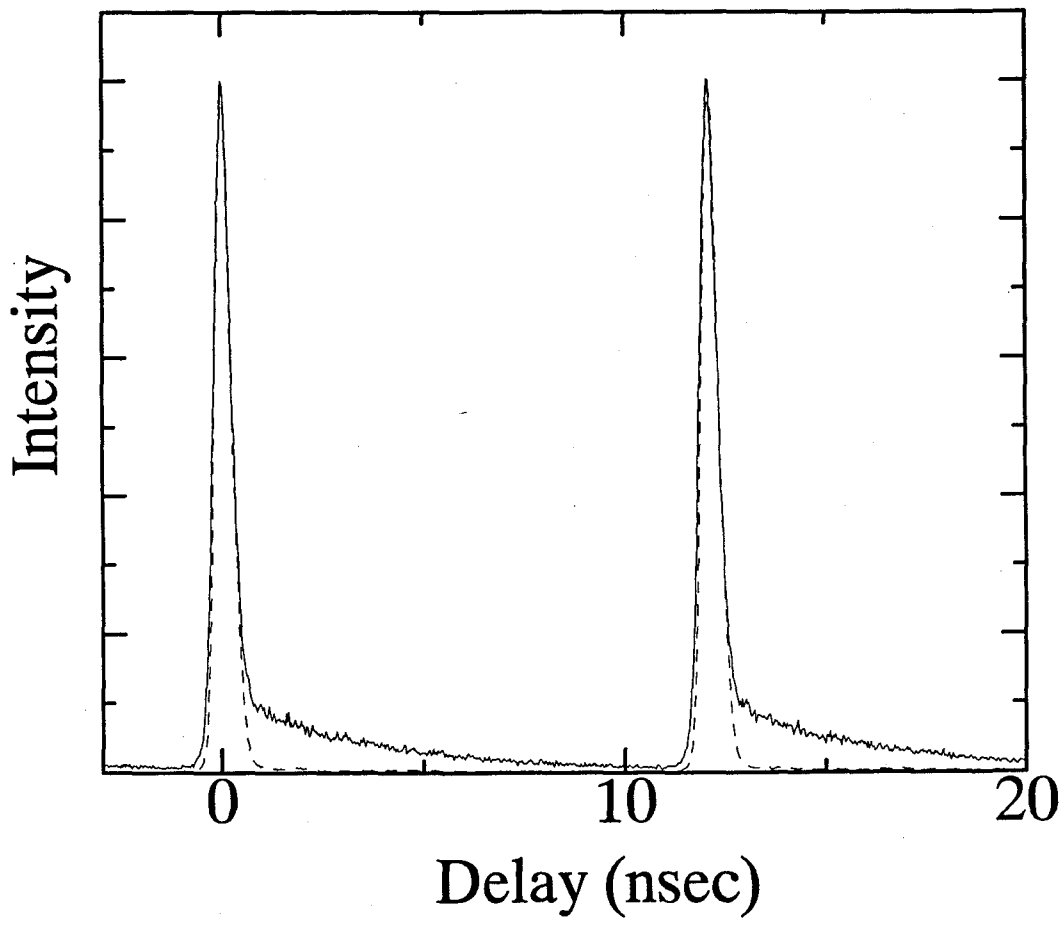

Figure 13: Time profiles of cw mode-locked dye laser pulses (broken line) and fluorescence (solid line). The driving frequency of the mode-locker was 40.8MHz.

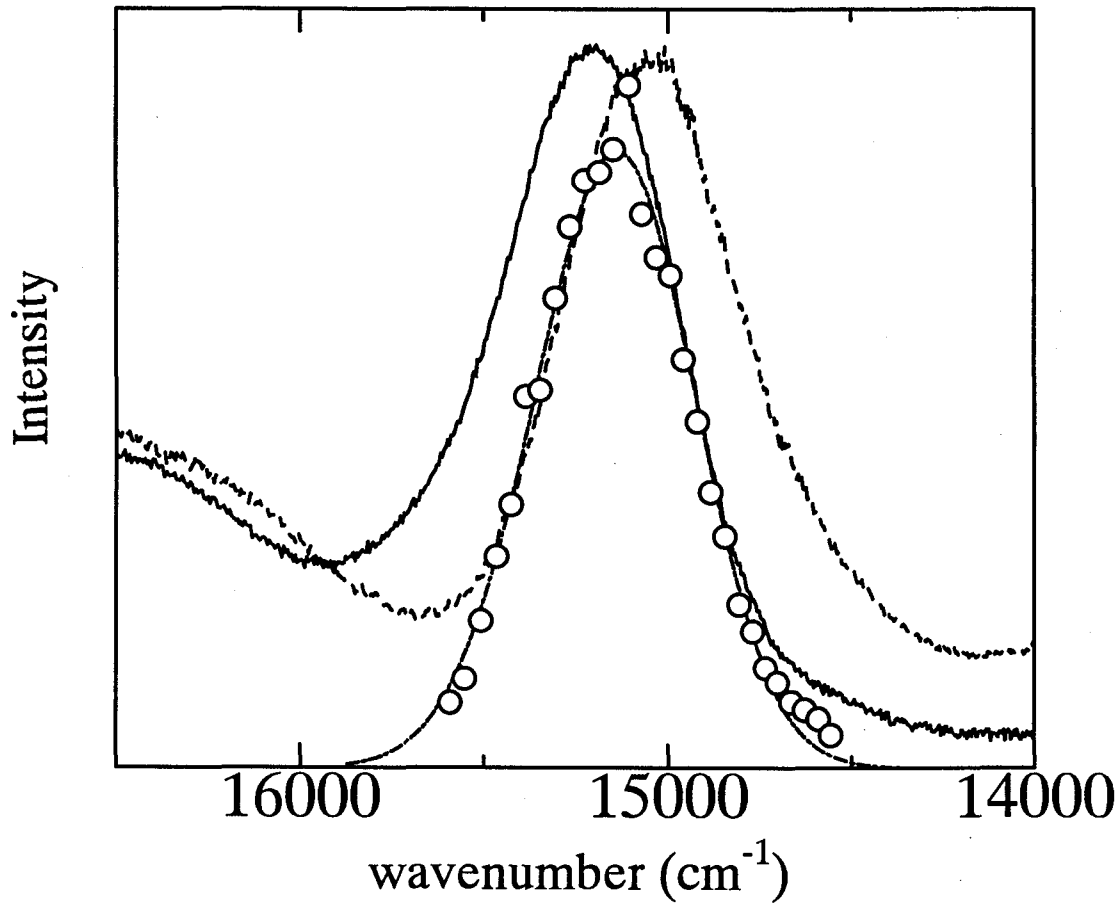

Figure 14: Distribution of the zero-phonon fluorescence intensity (circles) and fitted site-energy distribution function(dotted broken line) for chlorophyll b-doped propylene glycol glass together with absorption (solid line) and off-resonance fluorescence (broken line) spectra . This fitting function is a Gaussion function. Zero-phonon fluorescence intensities have been corrected for the reabsorption effect.

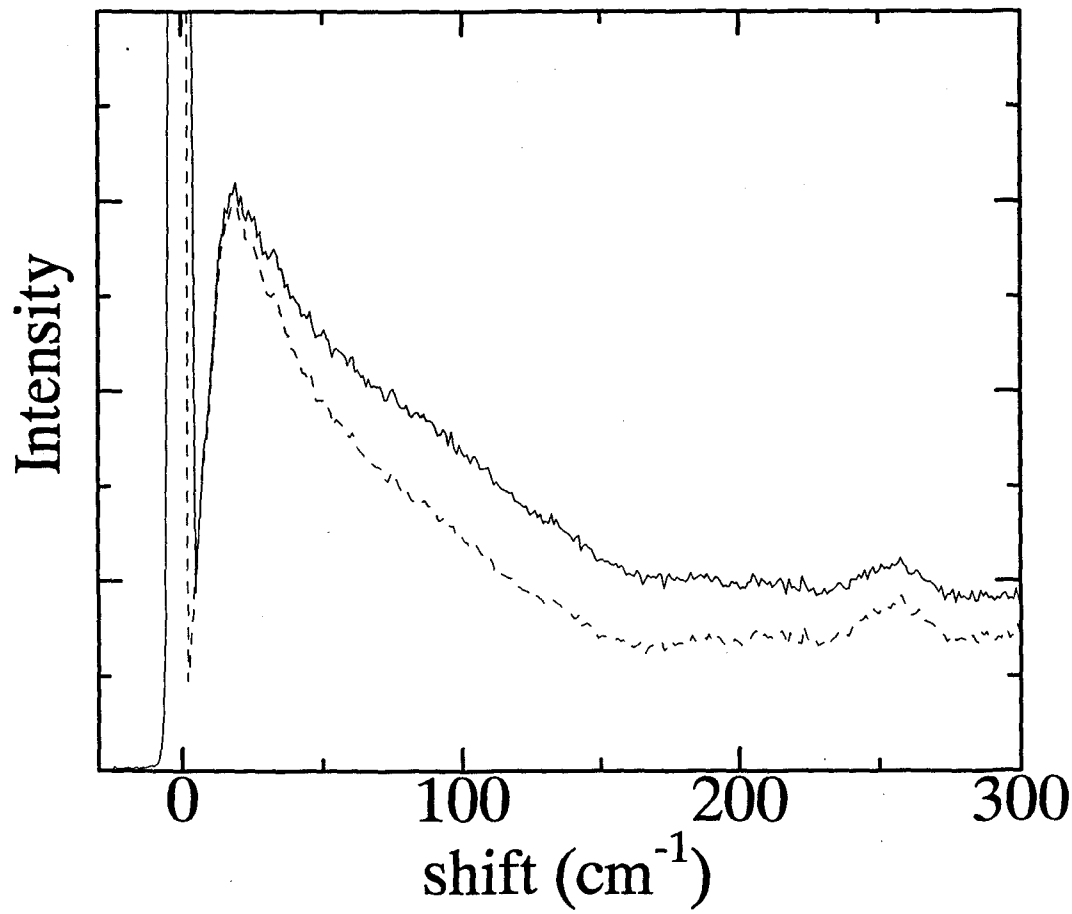

Figure 15: Site-selective excitation spectrum (solid line) together with the single-site spectrum (broken line) for chlorophyll b-doped 1-propanol glass at 4K.

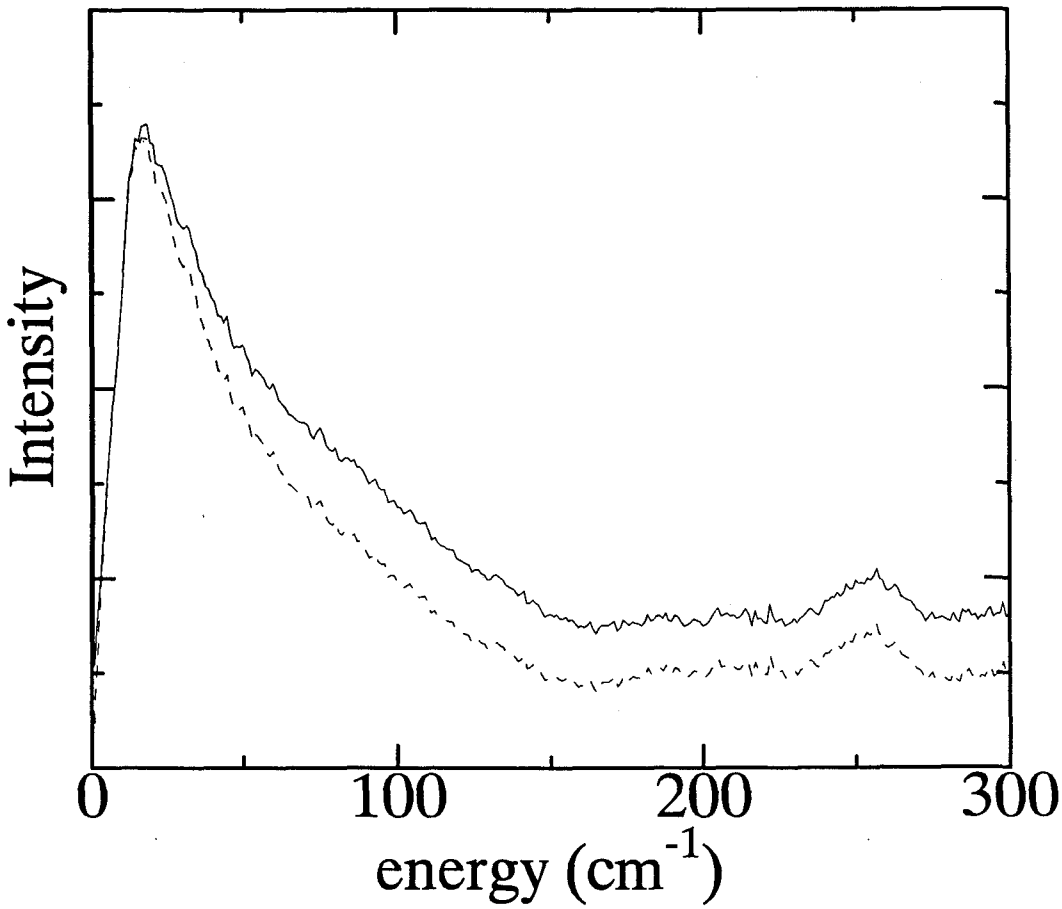

Figure 16: WDOS (broken line) and single-site spectrum (solid line) for chlorophyll b-doped 1-propanol glass.

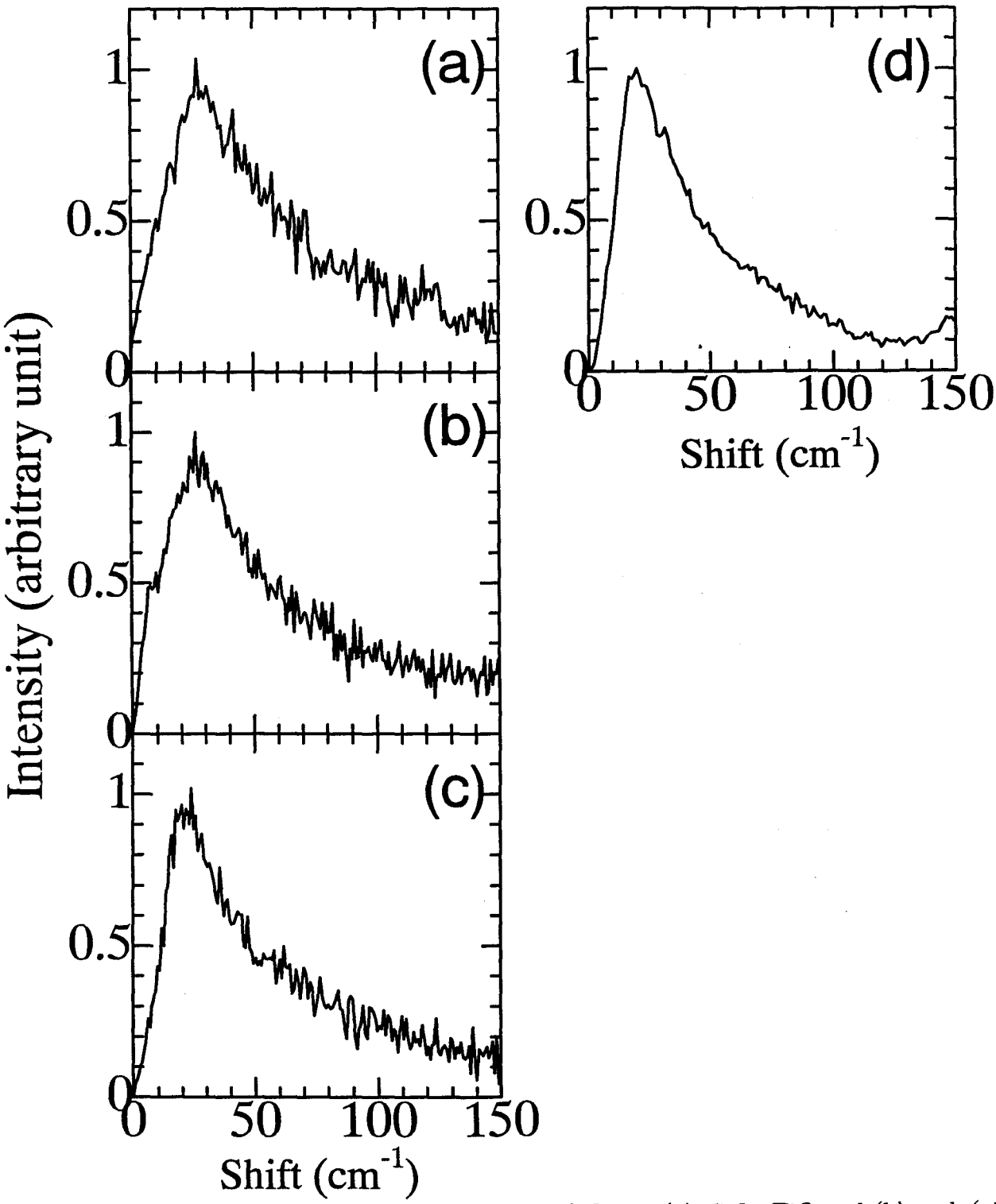

Figure 17: WDOS spectra for oxazine 4-doped SiO_2 gel (a), SiO_2-TiO_2 gel (b), poly(vinyl butyral) (c) and Zn-phthalocyanine-doped poly(butyl acrylate) (d).

chromophore	*host matrix*	*peak freq.* (cm^{-1})	*DWF*
Chlorophyll-b	poly(styrene)	13	0.37
Chlorin	poly(styrene)	13	0.36
Zn-Pc	poly(butyl acrylate)	20	0.55
oxazine 4	poly(vinyl butral)	22	0.39
oxazine 4	SiO_2	27	0.36
oxazine 4	SiO_2-TIO_2	27	0.34
Al-Pc	poly(styrene)	13	0.36
Zn-Pc	poly(styrene)	13	0.36
Li2-Pc	poly(styrene)	13	0.49
Mg-OEC	poly(styrene)	13	0.49
Mg-OEP	poly(styrene)	13	0.56
Mg-OEP	poly(methyl methacrylate)	14	0.41
Mg-OEP	poly(butadiene)	22	0.63
Mg-OEP	poly(isobutyrene)	19	0.66
Mg-OEP	epoxy resin	19	0.59
Zn-PP	Myoglobin	29	0.55

Table 3: Peak frequencies and Debye-Waller factors(DWFs) of WDOS spectra for various dye-doped polymeric systems. Six systems at the top of this table were newly investigated in this work. See reference [63] for the other systems.

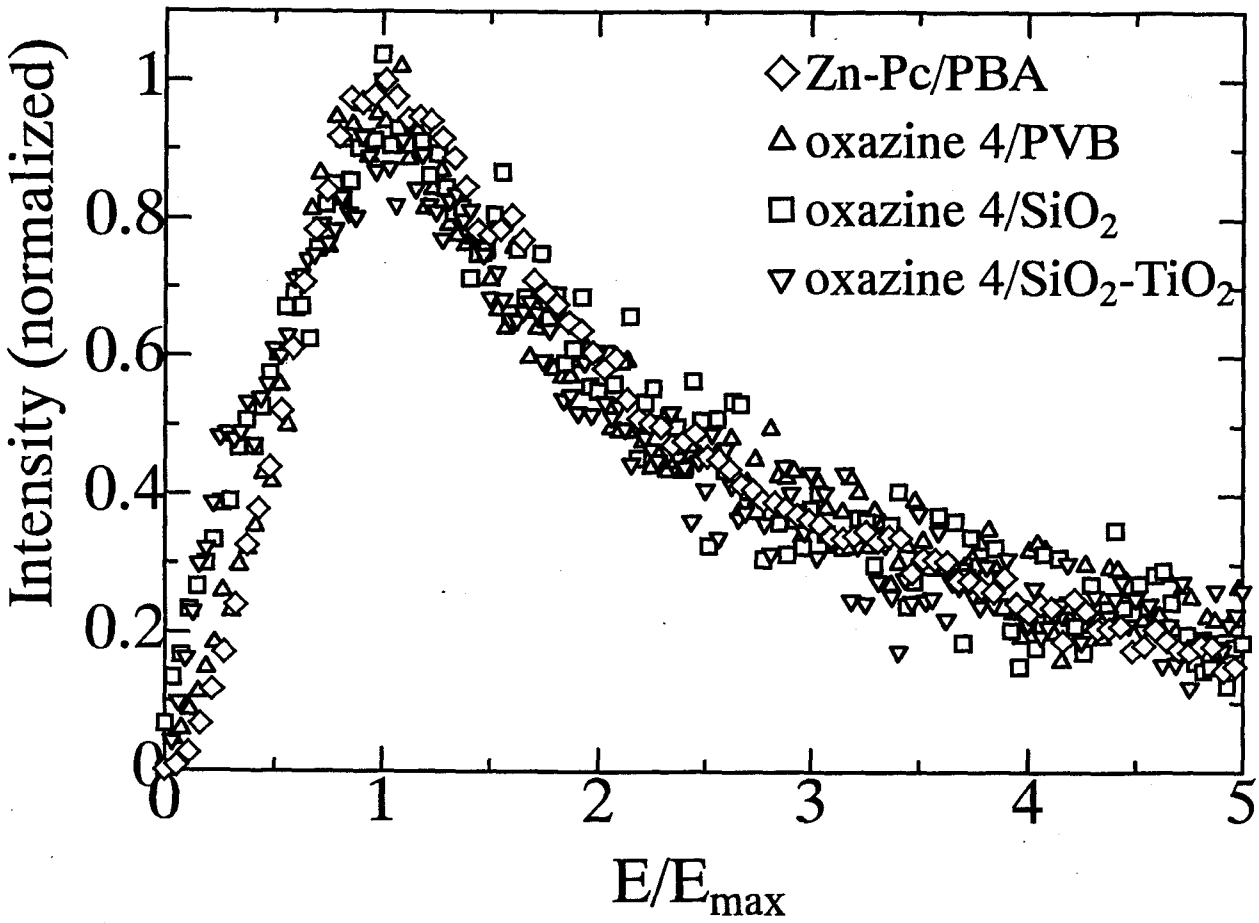

Figure 18: WDOSs spectra for various dye-doped polymeric disordered systems normalized by the peak frequencies and the peak intensities.

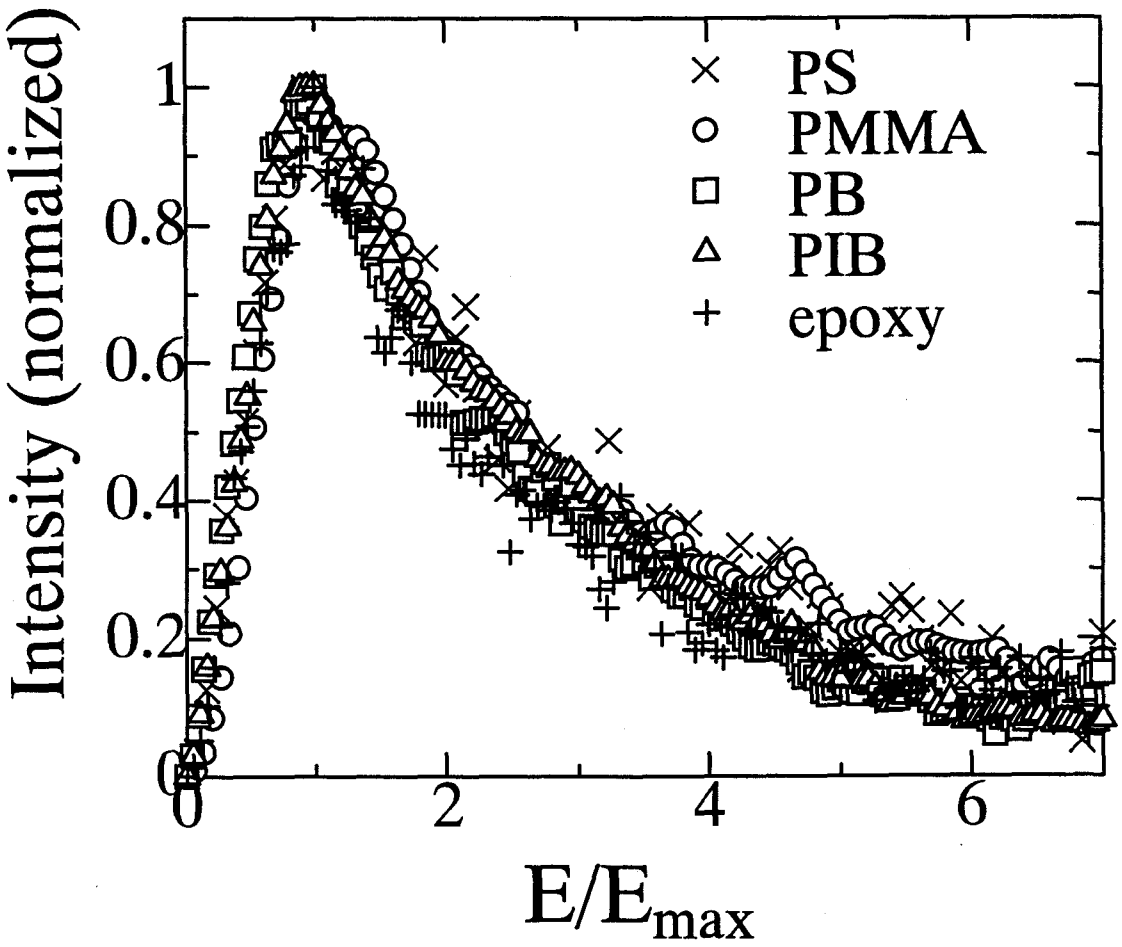

Figure 19: WDOSs spectra for MgOEP-doped organic polymers rescaled by the peak frequencies and the peak intensities.

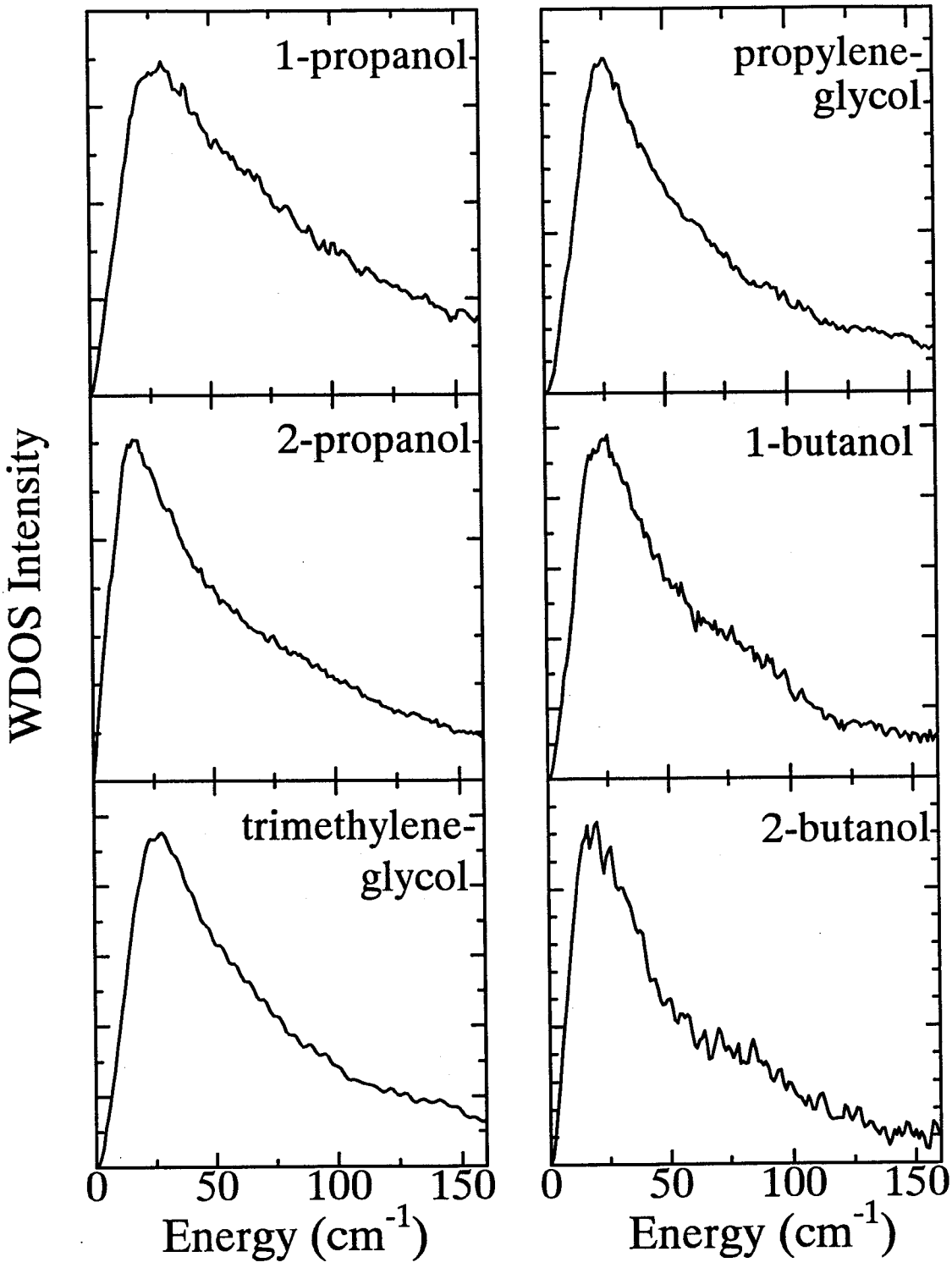

Figure 20: WDOS spectra for dye-doped alcoholic glasses.

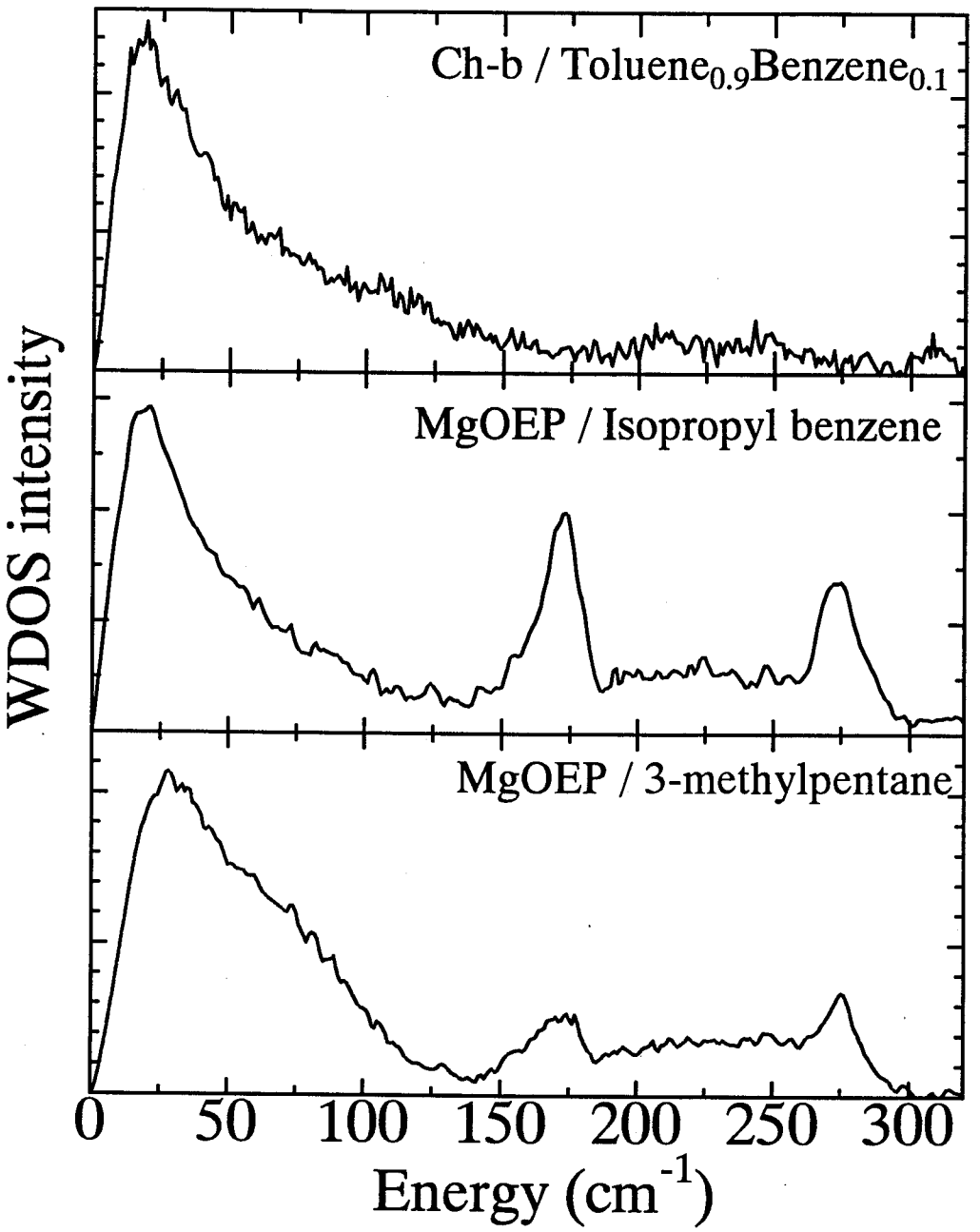

Figure 21: WDOS spectra for dye-doped non-alcoholic glasses.

chromophore	*solvent*	*peak freq.*(cm^{-1})	*DWF*
Chlorophyll-b	1-propanol	26	0.62
Chlorophyll-b	2-propanol	17	0.47
Chlorophyll-b	1-butanol	23	0.38
Chlorophyll-b	2-butanol	17	0.32
Chlorophyll-b	trimethylene glycol	25	0.35
Chlorophyll-b	propylene glycol	25	0.39
oxazine 1	glycerol	28	0.35
oxazine 4	1-propanol	25	0.45
Chlorophyll-b	toluene-benzene	18	0.38
MgOEP	isopropylbenzene	18	0.59
MgOEP	3-methylpentane	27	0.37

Table 4: Peak frequencies and Debye-Waller factors(DWFs) of WDOS spectra for various molecular glasses.

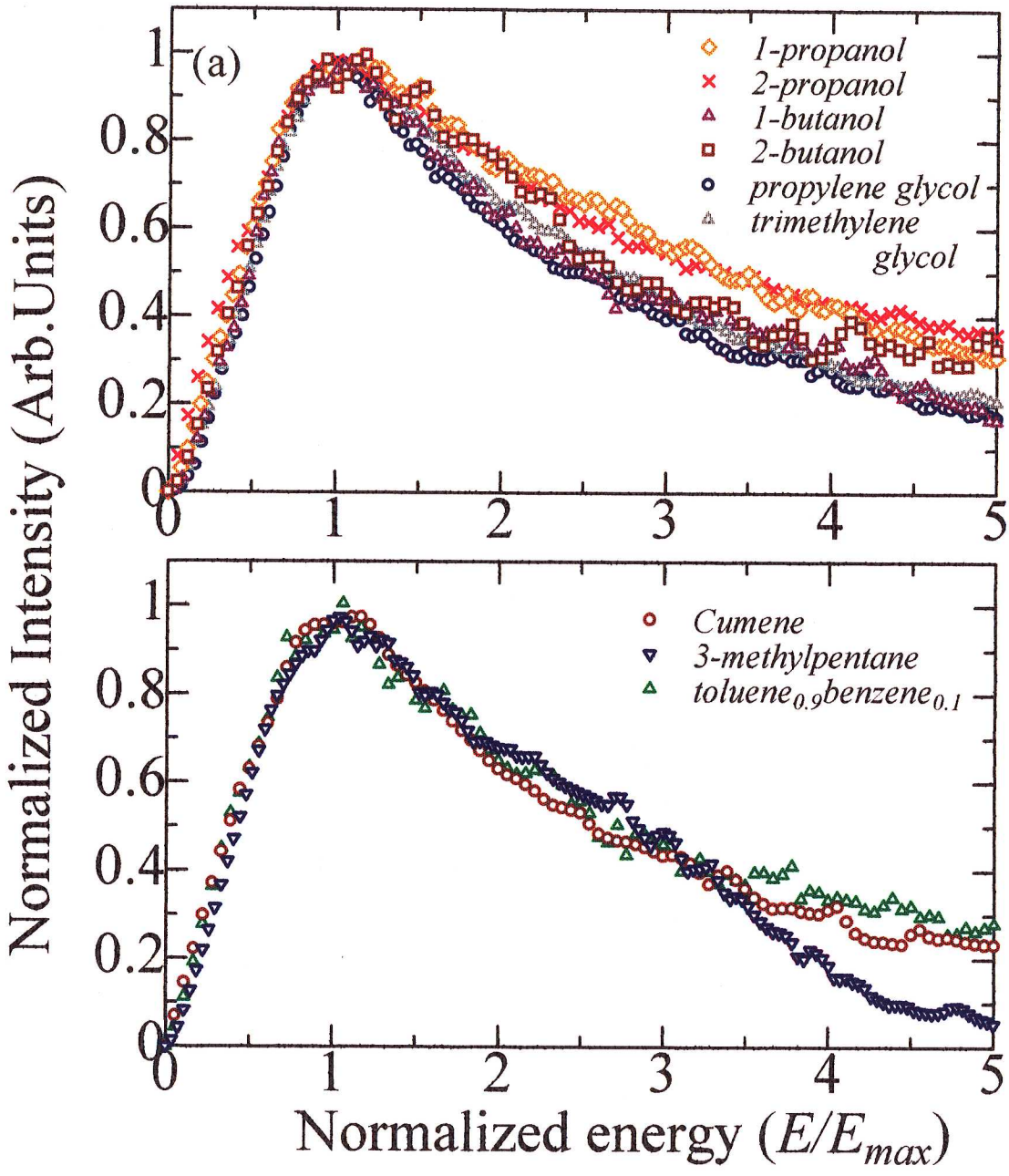

Figure 22: Rescaled WDOS spectra for alcoholic (a) and non-alcoholic (b) glasses.

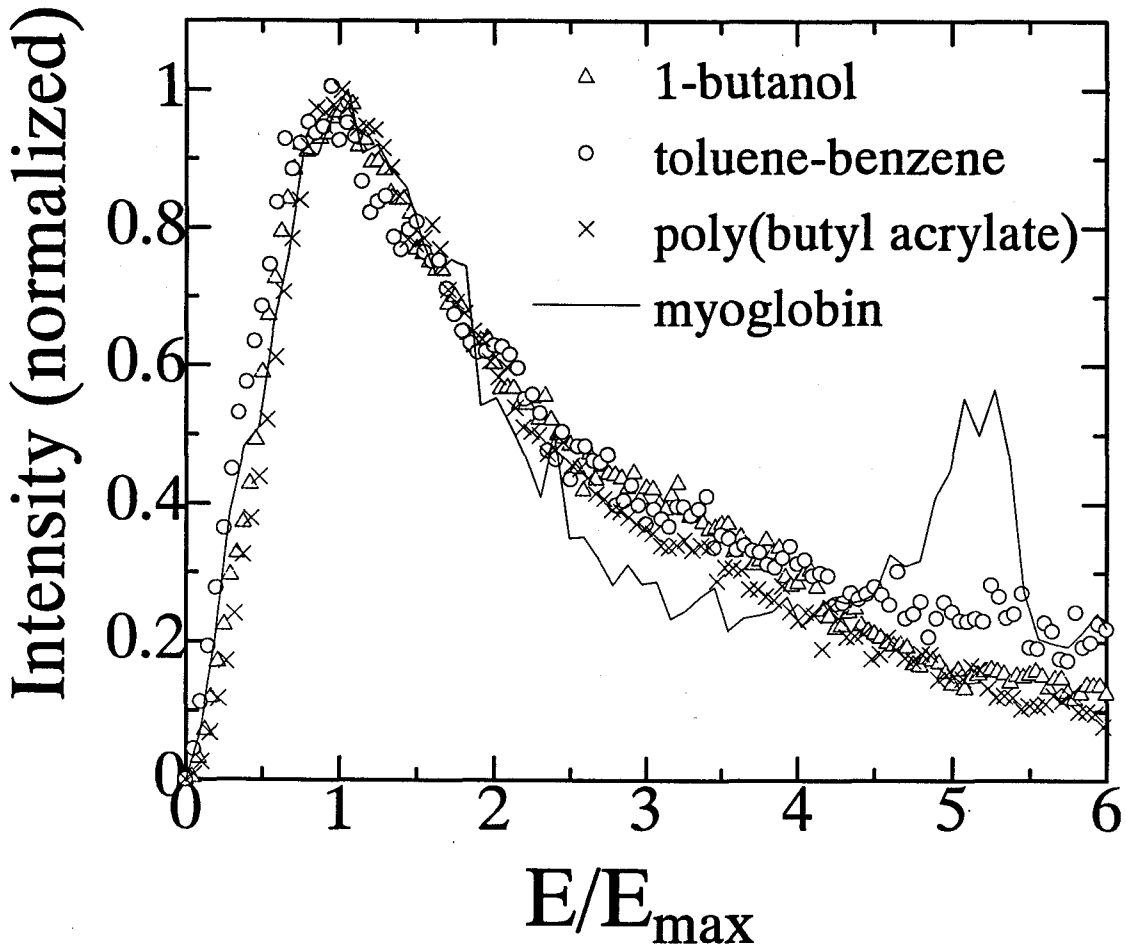

Figure 23: Rescaled WDOS spectrum for Zn-porphyrin-substituted myoglobin (solid line) together with those for dye-doped amorphous materials (symbols).

Low-frequency dynamics in various disordered materials examined via fluorescence spectroscopy of incorporated chromophores

Yoshiro Ichino

Dissertation in Physics
Graduate School of Science
Osaka University
1997

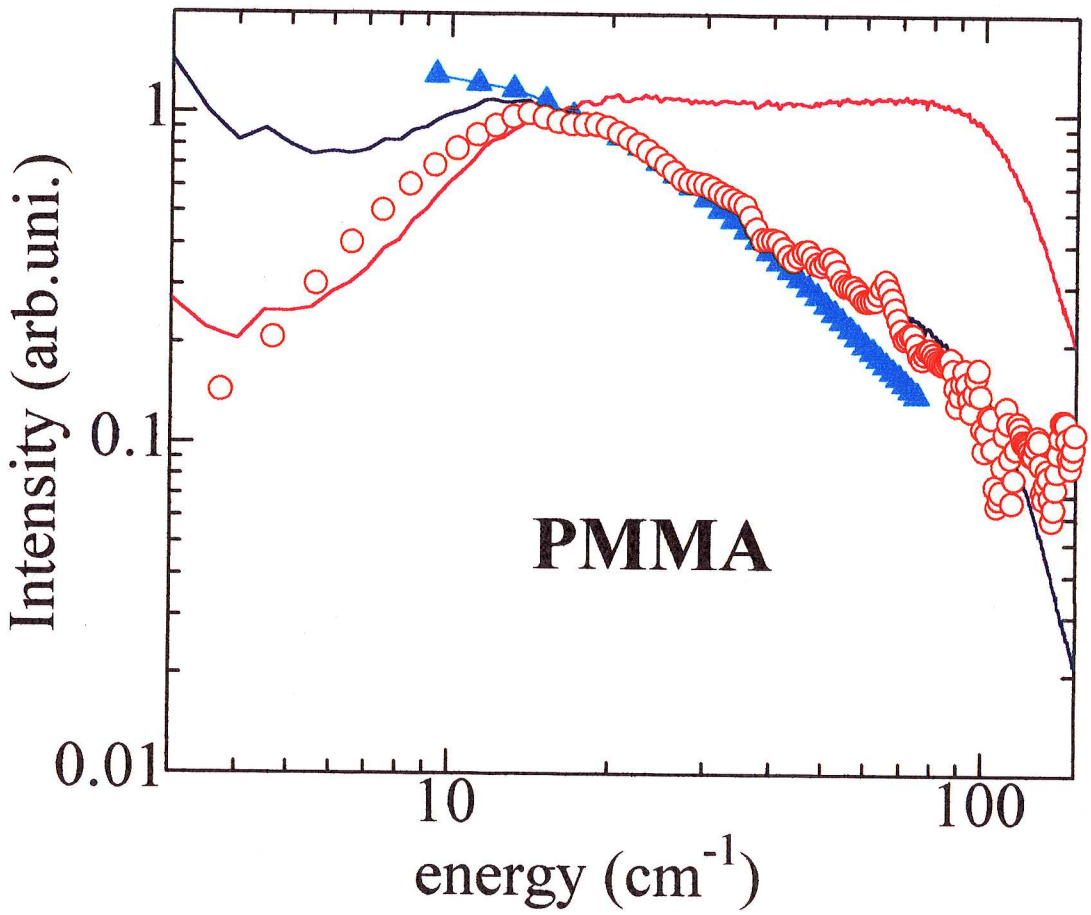

Figure 24: Comparison of WDOS spectra, Raman scattering and inelastic neutron scattering spectra for poly(methylmethacrylate)(PMMA), polystyrene(PS) and poly(butadiene)(PB). Blue and pink solid lines represent Raman scattering spectra given by $I(\omega)/\omega^2(n+1)$ and $I(\omega)/\omega(n+1)$ respectively. Triangles and circles represent neutron scattering given by $g(\omega)/\omega^2$ and WDOS spectra respectively.

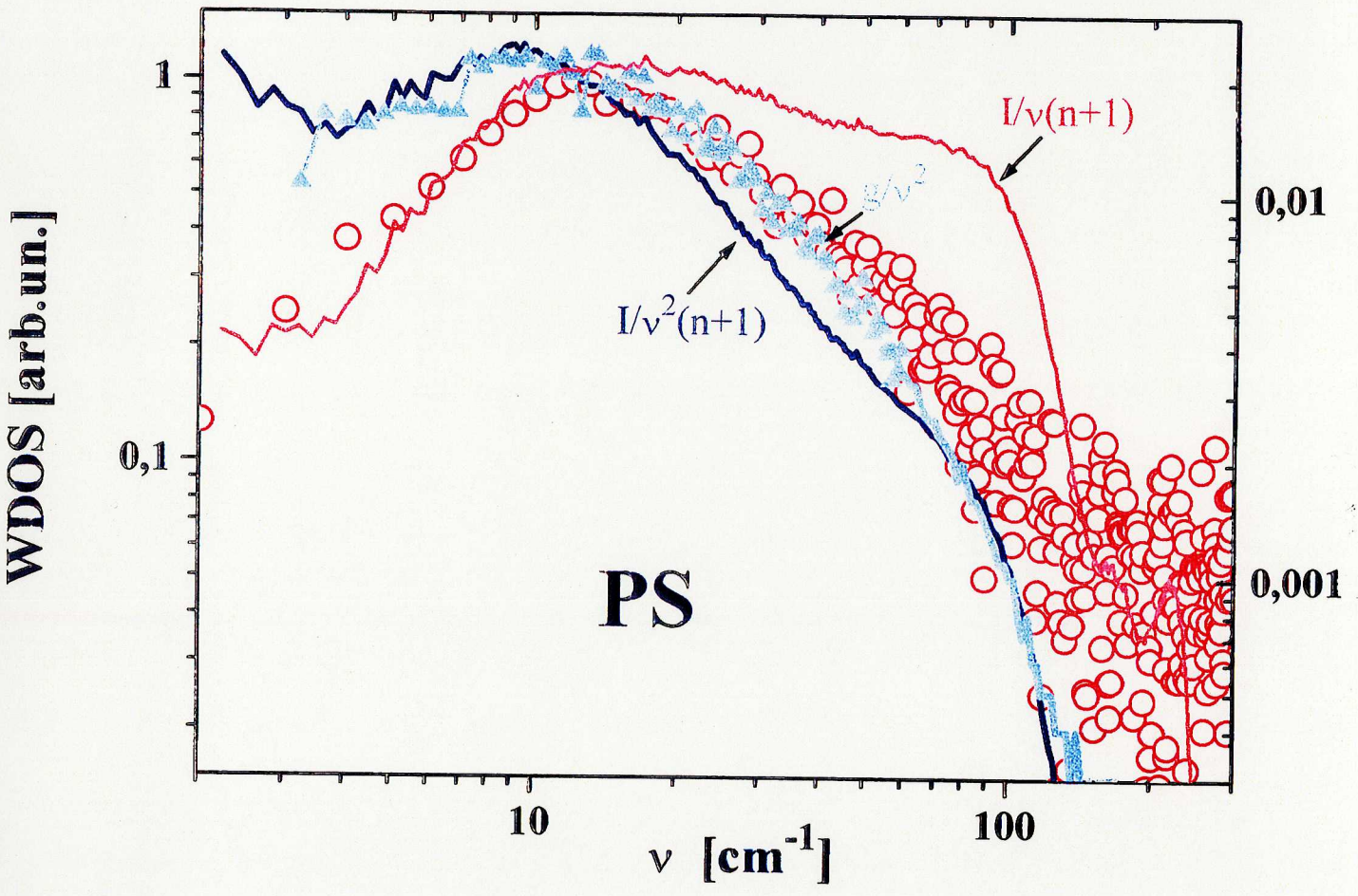
WDOS [arb.un.]
1
0,1
0,01
0,001
I/ν(n+1)
g/ν²
I/ν²(n+1)
PS
10
100
ν [cm⁻¹]

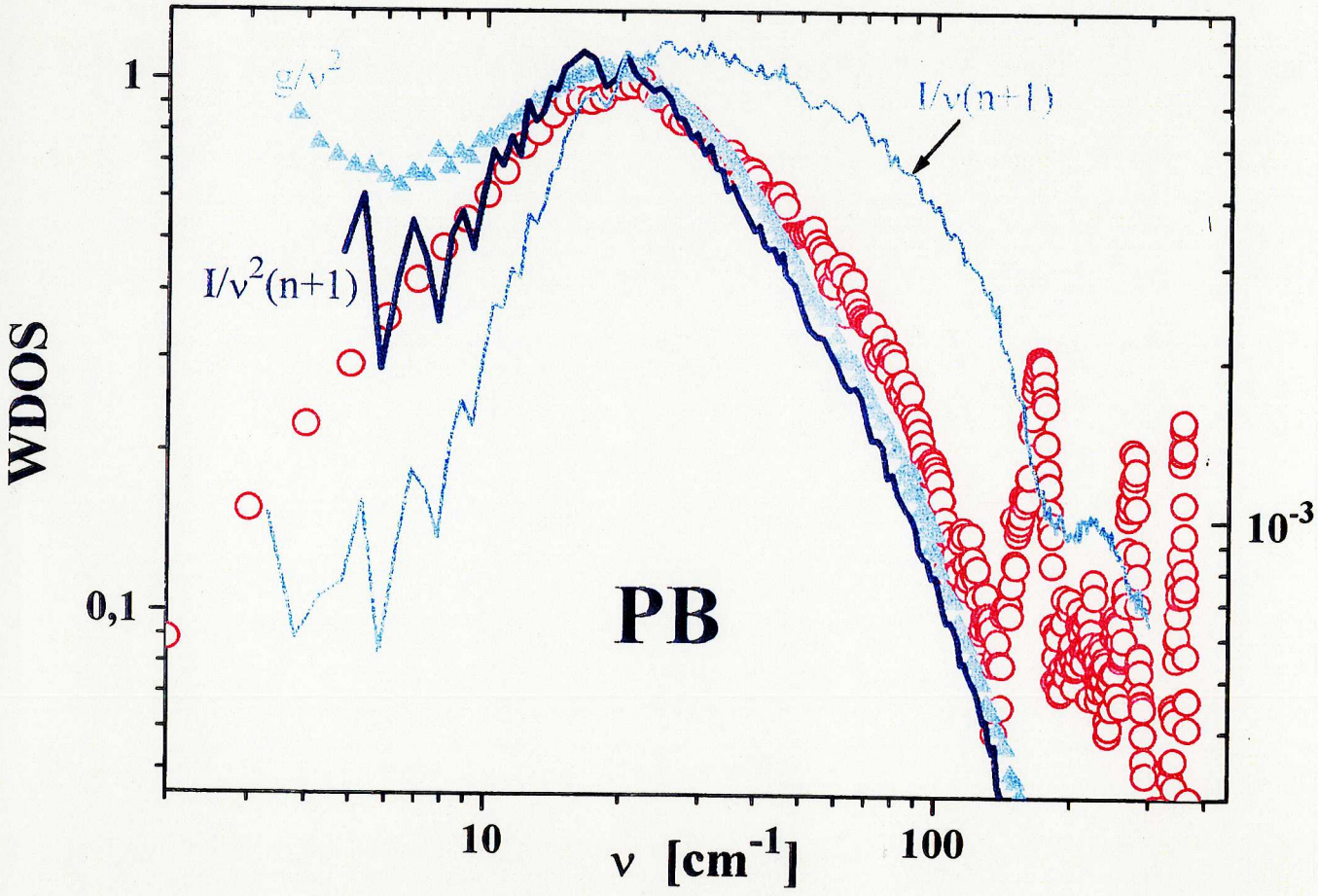
WDOS
1
0,1
10⁻³
g/ν²
I/ν(n+1)
I/ν²(n+1)
PB
10
100
ν [cm⁻¹]

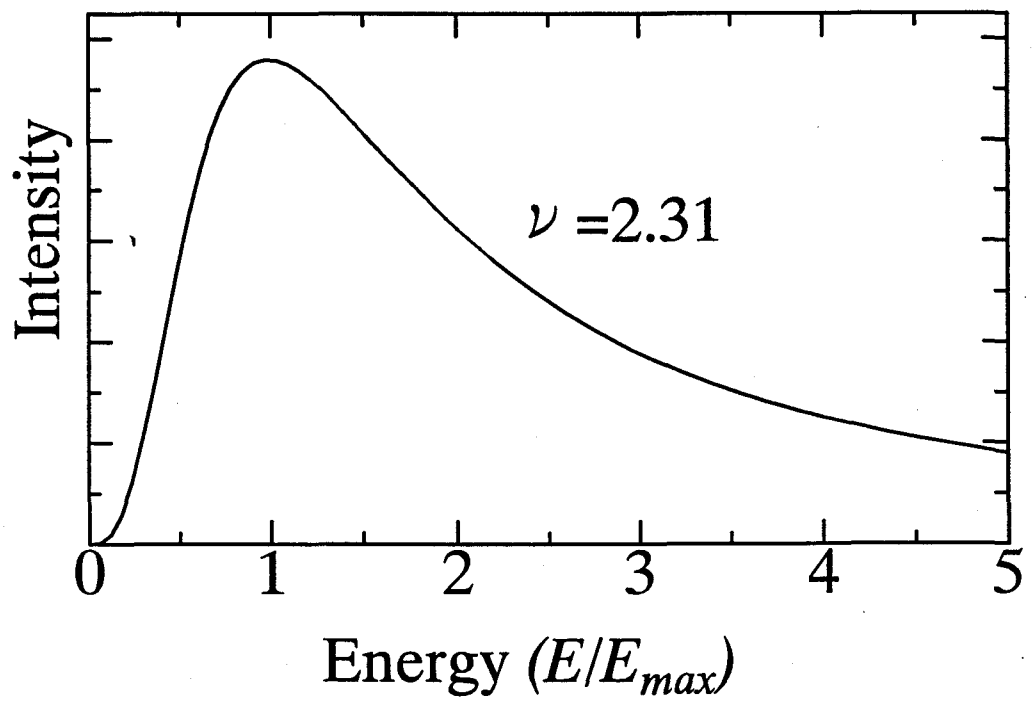

Figure 25: Theoretical function Eq.(4.32) obtained by the fracton model proposed by Ivanda and coworkers [19].

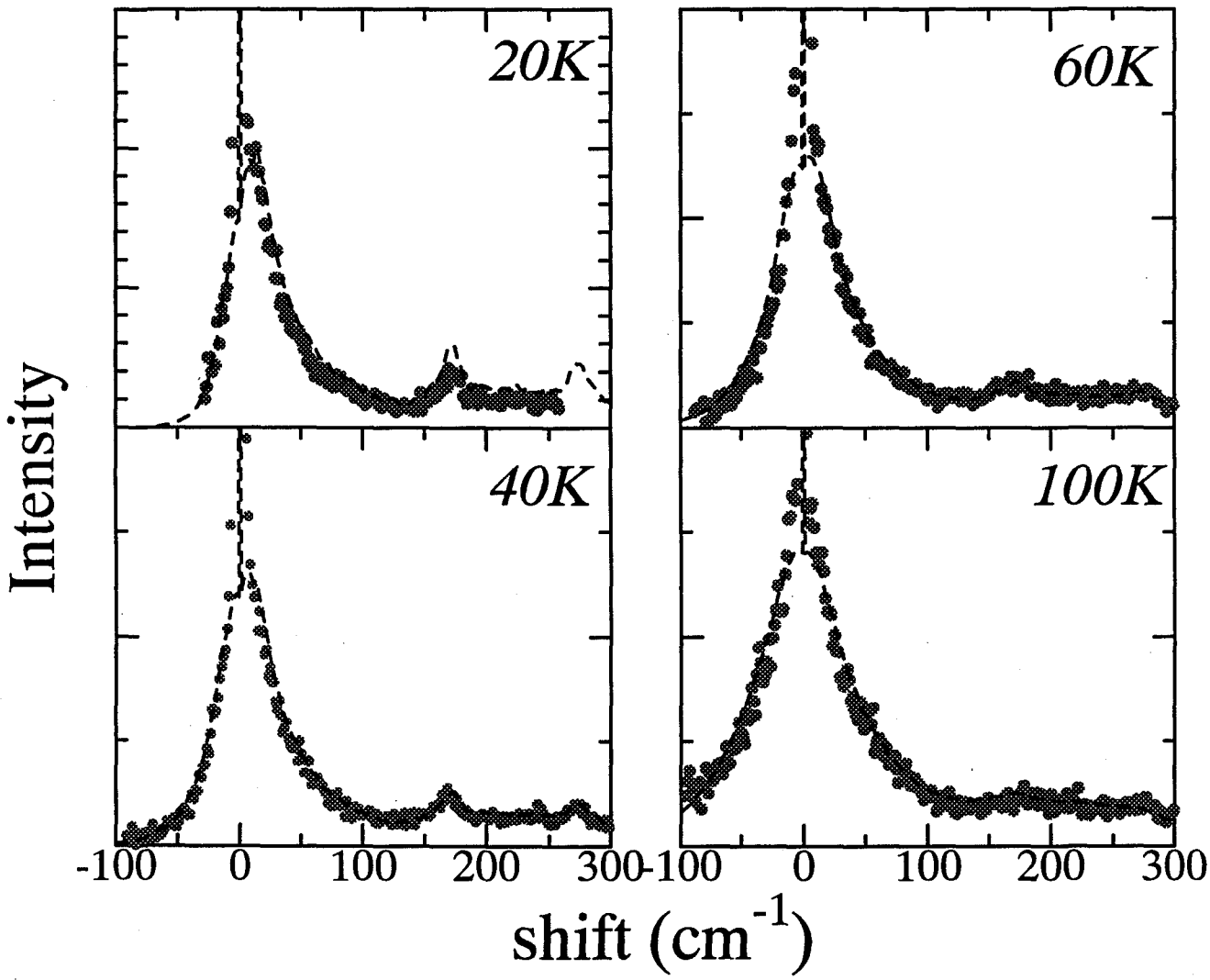

Figure 26: Measured (dots) and calculated (broken lines) site-selective fluorescence spectra for MgOEP-doped isopropylbenzene glass at various temperatures.

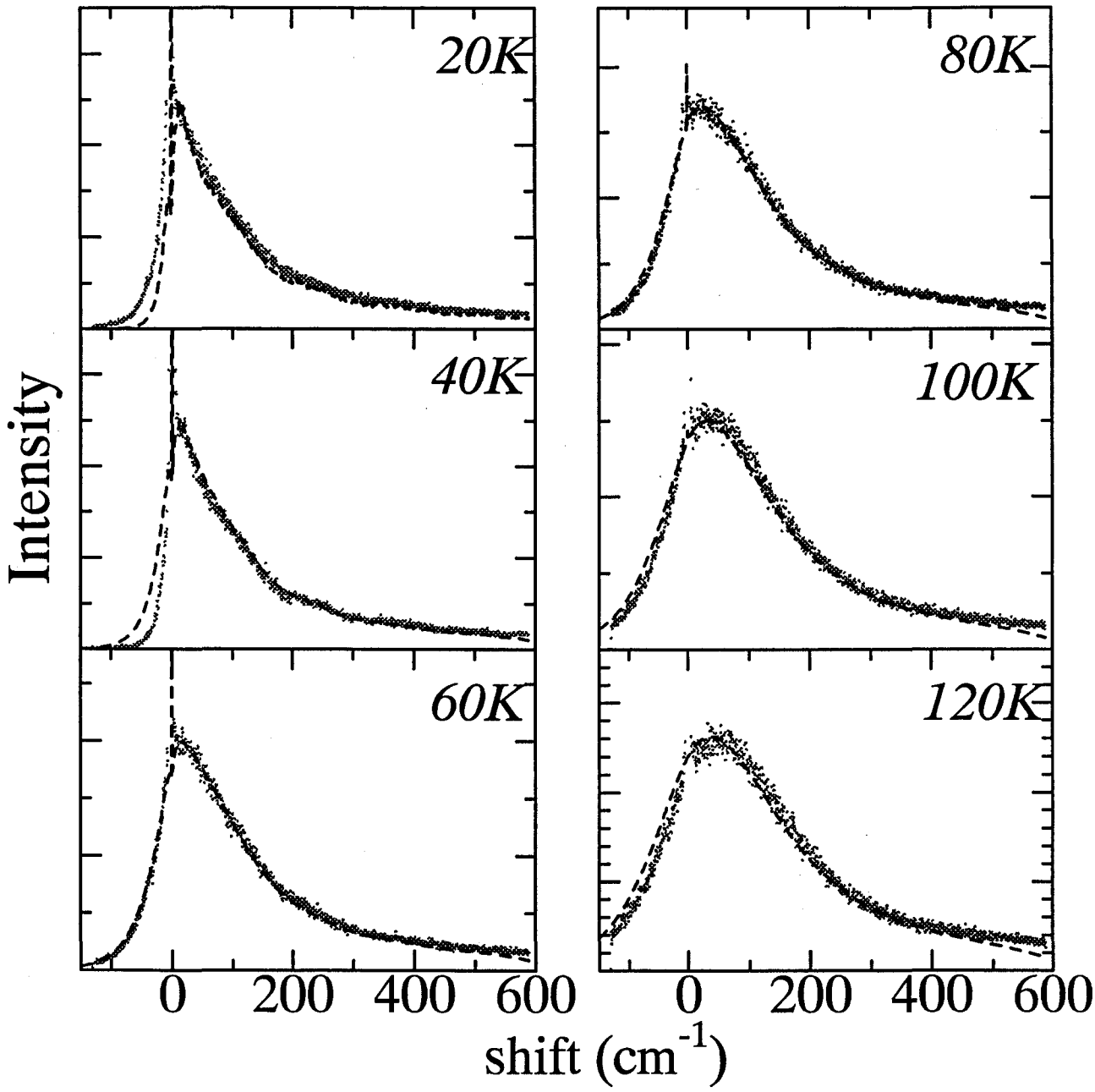

Figure 27: Measured (dots) and calculated (broken lines) site-selective fluorescence spectra for MgOEP-doped toluene$_{0.9}$-benzene$_{0.1}$ mixture glass at various temperatures.

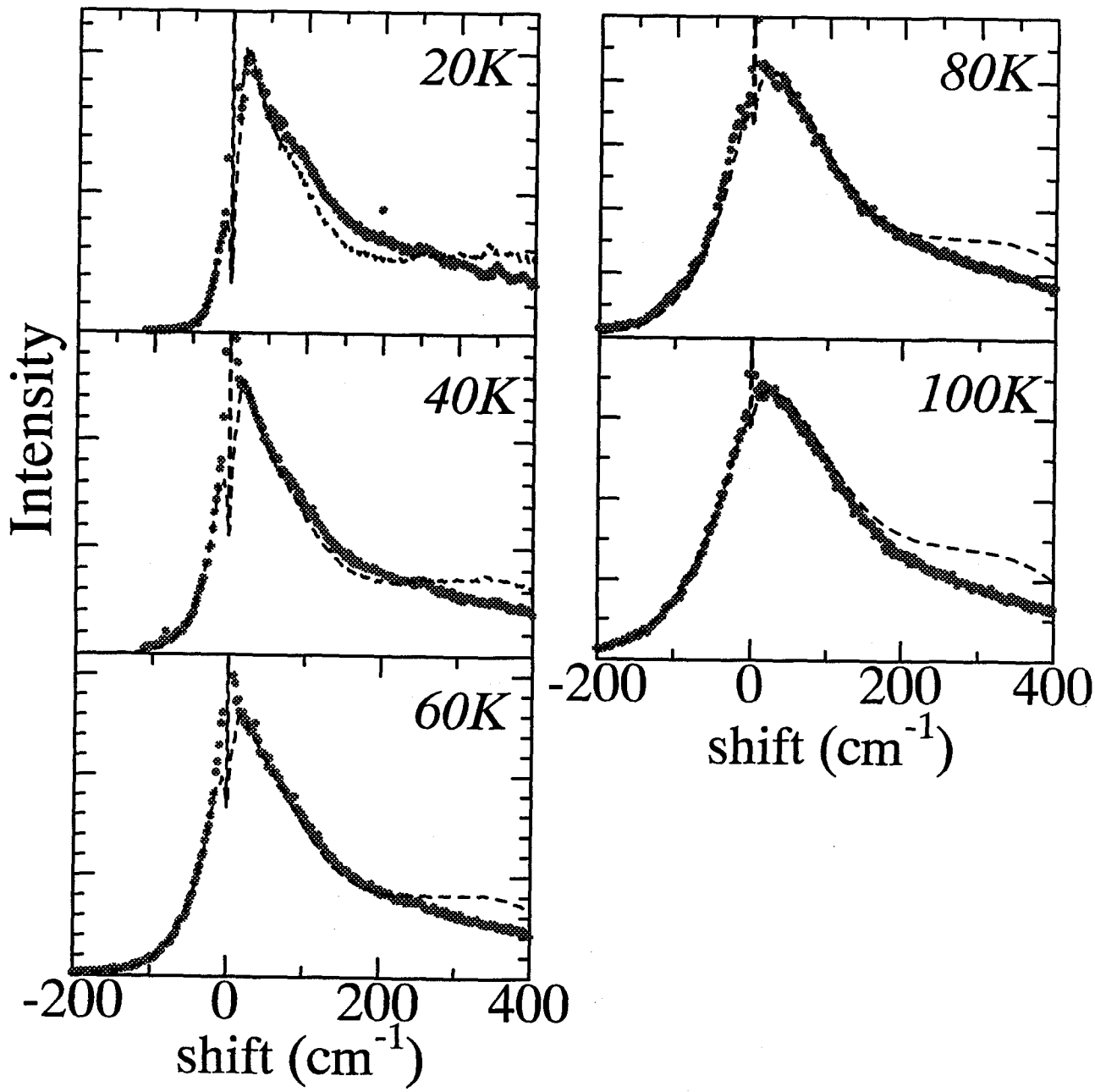

Figure 28: Measured (dots) and calculated (broken lines) site-selective fluorescence spectra for MgOEP-doped 1-butanol glass at various temperatures.

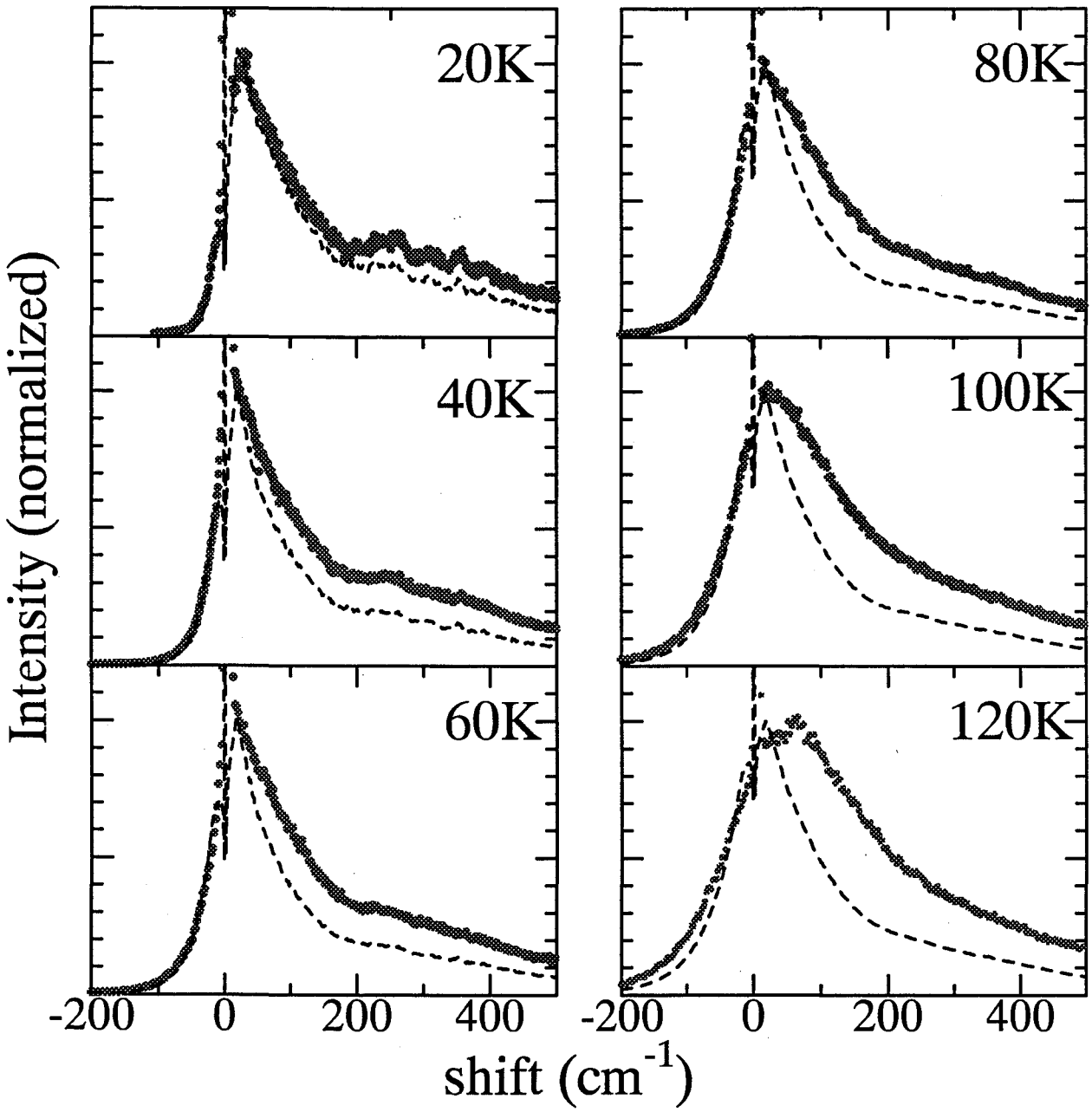

Figure 29: Measured (dots) and calculated (broken lines) site-selective fluorescence spectra for MgOEP-doped 1-propanol glass at various temperatures.

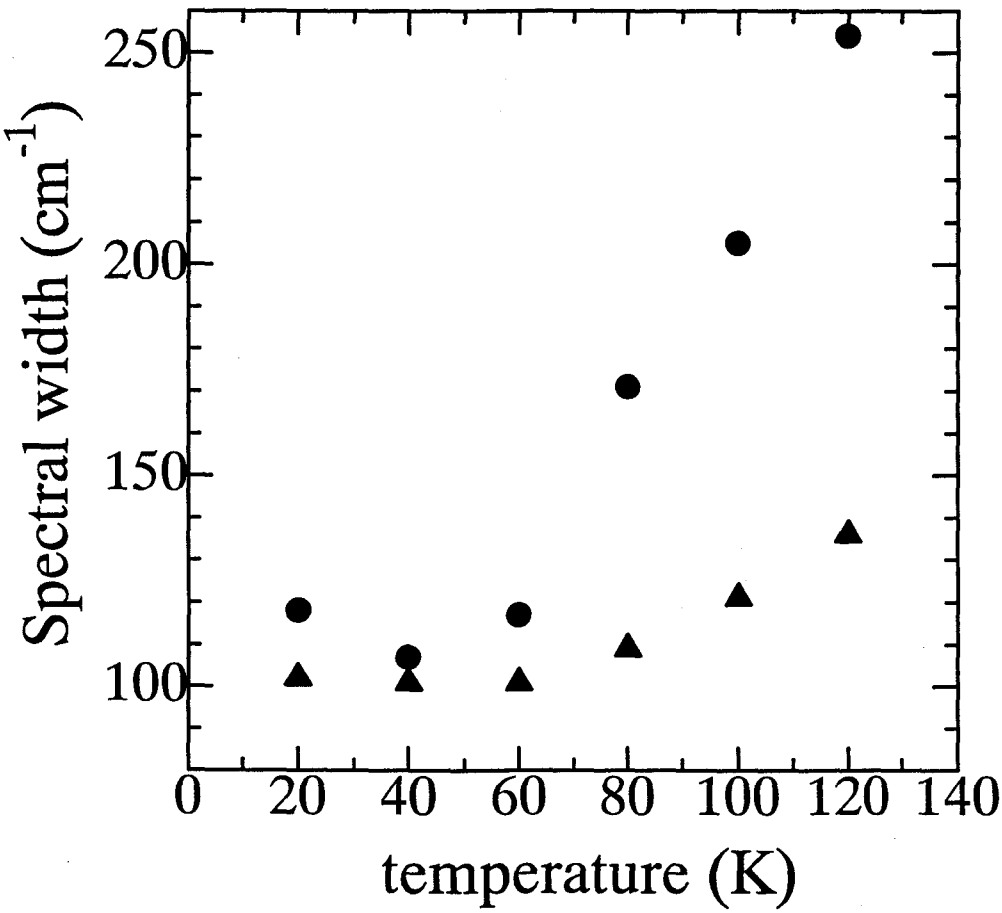

Figure 30: Temperature dependence of the bandwidth (in FWHM) of the measured (circles) and calculated (triangles) site-selective fluorescence spectra for chlorophyll b-doped 1-propanol below the glass transition temperature.

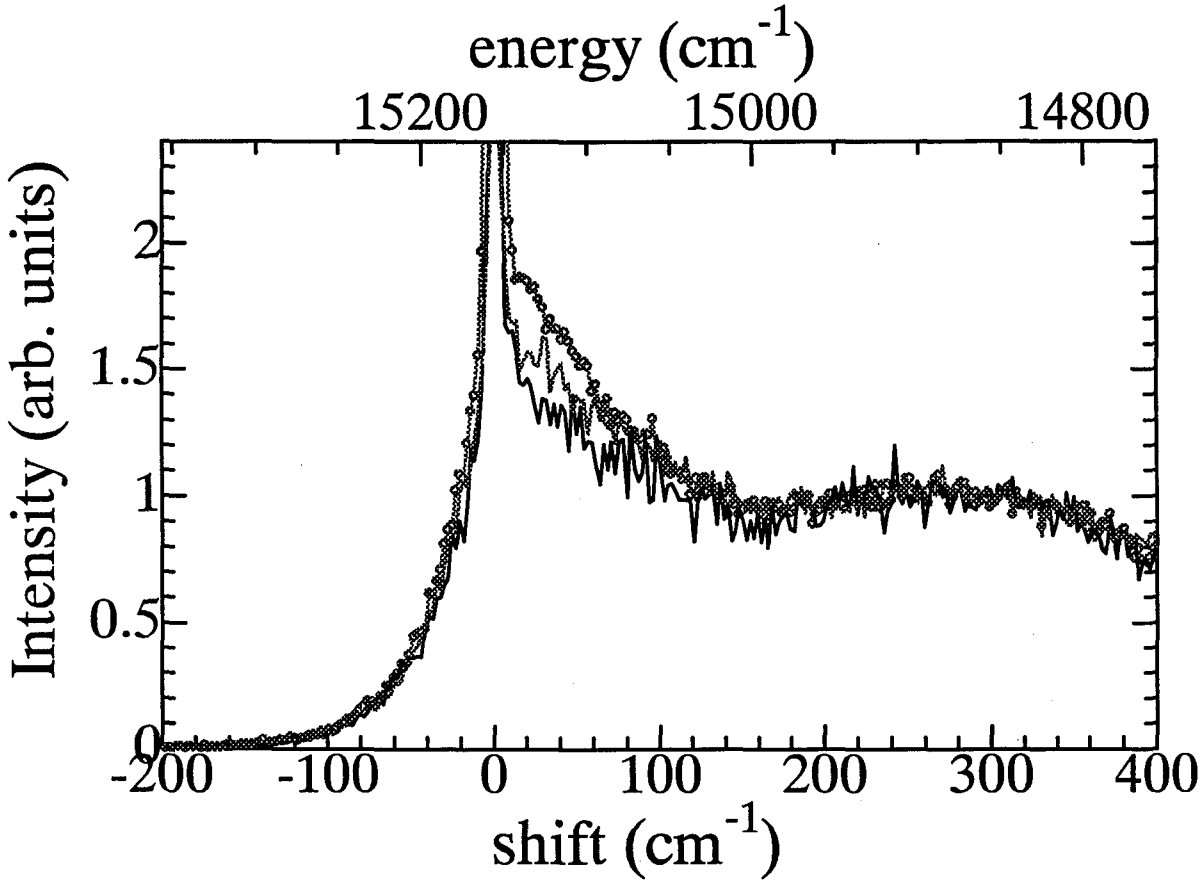

Figure 31: Time-resolved site-selective fluorescence spectra for chlorophyll b-doped 1-propanol at 60K with a delay-time window of 0-1nsec (circles), 2.5-3.9nsec (gray solid line) and 6.6-9.3nsec (black solid line). These spectra are normalized at both edges of higher and lower shift-energy.

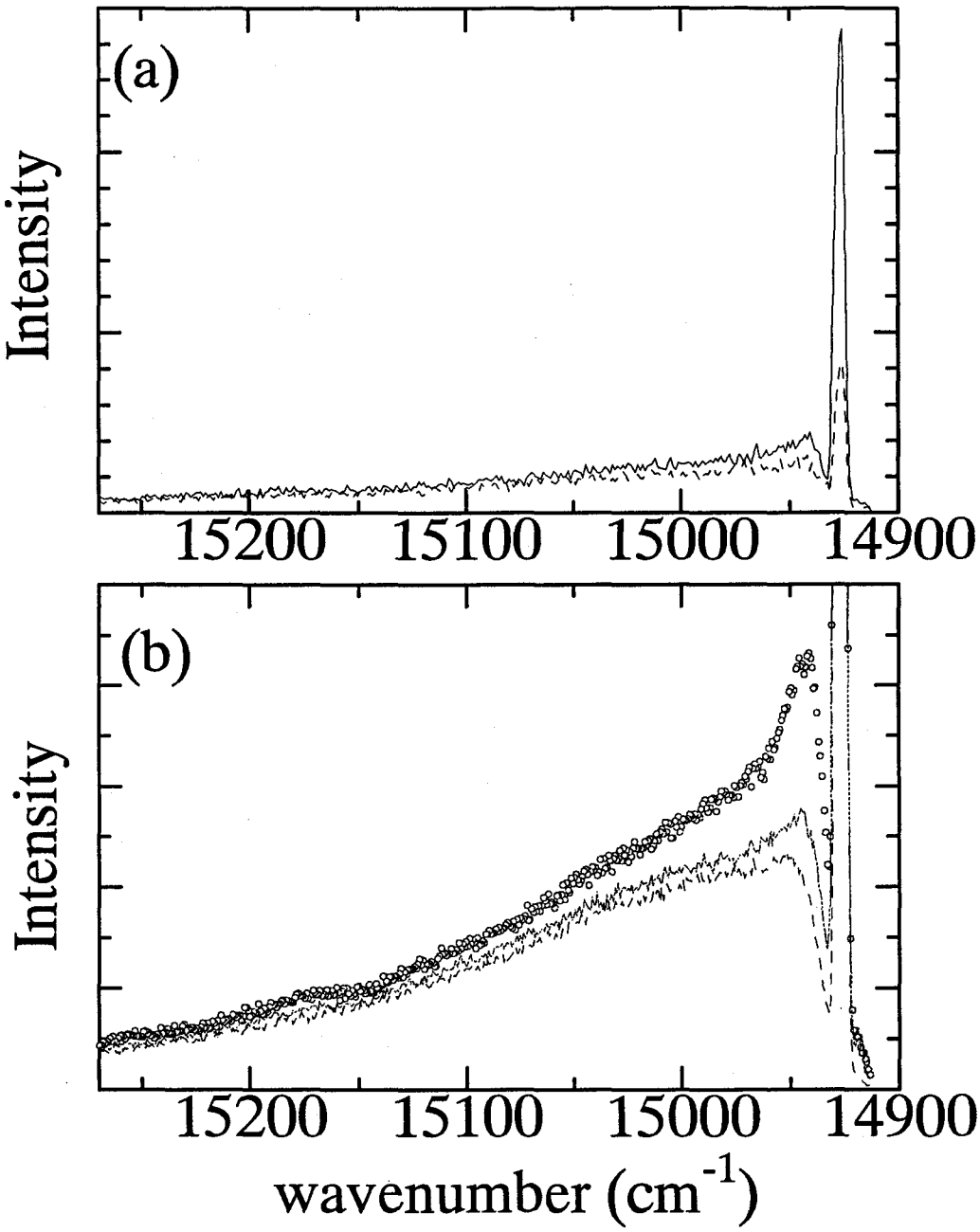

Figure 32: (a) Site-selective excitation spectra for chlorin e_6-doped polystyrene at 4K before (solid line) and after (broken line) hole-burning.
(b) Phonon-sideband components of the site-selective excitation spectra before hole-burning (circles), after a short-period hole-burning (gray solid line) and after a long-period hole-burning (black solid line).

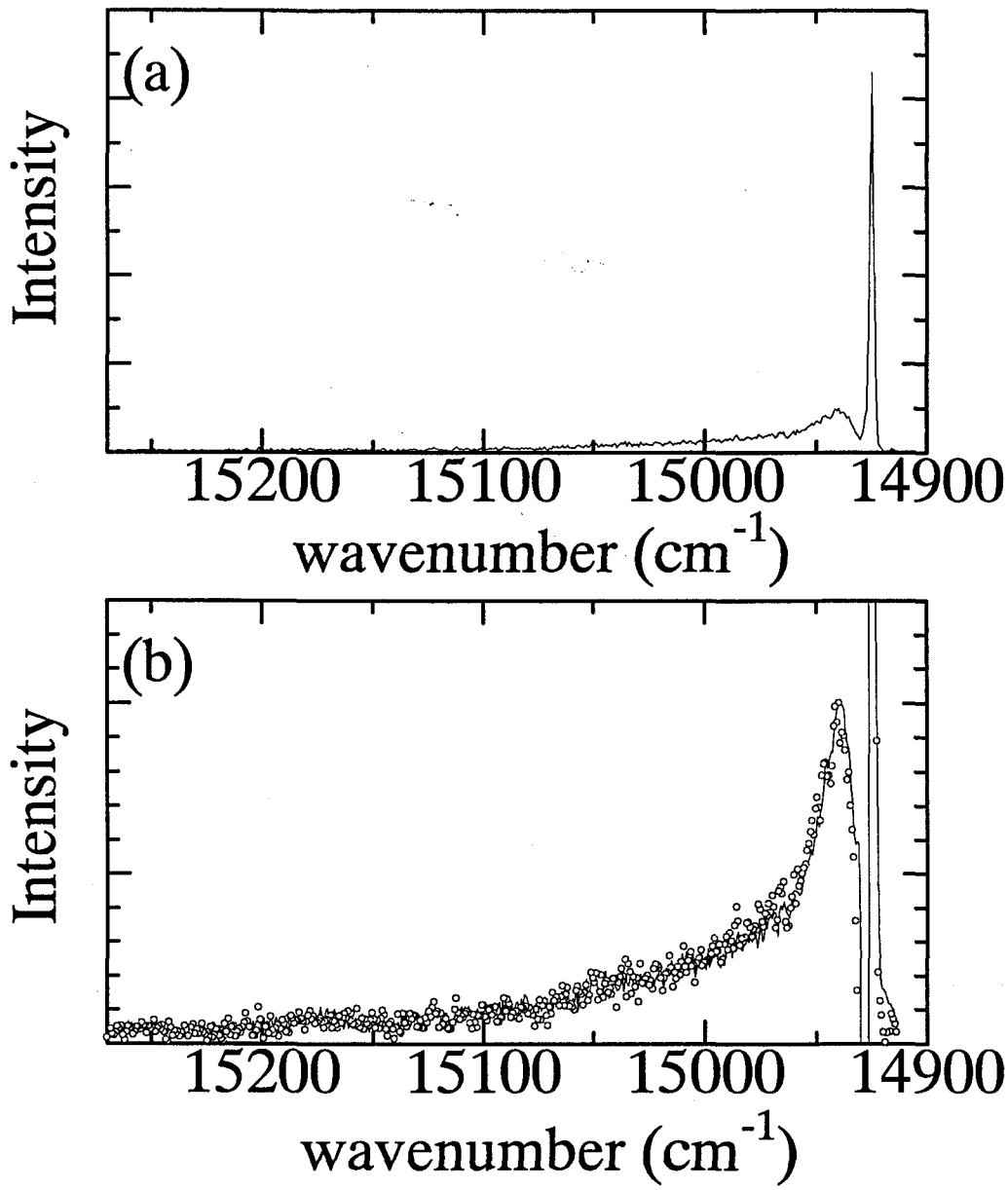

Figure 33: (a) Difference spectra of site-selective excitation spectra before and after hole-burning.
(b) Phonon-sideband components of difference spectra for a short-period (circles) and a long-period (solid line) hole-burning.

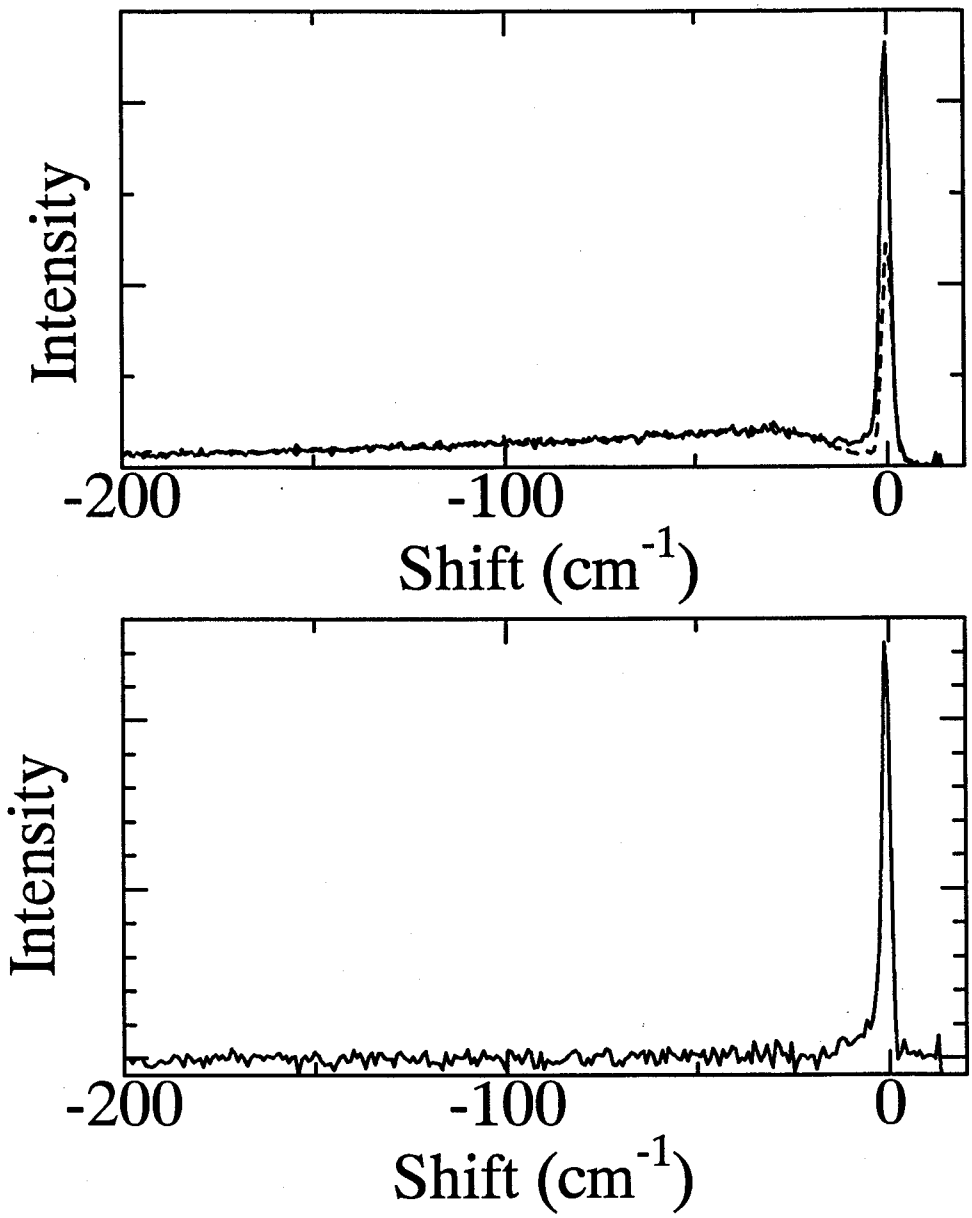

Figure 34: (a) Site-selective excitation spectra before (solid line) and after (broken line) hole-burning for oxazine 4-doped poly(vinyl butyral) at 4K.
(b) Difference spectrum of site-selective excitation spectra before and after hole-burning.

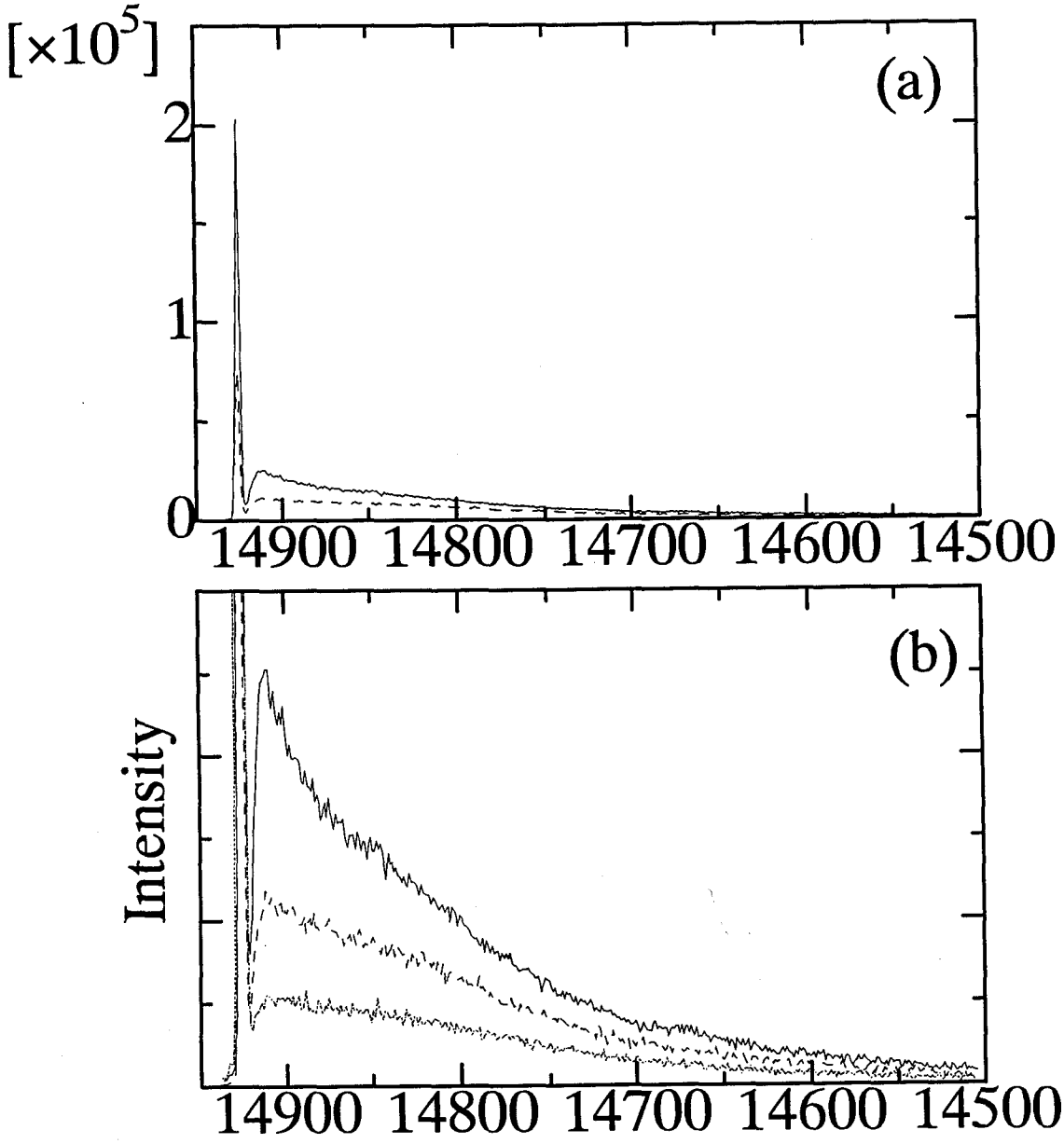

Figure 35: (a) Site-selective fluorescence spectra for chlorin e_6-doped polystyrene at 4K before (solid line) and after (broken line) hole-burning.
(b) Phonon-sideband components of the site-selective fluorescence spectra before hole-burning (black solid line), after a short-period hole-burning (broken line) and after a long-period hole-burning (gray solid line).

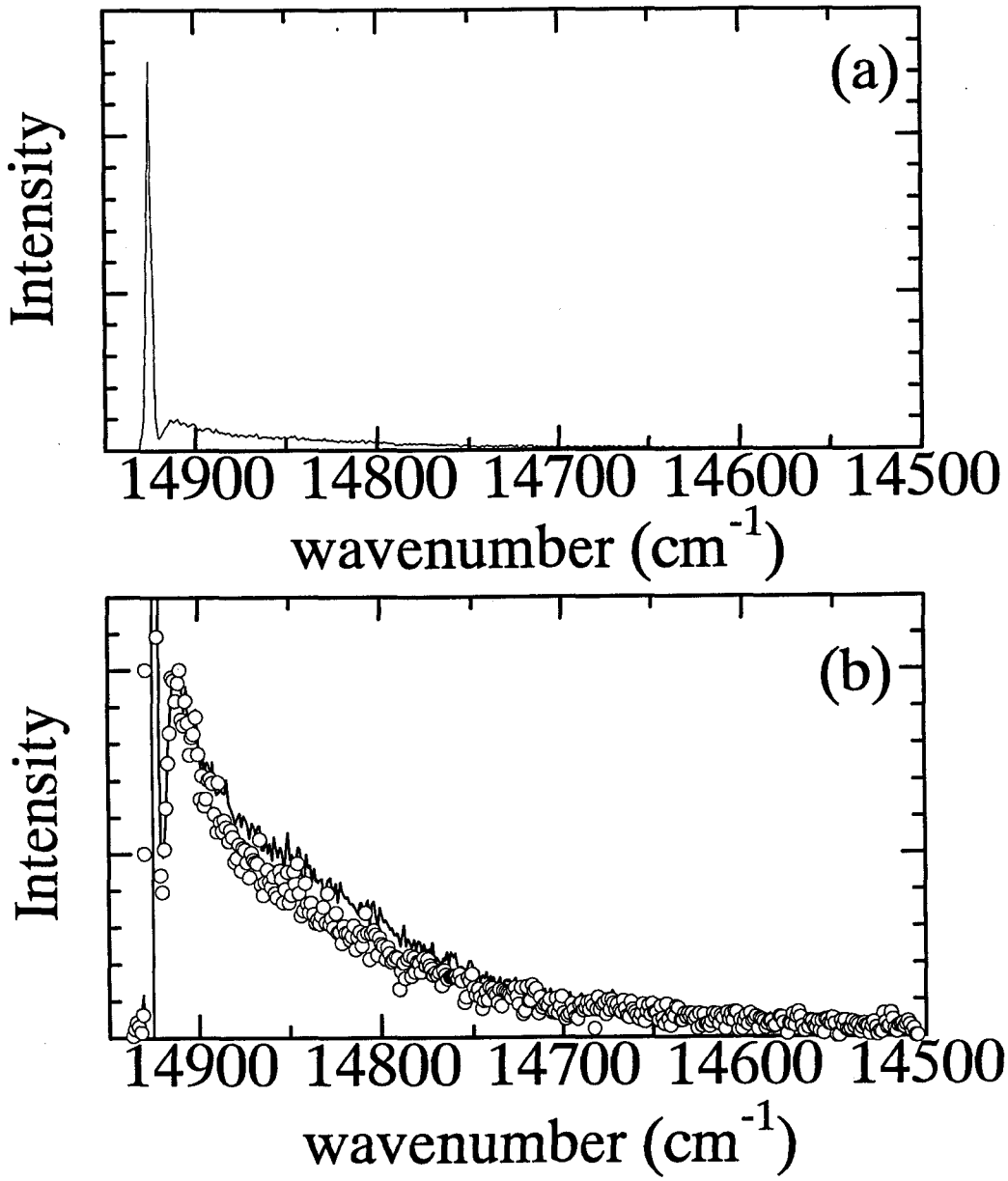

Figure 36: (a) Difference spectrum of site-selective fluorescence spectra before and after hole-burning.
(b) Phonon-sideband components of difference spectra for a short-period (solid line) and a long-period (circles) hole-burning.

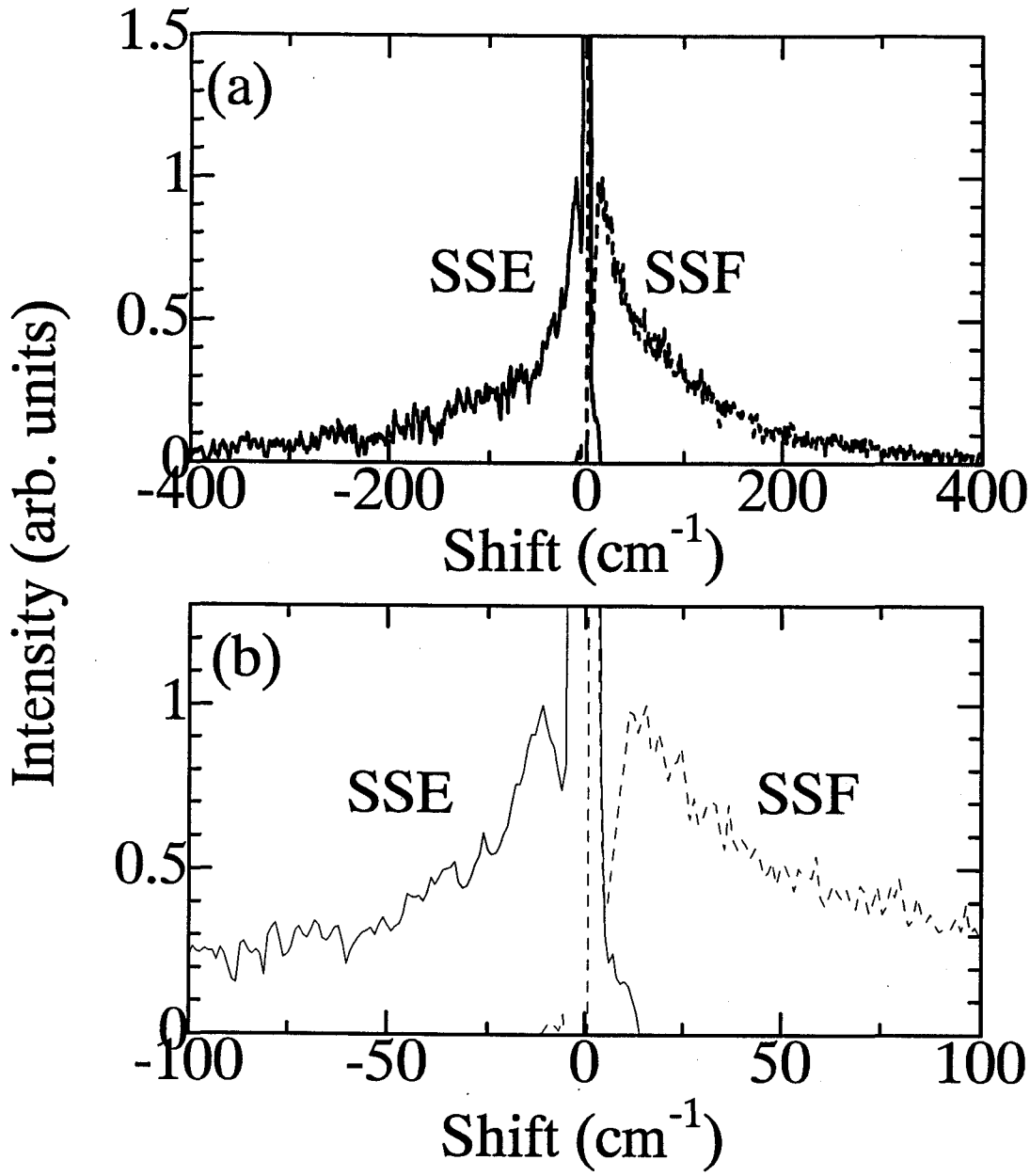

Figure 37: (a) Comparison of the difference spectra between the site-selective excitation spectra (SSE) and site-selective fluorescence spectra (SSF). Both intensities were normalized for the peak intensities of phonon-sidebands.
(b) The same comparison as (a) in a different scale.

Bibliography

[1] *Low-energy excitations in amorphous polymers*:
K.Inoue, T.Kanaya, S.Ikeda, K.Kaji, K.Shibata, M.Misawa, Y.Kiyanagi, J. Chem. Phys. **95**, 5332 (1991).

[2] *Low-energy excitation and fast motion near T_g in amorphous cis-1,4-polybutadiene*:
T.Kanaya, T.Kawaguchi, K.Kaji, J. Chem. Phys. **98**, 8262 (1993)

[3] *Raman scattering study of Boson peak of glass*:
S.Kojima, Jpn. J. Appl. Phys. **32** 2223, (1993)

[4] *Low-frequency Raman investigation of the liquid-glass transition in glycerol*:
S.Kojima, Phys. Rev. B **47**, 2924 (1993)

[5] O.Yamamuro, Private communications.

[6] *Inelastic neutron scattering study of low-energy excitations in glassy 1-butene*:
O.Yamamuro, T.Matsuo, K.Takeda, T.Kanaya, T.Kawaguchi, K.Kaji, J. Chem. Phys. **105**, 732 (1996).

[7] *Light scattering by low-energy excitations in glasses*:
A.P.Sokolov, Physica. B **219&220**, (1996).

[8] *Comparison of Raman- and neutron scattering data for glass-forming systems*:
A.P.Sokolov, U.Buchenau, W.Steffen, B.Frick, A.Wischnewski, Phys. Rev. B **52**, R9815 (1995).

[9] *The dynamics of strong and fragile glass formers: Vibrational and relaxational contributions*:
A.P.Sokolov, A.Kisliuk, D.Quitmann, A.Kudlik, E.Rössler, J. Non-Cryst. Solids **172**, 138 (1994).

[10] *Evaluation of density of vibrational states of glasses from low-frequency Raman scattering*:
A.P.Sokolov, A.Kisliuk, D.Quitmann, E.Duval, Phys. Rev. B **48**, 7692 (1993).

[11] *Log-normal spectrum of low-energy vibrational excitations in glasses*:
V.K.Malinovsky, V.N.Novikov, A.P.Sokolov, Phys. Lett. A **153**, 63 (1991).

[12] *Light scattering by fractons in polymers*:
V.K.Malinovsky, V.N.Novikov, A.P.Sokolov, V.A.Bagryanski, Chem. Phys. Lett. **143**, 111 (1988).

[13] *The nature of boson peak in Raman scattering in glasses*:
V.K.Malinovsky, A.P.Sokolov, Solid State Commun. **57**, 757 (1986).

[14] *Correlation effects on Raman scattering from low-frequency vibrational modes in fractal and disordered systems. I.Theory / II.Experimental Results*:
E.Duval, N.Garcia, A.Boukenter, J.Serughetti J. Chem. Phys. **99**, 2040 (1993).

[15] *Observation of Fractons in Silica Aerogels*:
E.Courtens, R.Vacher, J.Pelous, T.Woignier, Europhys. Lett. bf 6, 245 (1988).

[16] *Raman scattering measurements of acoustic superlocalization in silica aerogels*:
Y.Tsujimi, E.Courtens, J.Pelous, R.Vacher, Phys. Rev. Lett. **60**, 2757 (1988).

[17] *Pores in fractal aerogels and their incidence on scaling*:
R.Vacher, E.Courtens, E.Stoll, M.Böffgen, H.Rothuizen, J. Phys. Condens. Matter **3**, 6531 (1991).

[18] *Structure of random porous materials: Silica aerogel*:
D.W.Schaefer, K.D.Keefer, Phys. Rev. Lett. **56**, 2199 (1986).

[19] *Boson peak in the Raman spectra of amorphous gallium arsenide: Generalization to amorphous tetrahedral semiconductors*:
M.Ivanda, I.Hartmann, W.Kiefer, Phys. Rev. B **51**, 1567 (1995).

[20] M.Nakamura, O.Matsuda, K.Murase, *private communications.*

[21] *Microstructure of P-Se glasses and low-frequency Raman scattering*:
R.T.Phillips, M.K.Ellis, J. Non-Cryst. Solids **164-166**, 135 (1993).

[22] *Cluster size determination in amorphous structures using the Boson peak*:
I.Pócsik, M.Kods, Solid State Commun. **74**, 1253 (1990).

[23] *Interaction of soft modes and sound waves in glasses*:
U.Buchenau, Y.M.Galperin, V.L.Gurevich, D.A.Parshin, M.A.Ramos, H.R.Schober, Phys. Rev. B **46**, 2798 (1992).

[24] *Low-temperature specific heat and thermal conductivity of glasses*:
L.Gil, M.A.Ramos, A.Bringer, U.Buchenau, Phys. Rev. Lett. **70**, 182 (1993).

[25] *Neutron scattering study of the vibration-relaxation crossover in amorphous polycarbonates*:
U.Buchenau, C.Schönfeld, D.Richter, T.Kanaya, K.Kaji, R.Wehrmann, Phys. Rev. Lett. **73**, 2344 (1994).

[26] *Low-energy modes in phosphate glasses : A comparison with the soft potential model*:
A.Brodin, A.Fontana, L.Börjesson, G.Carini, L.M.Torell, Phys. Rev. Lett. **73**, 2067 (1994).

[27] *Low-frequency light scattering and structural defects in samarium phosphate glasses*:
G.Carini, M.Federico, A.Fontana, G.A.Saunders, Phys. Rev. B **47**, 3005 (1993).

[28] *The boson peak in glass formers of increasing fragility*:
A.K.Hassan, L.Börjesson, L.M.Torell, J. Non-Cryst. Solids **172-174**, 154 (1994).

[29] *Experimental study of the nature of the glass transition process in monohydroxy alcohols*:
S.S.N.Murthy, S.K.Nayak, J. Chem. Phys. **99**, 5362 (1993).

[30] *Nonexponential relaxations in strong and fragile glass formers*:
R.Böhmer, K.L.Ngai, C.A.Angell, D.J.Plazek, J. Chem. Phys. **99**, 4201 (1993).

[31] *Perspective on the glass transition*:
C.A.Angell, J. Phys. Chem. Solids **49**, 863 (1988).

[32] *Raman scattering selection-rule breaking and the density of states in amorphous materials*:
R.Shuker, R.W.Gammon, Phys. Rev. Lett. **25**, 222 (1970)

[33] *Model for Brillouin scattering in amorphous solids*:
A.J.Martin, W.Brenig, Phys. Stat. Sol. (b) **64**, 163 (1974)

[34] *Fracton interpretation of vibrational properties of cross-linked polymers, glasses, and irradiated quartz*:
S.Alexander, C.Laermans, R.Orbach, H.M.Rosenberg, Phys. Rev. B **28**, 4615 (1983)

[35] *Relaxation and nonradiative decay in disordered systems. I. One-fracton emission* :
S.Alexander, Ora Entin-Wohlman, R.Orbach, Phys. Rev. B **32**, 6447 (1985)

[36] *Vibrations of fractals and scattering of light from aerogels*:
S.Alexander, Phys. Rev. B **40**, 7953 (1989)

[37] *The determination of the site-energy distribution of organic molecules dissolved in glassy matrices*:
J.Fünfschilling, I.Zschokke-Gränacher and D.F.Williams, J. Chem. Phys. **75**, 3669 (1981).

[38] *The determination of the distribution of site energies of chlorophyll b in an organic glasses*:
J.Fünfschilling, I.Zschokke-Gränacher, Chem. Phys. Lett. **91**, 122 (1982).

[39] *Hole-burning spectroscopy as a tool to eliminate inhomogeneous broadening*:
J.Fünfschilling, D.Glatz, I.Zschokke-Gränacher, J. Lumin. **36**, 85 (1986).

[40] *Changes of the site distribution induced by hole burning*:
J.Fünfschilling, D.Glatz, I.Zschokke-Gränacher, J. Lumin. **40&41**, 511 (1988).

[41] *Quantitative determination of hole burning induced changes of site-energy in glassy matrices*:
D.Glatz, J.Fünfschilling, and I.Zschokke-Gränacher, J. Chem. Phys. **93**, 4652 (1990).

[42] *Relative importance of delocalized and pseudolocalized lattice vibrations in impurity vibron relaxation*:
G.J.Small, J. Chem. Phys. **58**, 2015 (1973).

[43] *One-phonon spectra in absorption and fluorescence spectra of molecular impurities: Breakdown of mirror symmetry*:
G.J.Small, Chem. Phys. Lett. **15**, 147 (1972).

[44] *Symmetry of quadratic-mode absorption and emission band shapes of impurities in solids*:
C.S.Kelly, Phys. Rev. B **6**, 4763 (1972).

[45] *Symmetry of vibrationally assisted electronic absorption and emission band shapes of impurities in solids*:
C.S.Kelly, Phys. Rev. B **8**, 1806 (1973).

[46] *Nonperturbative theory of temperature-dependent optical dephasing in crystals. IV. Microscopic model for pseudolocal phonons*:
D.Hsu, J.L.Skinner, J. Chem. Phys. **87**, 54 (1987).

[47] *Theory of he absorption and the fluorescence band shape of an impurity center in the Condon approximation*:
I.S.Osad'ko, Sov. Phys. JETP, **45**, 827 (1977).

[48] *Phonon structure in the fluorescence spectra of organic molecules in an n-paraffin matrix*:
I.S.Osad'ko, E.I.Al'shits, R.I.Personov, Sov. Phys. Sold State, **16** 1286 (1975).

[49] *Phonon wings and phonon-free lines in the spectra of doped n-paraffin crystals*:
R.I.Personov, I.S.Osad'ko, E.D.Godyaev, Sov. Phys. Solid State, **13**, 2224 (1972).

[50] *Relationship between electron-phonon coupling and intermolecular interaction parameters in dye-doped organic glasses*:
I.Renge, J. Opt. Soc. Am. B **9**, 719 (1992).

[51] *Phonon structure of impurity-related optical spectra in insulators*:
M.Mostoller, B.N.Ganguly and R.F.Wood, Phys. Rev. B **4**, 2015 (1971).

[52] *Zeeman effect of the $S_1 \rightarrow S_0$ transition of the two tautomeric forms of chlorin: A study by photochemical hole burning in an n-hexane host at 4.2K*:
A.I.M.Dicker, M.Noort, H.P.H.Thijssen, S.Völker and J.H.van der Waals Chem. Phys. Lett. **78**, 212 (1981).

[53] *Investigation of spectral forms of 5-cyano-octamethylisobacteriochlorin in Shpol'skii matrices*:
S.M.Arabei, S.F.Shkirman, K.N.Solovyov, Spectrochimica Acta, **48A**, 155 (1992).

[54] *Hole burning in the absorption spectrum of chlorin in polymer films: Stark effect and temperature dependence*:
F.A.Burkhalter,
G.W.Suter, U.P.Wild, V.D.Samoilenko, N.V.Rasumova, P.I.Personov, Chem. Phys. Lett. **94**, 483 (1983).

[55] *Thermal broadening of optical homogeneous linewidth in organic glasses and polymers studied via photochemical hole-burning*:
H.P.H.Thijssen, R.Van den Berg, S.Völker, Chem. Phys. Lett. **97**, 295 (1983).

[56] *Optical Dephasing of organic glassy systems studied by hole-burning: relation with excited state lifetimes*:
P.J.van der Zaag, B.C.Schokker, S.Völker, Chem. Phys. Lett. **180**, 387 (1991).

[57] J.P.Galaup, Private communication.

[58] *Inorganic and hybrid (organic-inorganic) sol-gel glasses doped with organic molecules: Fluorescence line narrowing, persistent hole-burning and spectral diffusion*:
J.P.Galaup, A.V.Veret-Lemarinier, S.Kulikov, S.Arabei, J.P.Boilot, F.Chaput, Proceedings of Spectral hole-burning and related spectroscopies: Science and applications, 358 (1994)

[59] *Universality in vibrational modes of various disordered materials examined by hole-burning-free FLN spectroscopy*:
Y.Ichino, Y.Kanematsu, T.Kushida, J. Lumin. **66&67**, 358 (1995).

[60] *Universal feature of vibrational modes of disordered materials investigated via optical spectra of doped probe molecules*:
Y.Ichino, Y.Kanematsu, T.Kushida, Physica B **219&220**, 377 (1996).

[61] *Site-selective fluorescence spectroscopy in dye-doped polymers: I. Determination of the site-energy distribution and the single-site fluorescence spectrum*:
J.S.Ahn, Y.Kanematsu, T.Kushida Phys. Rev. B **48**, 9058 (1993).

[62] *Site-selective fluorescence spectroscopy in dye-doped polymers: II. Determination of the weighted density of states of the vibrational modes*:
Y.Kanematsu, J.S.Ahn, T.Kushida Phys. Rev. B **48**, 9066 (1993).

[63] *Universal feature of weighted density of states of vibrational modes in dye-doped polymers*:
Y.Kanematsu, M.Enomoto, Y.Nishikawa, J.S.Ahn, T.Kushida, J. Lumin. **64**, 109 (1995).

[64] *Resonance fluorescence spectra of dye-doped polymers*:
Y.Kanematsu, J.S.Ahn, T.Kushida J. Lumin. **53**, 235 (1992).

[65] *Measurement of the resonance fluorescence spectrum in dye-doped amorphous systems*: J.S.Ahn, Y.Kanematsu, T.Kushida, J. Lumin. **48&49**, 405 (1991).

[66] *Polymer dependence of boson peak frequency studied by hole burning and Raman spectroscopies*: S.Saikan, T.Kushida, Y.Kanematsu, H.Aota, A.Harada, M.Kamachi, Chem. Phys. Lett. **166**, 358 (1990).

[67] *High-performance, time-correlated single photon counting apparatus using a side-on type photomultiplier*: S.Kinoshita, T.Kushida Rev. Sci. Instrum. **53**, 469 (1982).

[68] *Picosecond fluorescence spectroscopy by time-correlated single-photon counting*: S.Kinoshita, T.Kushida Anal. Instrum. **14**, 503 (1985).

[69] *Specific and non-specific solvent effects on chlorophyll a visible spectral maximum*: I.Renge, U.Mölder, I.Koppel, Spectrochim. Acta **41A**, 967 (1985).

[70] *Fluorescence-detected triplet kinetics study of the specifically solvated chlorophyll a and protochlorophyll in frozen solutions*: K.Mauring, I.Renge, P.Sarv, R.Avarmaa, Spectrochim. Acta **43A**, 507 (1987).

[71] *Vibrationally resolved optical spectra of Chlorophyll derivatives in different solid*: I.Renge, K.Mauring, P.Sarv, R.Avarmaa, J. Phys. Chem. **90**, 6611 (1986).

[72] I.Renge, Private Communications.

[73] *Solvation shell effects and spectral diffusion: Photon echo and optical hole burning experiments on ionic dyes in ethanol glass*: D.W.Pack, L.R.Narasimhan, M.D.Fayer, J.Chem. Phys. **92**, 4125 (1990)

[74] *Nonphotochemical hole burning of self aggregated dimers of chlorophyll a in polystyrene*: T.P.Carter, G.J.Small, J. Phys. Chem. **90**, 1997 (1986).

[75] *Hole-burning spectroscopy of organic molecules in amorphous silica*: R.Locher, A.Renn, U.P.Wild, Chem. Phys. Lett. **138**, 405 (1987).

[76] *Organic fluorescent dyes trapped in silica and silica-titania thin films by the sol-gel method: photophysical, film and cage properties*: D.Avnir, V.R.Kaufmann, R.Reisfeld, J. Non-Cryst. Solids **74**, 395 (1985).

[77] *Low-frequency Raman scattering from fractal vibrational modes in a silica gel*: A.Boukenter, B.Champagnon, E.Duval, J.Dumas, J.F.Quinson, J.Serughetti, Phys. Rev. Lett. **57**, 2391 (1986).

[78] *Raman study of gel-glass transformation in base-catalyzed silica*: K.Dahmouche, A.Boukenter, C.Bovier, J.Dumas, E.Duval, J.Serughetti, J. Non-Cryst. Solids **147&148**, 251 (1992).

[79] K.Kamitani, A.Makishima, *private communications.*

[80] *Sol-gel chemistry studied by ^{1}H and ^{29}Si nuclear magnetic resonance*:
L.W.Kelts, N.J.Effinger, S.M.Melpolder, J. Non-Cryst. Solids **83**, 353 (1986).

[81] *Photophysical hole burning in the resonance Raman excitation profile of the chlorophyll a dimer in solution*:
A.de Wilton, L.V.Haley, J.A.Koningstein, Chem. Phys. Lett. **97**, 538 (1983).

[82] T.Nakayama, Private communications.

[83] *Dynamical properties of fractal networks: Scaling, numerical simulations, and physical realizations*:
T.Nakayama, K.Yakubo, R.L.Orbach, Rev. Mod. Phys. **66**, 381 (1994).

[84] S.Kojima (unpublished).

[85] *Scattering investigation of acoustic localization in fused silica*:
M.Foret, E.Courtens, R.Vacher, J.B.Suck, Phys. Rev. Lett. **77**, 3831 (1996).

[86] *On the microscopic origin of the "boson" peak in glassy materials*:
F.J.Bermejo, A.Criado, J.L.Martinez, Phys. Lett. A **195**, 236 (1994).

[87] *Determination of weighted density of states of vibrational modes in Zn-substituted myoglobin*:
J.S.Ahn, Y.Kanematsu, M.Enomoto, T.Kushida, Chem. Phys. Lett. **215**, 336 (1993).

[88] *Biophysical aspects of neutron scattering from vibrational modes of proteins*:
P.Martel, Prog. Biophys. Mol. Bio. **57**, 129 (1992).

[89] *Protein dynamics: comparison of simulations with inelastic neutron scattering experiments*:
J.C.Smith, Quarterly Rev. Biophys. **24**, 227 (1991).